Impact of Receptors for Advanced Glycation End Products in Development of Chronic Pancreatitis & Pancreatic Ductal Adenocarcinoma

Dissertation

zur Erlangung des
Doktorgrades der Naturwissenschaften (Dr. rer. nat.)

der
Naturwissenschaftlichen Fakultät I - Biowissenschaften
der Martin-Luther-Universität
Halle-Wittenberg

vorgelegt von

Herr Richard Böhme (M.Sc.)

Die vorliegende Arbeit wurde in der Zeit vom 01.01.2017 bis 06.12.2023 an der Martin-Luther-Universität Halle-Wittenberg, Klinik für Innere Medizin I, unter der Leitung von Prof. Dr. med. Jonas Rosendahl und Prof. Dr. med. Patrick Michl angefertigt.

Gutachter

Prof. Dr. rer. nat. Guido Posern

Prof. Dr. rer. nat. Andrea Sinz

Prof. Dr. med. Patrick Michl (Universität Heidelberg)

Tag der öffentlichen Verteidigung: 12. Juni 2024

Table of Contents

List of Abbreviations

Abbreviation	Definition
2DG	2-Deoxy-D-Glucose
ACN	Acetonitrile
ACP	Alcoholic Chronic Pancreatitis
ADAM10	A Disintegrin and Metalloproteinase Domain-Containing Protein 10
ADM	Acinar-to-Ductal Metaplasia
AFL	Atypical Flat Lesions
AGE-R	Advanced Glycation End Product Receptor
AGEs	Advanced Glycation End Products
AKT	Protein Kinase B
AP	Acute Pancreatitis
AP-1	Activator Protein 1
Asn	Asparagine
ATF6	Transcription Factor 6
ATP	Adenosine Triphosphate
B2M	β2-Mikroglobulin
BRCA1	Breast Cancer Gene 1
BSA	Calf Serum Albumin
CALU	Calumenin
CDG	Congenital Disorder of Glycosylation
CDKN2A	Cyclin Dependent Kinase Inhibitor 2A
cDNA	Complementary DNA
CGGA	Chinese Glioma Genome Atlas
CHOP	C/EBP Homologous Protein
CID	Collisional Induced Dissociation
CML	Nε-(1-Carboxymethyl)-L-lysine
CP	Chronic Pancreatitis
CRD	Carbohydrate-Recognition-Binding Domain
C-type	Constant Domains
DAB	3,3’-Diaminobenzidine
DAD1	Defender Against Cell Death 1

DAMPs	Damage-Associated Molecular Patterns
DAPI	4′,6-Diamidino-2-Phenylindole
DDA	Data Dependent Acquisition
dDAD1	Drosophila DAD1
DDOST	Dolichyl-Diphosphooligosaccharide--Protein Glycosyltransferase Non-Catalytic Subunit
DEPs	Differentially Expressed Proteins and Phosphopeptides
dNTPs	Desoxy-Nucleotide Triphosphates
EDTA	Ethylenediaminetetraacetic Acid
eGFR	Estimated Glomerular Filtration Rate
EGFR	Epidermal Growth Factor Receptor
ELISA	Enzyme Linked Immunosorbent Assay
ER	Endoplasmic Reticulum
esRAGE	Endogenous Secretory RAGE
FBS	Fetal Bovine Serum
FC	Fold Change
FCS	Fetal Calf Serum
FDR	False Discovery Rate
FITC	Fluorescein Isothiocyanate
Gal-3	Galectin-3
GEO	Gene Expression Omnibus
GEPIA2	Gene Expression Profiling Interactive Analysis 2
GIIβ	Beta-Subunit of Glucosidase II
GO	Gene Ontology
GRB2	Growth Factor Receptor-Bound Protein-2
GSEA	Gene Set Enrichment Analysis
GTEx	Genotype-Tissue Expression
H&E	Hematoxylin and Eosin
H2DCFDA	2',7'-Dichlordihydrofluorescein-Diacetat
HaPanEU	Harmonizing Diagnosis and Treatment of Chronic Pancreatitis Across Europe
HCC	Hepatocellular Carcinoma
HCD	High Energy Collisional Dissociation
HEPES	4-(2-Hydroxyethyl)Piperazine-1-Ethanesulfonic Acid
HMGB1	High-Mobility Group Box Protein 1

HPASMC	Human Pulmonary Artery Smooth Muscle Cells
IHC	Immunohistochemistry
IL-1β	Interleukin-1 β
IPMN	Intraductal Papillary Mucinous Neoplasms
IRE1	Inositol-Requiring Enzyme1
IRE1α	Inositol-Requiring Transmembrane Kinase Endoribonuclease-1a
KD	Knockdown
kNN	K-Nearest Neighbors
KO	Knockout
KRAS	Kirsten Rat Sarcoma Virus
KRTCAP2	Keratinocyte Associated Protein 2
LC/MS-MS	Liquid Chromatography-Tandem Mass Spectrometry
LLO	Lipid-Linked Oligosaccharide
MAGT1	Magnesium Transporter 1
MAPK1	Mitogen-Activated Protein Kinase 1
MCN	Mucinous Cystic Neoplasms
MEM	Minimum Essential Medium
MMP9	Matrix Metallopeptidase 9
mRNA	Messenger-RNA
NaCl	Sodium chloride
NACP	Non-Alcoholic Chronic Pancreatitis
NCE	Normalized Collision Energies
NF-kB	Nuclear Factor Kappa-Light-Chain-Enhancer of Activated B Cells
OST	Oligosaccharyltransferase
OST4	OST Complex Subunit 4
OST-48	Oligosaccharyltransferase Subunit 48
PAAD	Pancreatic adenocarcinoma
PanIN	Pancreatic Intraepithelial Neoplasia
PARP	Poly-ADP-Ribose-Polymerase
PBS	Phosphate-Buffered Saline
PCLD	Polycystic Liver Disease
PDAC	Pancreatic Ductal Adenocarcinoma
PERK	PKR-like ER Kinase
pH	Potential of Hydrogen

PI	Propidium Iodide
PI3K	Phosphoinositid 3-Kinase
PKC	Protein Kinase C
PP cells	Pancreatic Polypeptide Cells
PPI	Protein-Protein-Interaction
PRC1	Polycomb Repressor Complex 1
PRKCSH	Protein Kinase C Substrate 80K-H
PTEN	Phosphatase and Tensin Homolog
PTM	Post-Translational Modification
PVDF	Polyvinylidene fluoride
qRT-PCR	Quantitative Real-Time Polymerase Chain Reaction
RAGE	receptor for advanced glycated end products
RNA	Ribonucleic Acid
ROS	Reactive Oxygen Species
ROTS	Reproducibility-Optimized Test Statistic
RPLP0	Ribosomal Protein Lateral Stalk Subunit P0
RPMI	Roswell Park Memorial Institute Medium
RPN1	Ribophorin 1
RPN2	Ribophorin 2
RT	Room Temperature
SD	Standard Deviation
SDS	Sodium Dodecyl Sulfate
Ser	Serine
SERBP1	Plasminogen Activator Inhibitor 1 RNA-Binding Protein
siRNA	Small Interfering RNA
SLC3A2	Solute Carrier Family 3 Member 2
SLC7A5	Solute Carrier Family 7 Member 5
SMAD4	SMAD Family Member 4
SNPs	Single Nucleotide Polymorphisms
SPSS	Statistical Package for the Social Sciences
sRAGE	soluble RAGE
STAT6	Signal Transducer and Activator of Transcription 6
STT3	Staurosporine and Temperature Sensitive 3
STT3A	STT3 OST Complex Catalytic Subunit A

STT3B	STT3 OST Complex Catalytic Subunit B
TCEP	Tris(2-Carboxyethyl)Phosphine
TCGA	The Cancer Genome Atlas
TFA	Trifluoroacetic Acid
Thr	Threonine
TiO2	Titanium Dioxide
TLR4	Toll-Like Receptor 4
TM	Tunicamycin
TMEM258	Transmembrane Protein 258
TMT	Tandem Mass Tag
TNF-α	Tumour Necrosis Factor α
TPM	Transcripts per Million
TP53	Tumor Suppressor Protein 53
TUSC3	Tumor Suppressor Candidate 3
UPR	Unfolded Protein Response
V-type	Variable Domains
YWHAZ	Tyrosine 3/Tryptophan 5 -Monooxygenase Activation Protein Zeta
ZC3H18	Zinc Finger CCCH-Type Containing 18

List of Figures

Page

List of Supplemental Figures

List of Tables

Page

List of Supplemental Tables

Acknowledgements

I express my deepest gratitude to my supervisors Prof. Dr. Guido Posern, Prof. Dr. Patrick Michl, Prof. Dr. Jonas Rosendahl and Prof. Dr. Andrea Sinz for their invaluable patience and feedback. Without my laboratory colleagues Dr. Helmut Laumen, Dr. Nico Hesselbarth, Dr. Julia Weißbach and M.Sc. Florian Sperling, who generously shared their knowledge, expertise and friendship, I would not have been able to complete this journey. Thank you very much. In addition, this endeavor would not have been possible without the generous support of the Wilhelm-Roux-Program, which funded my research.

I am also grateful to Prof. Dr. Monika Hämmerle, Dr. Alexander Navarrete Santos, Dr. Igor Kovacevic, Dr. Christian Ihling and M.Sc. Andreas Schmidt for their invaluable contributions and collaborative spirit throughout this research project. A special appreciation to all the technical assistants, Dana Reinicke, Katharina Theuerkorn, Claudia Ruffert, Thomas Brachmann, Susann Kostmann and Dirk Tänzler for their continuous support and invaluable insights.

Thanks are also owed to all the study participants and the co-authors of the "CP Serum Project", namely Carla Becker, Bettina Keil, Dr. Marko Damm, Dr. Sebastian Beer, Dr. Sebastian Rasch, Prof. Dr. Rick Schneider and Prof. Dr. Peter Bugert, who collected and processed the samples from patients and controls for this study.

Finally, I would be remiss in not mentioning my family, especially my parents, wife and child. Their belief in me has kept my spirits and motivation high throughout this process. I would also like to thank my dog for her endless patience.

Abstract

The pancreas is a multifaceted organ, providing both endocrine and exocrine functions to regulate essential metabolic processes. Continuous efforts focusing on the discovery of targeted therapies and reliable diagnostic biomarkers are being made for organ-related diseases such as chronic pancreatitis and pancreatic ductal adenocarcinoma (PDAC). Since these diseases are associated with age-related factors, advanced glycation end products (AGE) and their receptors are emerging targets which have the capability to modulate cellular functions and thereby influence pathogenesis and disease progression. AGEs and their soluble receptors sRAGE and Galectin-3 are known to activate inflammatory pathways and have been implicated in chronic inflammatory diseases, nonetheless no comprehensive data are available for chronic pancreatitis. To examine potential correlations, serum samples from 114 patients, including alcoholic and non-alcoholic chronic pancreatitis, and 40 healthy controls were collected and subsequently measured by ELISA in the course of the thesis. This comprehensive analysis revealed that both alcoholic and non-alcoholic chronic pancreatitis patients had significantly elevated serum AGEs and Galectin-3 levels compared to controls. In contrast, mean serum sRAGE levels were significantly reduced in chronic pancreatitis patients compared to controls. The simultaneous changes in ligand AGEs and their soluble receptors demonstrated the involvement of aging-related molecules in the pathogenesis of chronic pancreatitis. This may indicate the potential value of all three serum markers, AGE, sRAGE and Galectin-3, in the diagnosis and monitoring of chronic pancreatitis under defined conditions. In PDAC, RAGE and Galectin-3 have been discussed for their role in carcinogenesis and tumor progression. However, this study is the first to additionally assess the AGE receptors DDOST, a component of the oligosaccharyltransferase complex, and PRKCSH, the beta-subunit of glucosidase II, for phenotypic effects in pancreatic cancer. PDAC resections were evaluated by immunohistochemistry, and proliferation, ATP levels, endoplasmic reticulum stress, reactive oxygen species formation, and apoptosis were analyzed in four human PDAC cell lines. The observed effects for RAGE were limited to unchanged RNA expression in pancreatic cancer tissue compared to normal control and minimal protein expression in

resected PDAC tissue. The absence of significant changes in RAGE expression levels indicates that RAGE does not have a major role in pancreatic cancer. In contrast, both PRKCSH and Galectin-3 demonstrated increased RNA expression levels in pancreatic cancer tissues compared to normal controls, while *in vitro* experiments revealed reduced proliferation of the PDAC BXPC-3 cell line after knockdown of PRKCSH or Galectin-3. The results indicate a potential tumor promoting capacity of both receptors. As the proliferative effects were only observed in the *KRAS* wild-type cell line, a clinical relevance for PDAC patients is considered unlikely. However, it was confirmed that downregulation of Galectin-3 resulted in reduced migration activity in the *KRAS*-activated PDAC PA-TU-8988T cell line, highlighting its importance in the metastatic potential of PDAC. The most comprehensive results of this study were obtained for DDOST. Knockdown of DDOST resulted in decreased proliferation rates and viability, as well as increased endoplasmic reticulum stress, reactive oxygen species formation, and apoptosis in distinct PDAC cell lines. Using quantitative mass spectrometry, 30 differentially expressed proteins and phosphopeptides were identified following DDOST knockdown in PDAC PA-TU-8988T cell line. These were further analyzed for protein-protein interaction and correlation via the STRING and TCGA databases and annotated using the Gene Ontology database. Results reveal a potential tumor promoting function of DDOST in PDAC cell lines by intercepting cell stress events and thereby reducing apoptosis. The identified differentially expressed proteins and phosphopeptides highlight the role of DDOST in *N*-linked glycosylation and amino acid transport, but also in functional processes of pancreatic cancer progression. In conclusion, the findings of this study on the AGE receptors RAGE, PRKCSH, Galectin-3 and DDOST provide new potential either as promising biomarkers for early detection of chronic pancreatitis or as novel targets for PDAC therapies. DDOST, which has received little attention to date, may be an important link between protein *N*-linked glycosylation and tumor progression by contributing to protein homeostasis and protecting tumor cells from cytotoxic stress.

Zusammenfassung

Das Pankreas ist ein vielseitiges Organ, das sowohl endokrine als auch exokrine Funktionen zur Regulierung wichtiger Stoffwechselprozesse erfüllt. Kontinuierliche Bemühungen konzentrieren sich auf die Entdeckung gezielter Therapien und zuverlässiger diagnostischer Biomarker für organbezogene Krankheiten wie chronischer Pankreatitis und duktalem Pankreas-Adenokarzinom (PDAC). Da diese Krankheiten mit altersbedingten Faktoren in Verbindung gebracht werden, sind fortgeschrittene Glykationsendprodukte (AGE) und ihre Rezeptoren neue Ansatzpunkte, da sie die Fähigkeit haben, zelluläre Funktionen zu modulieren und dadurch die Pathogenese und den Verlauf der Krankheit zu beeinflussen. Es ist bekannt, dass AGEs und ihre löslichen Rezeptoren sRAGE und Galectin-3 Entzündungsprozesse aktivieren und bei chronischen Entzündungskrankheiten eine Rolle spielen, doch liegen bisher keine umfassenden Daten zur chronischen Pankreatitis vor. Um mögliche Zusammenhänge zu untersuchen, wurden im Rahmen dieser Arbeit Serumproben von 114 Patienten, einschließlich alkoholischer und nicht-alkoholischer chronischer Pankreatitis, und 40 gesunden Kontrollpersonen gesammelt und anschließend mittels ELISA gemessen. Diese umfassende Analyse ergab, dass sowohl Patienten mit alkoholischer als auch mit nicht-alkoholischer chronischer Pankreatitis im Vergleich zur Kontrollgruppe signifikant erhöhte Serumwerte von AGEs und Galectin-3 aufwiesen. Im Gegensatz dazu waren die mittleren Serumspiegel von sRAGE bei Patienten mit chronischer Pankreatitis signifikant niedriger als bei den Kontrollen. Die gleichzeitigen Veränderungen der Liganden AGEs und ihrer löslichen Rezeptoren zeigten, dass altersbedingte Moleküle an der Pathogenese der chronischen Pankreatitis beteiligt sind. Dies deutet auf den potenziellen Wert aller drei Serummarker, AGE, sRAGE und Galectin-3, für die Diagnose und Überwachung der chronischen Pankreatitis unter bestimmten Bedingungen hin. Im PDAC wurden RAGE und Galectin-3 bereits wegen ihrer Rolle in der Karzinogenese und Tumorprogression diskutiert. Diese Studie ist jedoch die erste, in der zusätzlich die AGE-Rezeptoren DDOST, eine Komponente des Oligosaccharyltransferase-Komplexes, und PRKCSH, die Beta-Untereinheit der Glucosidase II, auf ihre phänotypischen Auswirkungen beim Pankreaskarzinom untersucht wurden. PDAC-Resektionen wurden

immunhistochemisch ausgewertet, und Proliferation, ATP-Spiegel, Stress des endoplasmatischen Retikulums, Bildung reaktiver Sauerstoffspezies und Apoptose wurden in vier menschlichen PDAC-Zelllinien analysiert. Die beobachteten Auswirkungen auf RAGE beschränkten sich auf eine unveränderte RNA-Expression in Bauchspeicheldrüsenkrebsgewebe im Vergleich zur normalen Kontrolle und eine minimale Proteinexpression in Resektionsgewebe von PDAC. Das Fehlen signifikanter Veränderungen der RAGE-Expressionswerte deutet darauf hin, dass RAGE bei Bauchspeicheldrüsenkrebs keine wesentliche Rolle spielt. Im Gegensatz dazu zeigten sowohl PRKCSH als auch Galectin-3 eine erhöhte RNA-Expression in Bauchspeicheldrüsenkrebsgewebe im Vergleich zu normalen Kontrollen, während *In-vitro*-Experimente eine reduzierte Proliferation der PDAC-Zelllinie BXPC-3 nach Knockdown von PRKCSH oder Galectin-3 zeigten. Die Ergebnisse deuten auf eine potenziell tumorfördernde Wirkung der beiden Rezeptoren hin. Da die proliferativen Effekte nur in einer *KRAS*-Wildtyp-Zelllinie beobachtet wurden, ist eine klinische Relevanz für PDAC-Patienten unwahrscheinlich. Es wurde jedoch bestätigt, dass die Herunterregulierung von Galectin-3 zu einer verringerten Migrationsaktivität in der *KRAS*-aktivierten PDAC-Zelllinie PA-TU-8988T führte, was die Bedeutung dieses Rezeptors für das metastatische Potenzial von PDAC unterstreicht. Die umfassendsten Ergebnisse dieser Studie wurden für DDOST erzielt. Ein Knockdown von DDOST führte zu einer verringerten Proliferationsrate und Viabilität sowie zu erhöhtem Stress des endoplasmatischen Retikulums, Bildung reaktiver Sauerstoffspezies und Apoptose in verschiedenen PDAC-Zelllinien. Mithilfe der quantitativen Massenspektrometrie wurden 30 differentiell exprimierte Proteine und Phosphopeptide nach dem Knockdown von DDOST in der PDAC-Zelllinie PA-TU-8988T identifiziert. Diese wurden mittels der STRING- und TCGA-Datenbanken auf Protein-Protein-Interaktion und Korrelation untersucht und auf Basis der Gene Ontology-Datenbank annotiert. Die Ergebnisse zeigen eine potenziell tumorfördernde Funktion von DDOST in PDAC-Zellen, indem es Zellstressereignisse abfängt und dadurch die Apoptose reduziert. Die identifizierten differentiell exprimierten Proteine und Phosphopeptide unterstreichen die Rolle von DDOST bei der *N*-Glykosylierung und dem Aminosäuretransport, aber auch bei funktionellen Prozessen der Progression des Pankreaskarzinoms. Zusammenfassend lässt sich sagen, dass die Ergebnisse dieser Studie zu den AGE-Rezeptoren RAGE,

PRKCSH, Galectin-3 und DDOST sowohl als vielversprechende Biomarker für die Früherkennung von chronischer Pankreatitis als auch als neue Ansätze für PDAC-Therapien dienen können. DDOST, dem bisher wenig Aufmerksamkeit zugewendet wurde, könnte ein wichtiges Bindeglied zwischen der *N*-Glykosylierung von Proteinen und der Tumorprogression sein, indem es zur Proteinhomöostase beiträgt und Tumorzellen vor zytotoxischem Stress schützt.

1 Introduction

1.1 Pancreas

The pancreas, a multifunctional gland located in the abdominal cavity, plays a crucial role in distinct physiological processes. This gland is pivotal in both endocrine and exocrine functions, contributing to the regulation of blood glucose levels, digestion, and thus the release of numerous essential hormones and enzymes.

Inside the gastrointestinal tract, the pancreas is located secondary retroperitoneal in the abdomen, between the stomach, small intestine and spleen. Macroscopically, it appears as an elongated structure, approximately 14 to 25 centimeters in length (Longnecker et al., 2018). Divided into distinct regions such as the head, neck, body, and tail, the pancreas is organized into lobules and is composed of exocrine tissue and endocrine glands. The head of the pancreas is adjacent to the duodenum, while the tail extends towards the spleen (Longnecker et al., 2018). The endocrine function of the pancreas comprises the secretion of hormones into the bloodstream. This endocrine role is performed by clusters of cells called islets of Langerhans, which are distributed throughout the pancreas (In't Veld & Marichal, 2010). These islets contain different types of cells, each responsible for the synthesis and secretion of specific hormones. Beta cells secrete insulin, a hormone critical for glucose homeostasis. Insulin facilitates the uptake of glucose from the bloodstream into cells, thereby lowering blood glucose levels. Beta cell dysfunction can lead to conditions such as diabetes mellitus (Atkinson et al., 2020). Alpha cells produce glucagon, a hormone that counteracts to insulin. Glucagon stimulates the release of stored glucose from the liver, raising blood glucose levels when needed. Delta cells release somatostatin, a hormone that inhibits the release of both insulin and glucagon, thereby exerting regulatory control over blood glucose levels. Epsilon cells produce ghrelin, a hormone associated with appetite regulation and growth hormone release. PP cells help to synthesize and to regulate the release of pancreatic polypeptides (Atkinson et al., 2020). The exocrine function of the pancreas involves the secretion of digestive enzymes and fluids into the duodenum, contributing to the digestion and absorption of nutrients (Petersen, 2018). Exocrine

pancreatic acinar cells are organized into clusters known as acini, which release digestive enzymes into a network of ducts leading to the small intestine. These enzymes, including amylase, lipase, and proteases, are crucial for cleaving carbohydrates, lipids, and proteins, respectively. Their activities facilitate the digestion of ingested food and allow for the subsequent absorption of nutrients by the intestinal mucosa (Petersen, 2018). The function of ductal epithelial cells is to secrete bicarbonate to regulate the pH of digestive secretions and pass it to the intestine, thereby protecting acinar cells from damage by pancreatic stressors (Zeng et al., 2018).

1.2 Chronic Pancreatitis

Pancreatitis is an inflammation of the pancreatic tissue, which is divided into an acute and a chronic form. The acute inflammation is physiologically self-limiting, since after the release of proinflammatory cytokines, anti-inflammatory cytokines are also released promptly. In chronic courses, one of these two mechanisms most likely is impaired, leading to persistent inflammation (Coussens & Werb, 2002).

Chronic pancreatitis (CP) is a recurrent or continuous inflammatory disease of the pancreas that results in the replacement of the pancreatic parenchyma with fibrotic tissue (Lowenfels & Maisonneuve, 2018). The incidence ranges from 4 per 100,000 inhabitants in the United States and the United Kingdom to rates of 5 to 13 per 100,000 in European countries (Lévy et al., 2014). Patients may experience intermittent or continuous pain and irreversible morphologic changes in both endocrine and exocrine glands with permanent loss of function (Löhr et al., 2017). The most common cause of developing chronic inflammation is alcohol abuse, but other causes may include gene mutations, obstruction, hypertriglyceridemia, hypercalcemia, or autoimmune disorders (Masamune & Shimosegawa, 2018). The underlying pathomechanisms range from premature intrapancreatic protease activation to local and systemic inflammatory processes involved in initiating and progressing the disease (Habtezion et al., 2019). Similar to other inflammatory diseases, damaged pancreatic tissue releases damage-associated molecular patterns (DAMPs) that can stimulate the inflammatory response and thereby influence the development of CP (Habtezion et al., 2019; Hoque et al., 2012; Yasuda et al., 2006). As a result, patients with chronic pancreatitis have an increased risk

of developing pancreatic ductal adenocarcinoma (PDAC) (Guerra et al., 2007; Lowenfels & Maisonneuve, 2006, 2018). The cumulative risk of developing pancreatic cancer is 40 to 55 % for individuals with hereditary pancreatitis (Yadav & Lowenfels, 2013). In fact, both CP and PDAC share similar histologic features, including massive immune cell infiltration and fibrosis. However, the majority of patients with PDAC do not have a history of either acute or chronic pancreatitis (Yadav & Lowenfels, 2013).

1.3 Pancreatic Ductal Adenocarcinoma

PDAC to date is a devastating disease characterized by late diagnosis, early metastasis, limited response to chemotherapy, and poor prognosis (Neoptolemos et al., 2018). Although significant advances have been made in understanding the pathobiology of this disease in recent decades, PDAC is predicted to become the third leading cause of cancer-related mortality in Europe by 2025 (Ferlay et al., 2016), reflecting the lack of successful therapies, but also the increasing prevalence of obesity, diabetes and alcohol consumption (Arnold et al., 2020). The incidence rates of pancreatic cancer in North America (7.6 per 100,000 people) and Europe (7.7 per 100,000 people) are the highest worldwide (Bray et al., 2018), while the survival rates are the lowest of any major tumor type. However, in recent years, a small but significant increase in survival rates has been reported in the United States, from 4-5 % to as high as 8 % (Mocci & Klein, 2018).

Initially, PDAC arises from exocrine tissue, which is characterized by high protein expression and secretion capacity. Acinar cells, the main component of exocrine tissue, produce digestive enzymes, including amylases, proteases, and lipases. In contrast, ductal cells are responsible for the production and secretion of bicarbonate ions. The bicarbonate buffering system contributes to the maintenance of acid-base homeostasis to regulate the pH of the pancreatic extracellular fluid and neutralize acidic gastric acid (Marstrand-Daucé et al., 2023; Steward et al., 2005). When the homeostatic balance in the pancreas is disturbed by inflammation or cellular injury, acinar cells dedifferentiate into duct-like cells in response. This acinar-to-ductal metaplasia (ADM) is a cellular process and essential for regeneration. ADM involves changes in the expression of genes that control cell differentiation, proliferation, and survival to give the opportunity to proliferate and thereby replace the existing tissue damage (Marstrand-Daucé et al.,

2023). While ADM is initially a protective mechanism, metaplasia is a reversible process that allows acinar regeneration (Mills et al., 2019). Recent studies have demonstrated that under sustained stress, ADM becomes persistent and cells are highly susceptible to oncogenic stimuli (Benitz et al., 2015; Quilichini et al., 2019; Storz, 2017). An accumulation of genetic alterations leads to the formation of precursor lesions such as pancreatic intraductal neoplasia (PanIN) and intraductal papillary mucinous neoplasia (IPMN), while PanIN are found in >80 % of invasive pancreatic cancers and are therefore the most common precursor of PDAC (Andea et al., 2003; Bazzichetto et al., 2020; Maitra et al., 2005). In early lesions, the oncogenic activation of *KRAS* (Kirsten rat sarcoma) induces PanIN and IPMN development (Baumgart et al., 2010; Kojima et al., 2007; Shi et al., 2009), with >90 % of *KRAS* mutations being G12D, G12V or G12R (Network, 2017; Qian et al., 2018; L. Zhu et al., 2007). The inactivation of the tumor suppressor genes *CDKN2A* (cyclin dependent kinase inhibitor 2A), *TP53* (tumor suppressor protein 53), and *SMAD4* (SMAD family member 4) occur as very late events, often in the presence of pre-existing invasion (Hosoda et al., 2017; S. Jones et al., 2008). The simultaneous deregulation of the PTEN/PI3K/AKT (phosphatase and tensin homolog/ phosphoinositid 3-kinase/ protein kinase B) and MAPK (mitogen-activated protein kinase) pathways acts in a synergistic manner to promote the development of PDAC (Collins et al., 2014; Eser et al., 2013; Hill et al., 2010). Thus, PDAC carcinogenesis may begin with the formation of an ADM and progress to an invasive tumor via precursor lesions such as PanIN or IPMN.

1.4 Protein Modification

The intricate structures and diverse functions of proteins are not static but can undergo a variety of modifications that significantly affect their activity, stability, localization and interactions. Protein modifications, which include covalent and non-covalent changes, play a central role in the regulation of cellular processes and signal transduction pathways (Ramazi & Zahiri, 2021).

Proteins are assembled from linear sequences of amino acids, with the sequence dictating their three-dimensional structures and functional properties. However, the functional diversity of proteins is often extended by post-translational modification

(PTM) of specific amino acid residues (Walsh et al., 2005). PTMs are enzymatic or non-enzymatic processes that introduce chemical modifications to specific amino acids, thereby altering the properties of the protein. These modifications can involve the addition of chemical features such as phosphoryl, acetyl, methyl, ubiquitin, or glycosyl groups, among others (Y.-C. Wang et al., 2014). These covalent modifications can lead to conformational changes, changes in subcellular localization, or the creation of interaction sites for other proteins, nucleic acids, or small molecules (S. Wang et al., 2022).

The orchestration of PTMs is highly regulated and of crucial relevance in many biological processes (Seo & Lee, 2004). For example, phosphorylation, the addition of a phosphate group to specific serine, threonine, or tyrosine residues, acts as a molecular switch in signaling cascades. This modification can lead to conformational changes, protein-protein interactions, and activation or inactivation of enzymatic activity (Walsh et al., 2005). In addition, non-covalent interactions also affect protein function. For example, chaperones transiently interact with proteins to promote proper folding, prevent aggregation, and assist in intracellular trafficking (Tompa, 2016). Ligand-binding interactions allow proteins to specifically recognize and interact with other molecules, facilitating processes such as enzymatic catalysis, molecular transport, and signal transduction (Tompa, 2016).

Dysregulation of PTMs has been implicated in a variety of human diseases, including cancer, neurodegenerative disorders, and metabolic syndromes. As a result, the field of proteomics, which aims to comprehensively analyze and quantify protein modifications on a global scale, has emerged as a powerful tool for investigating cellular dynamics and identifying potential therapeutic targets (Seo & Lee, 2004; Tolani et al., 2021).

1.5 *N*-linked Glycosylation

Among the PTMs, glycosylation, the covalent attachment of carbohydrate or glycan to non-carbohydrate structures, usually proteins or lipids, emerges as a key process that modulates protein structure, stability, function, and cellular localization (Stowell et al., 2015). Approximately half of all human proteins are glycoproteins, most of which are *N*-linked glycosylated (Apweiler et al., 1999).

Secretory proteins undergo *N*-linked glycosylation during their endoplasmic reticulum (ER) transit (Bause, 1983). The *N*-linked glycosylation pathway begins with the synthesis of a lipid-linked oligosaccharide precursor, commonly referred to as the lipid-linked oligosaccharide (LLO), in the ER membrane. This precursor is initially assembled by the sequential addition of N-acetylglucosamine, mannose, and glucose on a dolichol pyrophosphate lipid carrier to form a conserved core oligosaccharide structure composed of two glucosamines, nine mannoses, and three glucoses (Freeze, 1998). The pre-assembled core oligosaccharide is subsequently transferred from dolichol to specific asparagine (Asn) residues within the consensus sequence Asn-Xaa-Ser/Thr motif (Sequon) of the nascent polypeptide chain, by the oligosaccharyl transferase (OST) complex, as it enters the ER lumen (Bause, 1983). The OST complexes, which catalyze the *N*-linked glycosylation, consist of 12 proteins, including STT3 OST complex catalytic subunit A and B (STT3A, STT3B), ribophorin 1 (RPN1), ribophorin 2 (RPN2), dolichyl-diphosphooligosaccharide--protein glycosyltransferase non-catalytic subunit (DDOST), defender against cell death 1 (DAD1), OST complex subunit 4 (OST4), transmembrane protein 258 (TMEM258), keratinocyte associated protein 2 (KRTCAP2), magnesium transporter 1 (MAGT1), and tumor suppressor candidate 3 (TUSC3) (Bai et al., 2018).

After attachment of the glycan moiety, the protein enters the lumen of the ER, where the glycan structure undergoes a series of processing steps catalyzed by various glycosidases and glycosyltransferases (Aebi, 2013). These enzymes work together to truncate and elongate the glycan chains, resulting in a variety of mature *N*-linked glycan structures. The extent and nature of glycan processing is influenced by factors such as the folding state of the protein, its intended cellular destination, and the specific glycan processing enzymes present in the ER (Aebi, 2013).

The consequences of *N*-linked glycosylation on protein structure and function are manifold. The glycan moieties can serve as recognition signals for chaperones and quality control mechanisms, affect protein folding by increasing the stability of the unfolded polypeptide, prevent aggregation, and allow localization of cell surface glycoproteins to the cell surface (Imperiali & O'Connor, 1999). Additionally, they can modulate protein-protein interactions, receptor binding, and enzymatic activities, thereby affecting cellular signaling pathways (Esmail & Manolson, 2021; Moremen et al., 2012). Furthermore, the glycans can influence protein solubility, half-life, and

immunogenicity. This biological versatility makes *N*-linked glycosylation a key player in various physiological processes, including embryonic development, immune response, cell adhesion, and host-pathogen interactions (Esmail & Manolson, 2021).

Aberrant *N*-linked glycosylation is widely recognized as an important characteristic of several cancers including colorectal, breast, skin and liver, correlating with tumor development, progression, metastasis and chemoresistance (Cui et al., 2018; Legler et al., 2018; Pinho & Reis, 2015; L. Tang et al., 2019; Very et al., 2018). Knockdown (KD) of Drosophila DAD1 (dDAD1) in *Drosophila melanogaster* or human RPN1 in breast cancer cells induces ER stress-dependent apoptosis, whereas expression levels of several OST subunits, including RPN1, RPN2, STT3A, STT3B, and DDOST, are upregulated in breast cancer tissue (Ding et al., 2021; Y. Zhang et al., 2016). Interestingly, inhibition of the OST complex and thereby *N*-linked glycosylation of proteins was found to induce ER stress-dependent apoptosis (Ding et al., 2021; Y. Zhang et al., 2016). In PDAC cell lines, the glycolytic inhibitor 2-deoxy-D-glucose (2DG) was found to reduce protein N-glycosylation and induces ER-related apoptosis (Ishino et al., 2018). Protein processing in the ER of tumor cells is often impaired either intrinsically, exemplarily by oncogenic activation, or extrinsically, by hypoxic, acidic and nutrient-deprived milieu (Ma & Hendershot, 2004). KD of Selenoprotein T (SelT), which interacts with KRTCAP2 and stabilizes OST subunits, resulted in a defect in ER-associated degradation of unfolded proteins (Hamieh et al., 2017). Consequently, impaired proteostasis and accumulation of misfolded proteins in ER lumen cause ER stress. This leads to the induction of the unfolded protein response (UPR) to increase clearance capacity and restore ER proteostasis. The UPR is an important cytoprotective response, prolonged ER stress can lead to apoptosis (Ma & Hendershot, 2004; Urra et al., 2016).

1.6 Glycation and Advanced Glycation End Products (AGE)

In 1912, Louis Camille Maillard described a non-enzymatic browning reaction when sugars and amino acids were heated (Ruan et al., 2018). The observed reaction is glycation and the resulting products are advanced glycation end products (AGEs).

At the molecular level, glycation starts with the initial reversible reaction between the carbonyl group of a reducing sugar and a free amino group of a protein, mostly an

arginine or lysine residue, in a nucleophilic addition reaction. This leads to the formation of a reversible Schiff base product. It´s amount correlates with the glucose concentration available in the reaction system (Brownlee et al., 1984). Further rearrangement of this Schiff base leads to formation of the amadori product. Over time, the amadori product undergoes oxidation, condensation or dehydration, resulting in the formation of stable and irreversible AGEs (Brownlee, 1995; Monnier, 1990; Vistoli et al., 2013). Because of the high variety of available proteins reacting with different glycating agents during glycation, the amount of existing AGE structures is high (Henle, 2005).

Some of these AGEs can accumulate in various tissues, such as the skin, blood vessels, kidneys, and the nervous system, through the integration in certain proteins, if the exogenous intake or endogenous formation is higher than the excretion from the body (Aldini et al., 2013; Dyer et al., 1991; Uribarri et al., 2015). These accumulations can cause structural alterations and functional impairments in affected proteins, by conformational changes, altered enzymatic activity, reduced solubility, and increased susceptibility to proteolytic degradation (Avery & Bailey, 2006; Gautieri et al., 2017; Roncero-Ramos et al., 2014). The accumulation of AGEs has also been implicated in promoting protein aggregation, oxidative stress, and inflammation, all of which contribute to disease progression (Clarke et al., 2016; Gawandi et al., 2018; Ott et al., 2014). Thereby, normal cellular processes can be disrupted and the development of various diseases, such as diabetes, neurodegenerative diseases like multiple sclerosis, Alzheimer's and Parkinson's, cardiovascular and cancer diseases are promoted (Jakuš & Rietbrock, 2004; Uribarri et al., 2015; Vicente Miranda et al., 2016; Wetzels et al., 2017; Yamagishi & Matsui, 2011).

In contrast to the receptor-independent effects, AGEs have a complex receptor system that can be divided in two categories. AGE-binding receptors, such as DDOST, PRKCSH and various scavenger receptors (Table 1) have been described to catabolize and degrade AGEs (Araki et al., 1995; Cai et al., 2010; Jono et al., 2002; Ohgami, Nagai, Ikemoto, et al., 2001; Ohgami, Nagai, Miyazaki, et al., 2001; Tamura et al., 2003; Thornalley, 1998). The receptor for advanced glycation end products (RAGE) and Galectin-3 (Gal-3) bind AGEs and activates downstream inflammatory signal cascades like the MAPK or the nuclear factor kappa-light-chain-enhancer of activated B cells (NF-κB) pathways (Braach et al., 2014; Ott et al., 2014; Pricci et al., 2000).

Table 1: Receptors for AGEs

	Receptor Name	Receptor Type (Aliases; Uniprot ID)	Ligands (Function)	Reference
	RAGE	(AGER; Q15109)	S100 proteins, β-amyloid, phosphatidylserine, HMGB1	(Neeper et al., 1992)
	DDOST	(AGE-R1, OST-48; P39656)	(48 kDa subunit of the OST complex)	(Yamagata et al., 1997)
	PRKCSH	(AGE-R2, 80K-H; P14314)	(β-subunit of glucosidase II)	(Thornalley, 1998)
	Gal-3	(AGE-R3; P17931)	β-galactosides	(Pricci et al., 2000)
Scavenger Receptors	Stabilin-1	Scavenger, class H (Stab1, FEEL1; Q9NY15)	low-density lipoproteins (LDL), Gram-positive and Gram-negative bacteria	(Tamura et al., 2003)
	Stabilin-2	Scavenger, class H (Stab2, FEEL2; Q8WWQ8)	hyaluronan, LDLs, oligonucleotides, bacteria	(Tamura et al., 2003)
	MSR1	Scavenger, class A (SR-AI; P21757)	LDLs	(Araki et al., 1995)
	SCARB1	Scavenger, class B (SR-BI; Q8WTV0)	phospholipids, cholesterol, high-density lipoprotein (HDL), cholesterol ester	(Shen et al., 2018)
	CD36	Scavenger, class B (SCARB3; P16671)	collagen, LDL, phospholipids	(Ohgami, Nagai, Ikemoto, et al., 2001)
	OLR1	Scavenger, class E (LOX-1; P78380)	LDL, HSP70	(Jono et al., 2002)

1.7 RAGE

The multi-ligand receptor RAGE, a member of the immunoglobulin superfamily, is one of the best-characterized AGE receptors (Ramasamy et al., 2008). First described in 1992, RAGE has an approximate molecular mass of 35 kDa, but due to post-translational modification can be detected between 45 and 50 kDa (Neeper et al., 1992). Full-length RAGE consists of an extracellular domain, a transmembrane domain, and a cytosolic domain. The extracellular domain is composed of three subdomains, one variable (V-type) and two constant (C-type) domains. The V-type domain provides multiple ligand

binding sites and is required for signal transduction. The transmembrane domain anchors the receptor in the plasma membrane, while the cytosolic domain transduces signals into the cell (Lee & Park, 2013). RAGE is expressed in various cell types, including immune cells such as monocytes and macrophages, T lymphocytes, as well as endothelial cells and fibroblasts (Akirav et al., 2012; Y. Liu et al., 2010; Ohashi et al., 2010; Pollreisz et al., 2010; Y. Wang et al., 2010). The expression of RAGE has been observed to be very low in adult tissues, including the pancreas, but high during embryonic development and in various cancer diseases, revealing its oncogenic potential (Brett et al., 1993; Chen et al., 2020; Hori et al., 1995).

There are more than 20 different alternative splice forms of the full-length RAGE protein identified (Falcone et al., 2013). One of the major splice variants is the well-characterized soluble RAGE (sRAGE), which lacks the C-terminal domain but contains all C- and V-type domains. It can be released extracellularly by proteolytic cleavage of its transmembrane domain by metalloproteinases like ADAM10 (A disintegrin and metalloproteinase domain-containing protein 10) and MMP9 (Matrix metallopeptidase 9) (Raucci et al., 2008; Yonekura et al., 2003; L. Zhang et al., 2008). Another splice variant is endogenous secretory RAGE (esRAGE), an isoform that lacks the signaling domain similar to sRAGE and additionally lacks the transmembrane domain (Yonekura et al., 2003). Both splice variants are secreted into the extracellular space and are unable to transduce signals into the cell. Because sRAGE and esRAGE share the same ligand binding specificity as full-length RAGE, they act as extracellular decoy receptors that bind AGEs, resulting in reduced activity of intercellular signaling pathways via RAGE, thereby providing cytoprotection (Park et al., 1998; Yan et al., 2010; Yonekura et al., 2003).

As a pattern recognition receptor, RAGE binds a wide variety of DAMPs, such as β-amyloid, phosphatidylserine, S-100 proteins, the high-mobility group box protein 1 (HMGB1) and AGEs (Ramasamy et al., 2012; Teissier & Boulanger, 2019). In PDAC, promotion of cell survival has been observed by enhancing ATP production and autophagy along with a reduction in apoptosis (Hori et al., 1995; Kang et al., 2014; Leclerc & Vetter, 2015). When AGEs or other ligands bind to RAGE, a wide range of signaling cascades are induced, including the PI3K/Akt and MAPK pathways, resulting in increased generation of reactive oxygen species (ROS) and the activation of transcription factors such as NF-κB, AP-1 and STAT-3 (Herold et al., 2007; Negre-Salvayre et al., 2009;

Riehl et al., 2009; Vazzana et al., 2009). In fact, the full function of RAGE and it´s signaling network has not yet been fully understood. However, reduced serum levels of sRAGE have been reported to be associated with pancreatic diseases such as diabetes mellitus and acute pancreatitis (AP), but no data are available on CP (Kocsis et al., 2009; Lindström et al., 2009). Whether sRAGE is a suitable biomarker for cardiovascular or coronary artery disease has been controversially discussed, with particular preference for the ratio of AGE/sRAGE as a possible universal marker (Katakami, 2017; Prasad, 2019). Notably, previous studies have shown that some variants of *RAGE* single nucleotide polymorphisms (SNPs) correlate with serum sRAGE levels in diabetes patients or are associated with diabetic complications (Lim et al., 2017; Serveaux-Dancer et al., 2019). In pancreatic cancer, RAGE was associated with the development and progression of ductal neoplasia (Azizan et al., 2017; DiNorcia et al., 2012; Leclerc & Vetter, 2015). Inhibition of RAGE has been shown to reduce MAPK activity downstream of KRAS in PDAC cell lines and prolong survival *in vivo* (Azizan et al., 2017; DiNorcia et al., 2012). A previous review summarized that by inhibiting the interaction of RAGE with its ligands, cancer development can be inhibited and this may be an effective strategy for the treatment of numerous types of cancer (Faruqui et al., 2022). In summary, RAGE and it´s soluble isoforms are potential biomarkers and might be therapeutic targets in many diseases, as altered levels are associated with inflammation, fibrosis and cancer development. However, further characterization of RAGE is required to elucidate its role in CP and PDAC.

1.8 DDOST

DDOST is the non-catalytic subunit and key component of the OST complex that catalyzes *N*-linked glycosylation within the ER lumen. Within the OST complex, DDOST has been shown to be required for substrate binding and mediation of *N*-linked glycosylation, whereas DDOST KD reduced *N*-glycosylation of newly synthesized proteins (Tu et al., 2022). Further, the implication of *DDOST* mutations in congenital disorders of glycosylation (CDG) indicated that DDOST is essential for the activity and stability of the OST complex (M. A. Jones et al., 2012) and in mice, a knockout (KO) of *DDOST* has been found to be homozygous lethal (Dickinson et al., 2016).

DDOST mRNA has been found to be highly expressed in the heart and pancreas cells of mouse and human (Yamagata et al., 1997). The mRNA expression of *DDOST* among gliomas and normal brain tissue was compared in a recent study using the Gene Expression Omnibus (GEO) and the Chinese Glioma Genome Atlas (CGGA) databases. In glioma patients, high levels of *DDOST* correlated with increased aggressiveness and an aberrant immunosuppressive microenvironment. (Chang et al., 2022). In hepatocellular carcinoma (HCC), high mRNA levels of *DDOST* expression have been found to be associated with poorer overall and disease-specific survival (C. Zhu et al., 2021). Proteomic data identified DDOST as tissue-specific expressed in the pancreas (L. Jiang et al., 2020). However, an association with pancreatic cancer has not been reported to date. In addition to its known function as a subunit of the OST complex, DDOST was identified as a potential receptor for advanced glycation end products (AGE-R1 / OST-48) and as such acted as a suppressor of cell oxidative stress and activation signaling through the epidermal growth factor receptor (EGFR) in mesangial and embryonic kidney cells (Cai et al., 2006; Y. M. Li et al., 1996). In summary, DDOST expression impacts diverse cancers and congenital disorders of glycosylation, however, little is known about the function of DDOST, especially in the progression of PDAC.

1.9 PRKCSH

The protein kinase C (PKC) substrate 80K-H (PRKCSH), which encodes the beta-subunit of glucosidase II (GIIβ), an *N*-linked glycan-processing enzyme in the ER, was originally identified during a search for PKC substrates (Hirai & Shimizu, 1990). Although, PRKCSH was found to be a poor PKC substrate, the ability to bind AGEs suggested other functions (Y. M. Li et al., 1996). Later, sequencing of *PRKCSH* revealed high homology to human and bovine DNA encoding GIIβ (Arendt & Ostergaard, 1997). Glucosidase II plays an integral role in the regulation of glycoprotein folding and maturation by cleaving two glucose residues of Glc3Man9GlcNAc2 N-glycans on newly synthesized proteins, and thereby regulating their binding to calnexin in the ER (Ellgaard et al., 1999). PRKCSH/GIIβ is located in the ER lumen and functions in the early secretory route of the cell. It is ubiquitously expressed in the human body and highly expressed in lumen-forming epithelial tissues such as liver, kidney and the pancreas (Drenth et al., 2003; A. Li et al.,

2003). PRKCSH/GIIβ has no enzymatic activity but is required for GIIα maturation and retention in the ER (D'Alessio et al., 1999; Treml et al., 2000). In addition, as an alternatively spliced protein, the ~80 kDa PRKCSH has a comprehensive domain structure indicating that it may be regulated by Ca^{2+} binding motifs and putative growth factor receptor-bound protein-2 (Grb2) binding domains (Arendt & Ostergaard, 2000).
In 2003, PRKCSH was identified as the first causative gene for polycystic liver disease (PCLD), with disease causing mutations in PRKCSH found in ~25 % of PCLD patients (Drenth et al., 2003; A. Li et al., 2003). In lung cancer cells, KO of PRKCSH/GIIβ led to reduced growth and metastatic potential through inhibition of receptor tyrosine kinases (Khaodee et al., 2019), and in liver cancer, PRKCSH was shown to regulate inositol-requiring transmembrane kinase endoribonuclease-1α (IRE1α) signaling by physical interaction under ER stress conditions (Shin et al., 2019). Bioinformatic analysis suggested that a PRKCSH deficiency potentially promotes G2/M arrest in response to cellular stress in lung cancer cells through induction of signal transducer and activator of transcription 6 (STAT6) translocation and tumor protein P53 (TPR53) activation (Lei et al., 2022). In addition, PRKCSH has been identified as a positive regulator of the Wnt/β-catenin pathway in 60 different cancer cell lines and proven in HEK293T cells (Rauscher et al., 2018). In summary, PRKCSH expression has been shown to be relevant in the regulation of glycoprotein folding and maturation, but little is known about the function of PRKCSH in the progression of PDAC.

1.10 Gal-3

Gal-3, encoded by the *LGALS3* gene, is a member of the lectin family, of 14 mammalian galectins (Barondes et al., 1994). The ~30 kDa protein Gal-3 contains a carbohydrate-recognition-binding domain (CRD) that enables the binding of β-galactosides (Verkerke et al., 2022). As such, it plays multiple roles in a broad variety of functions including cell-cell adhesion, cell-matrix interactions, macrophage activation, angiogenesis, metastasis and apoptosis (Dumic et al., 2006; Elola et al., 2007; F.-T. Liu & Rabinovich, 2005; Nakahara & Raz, 2006). Gal-3 is expressed in various cell types, such as blood vessels, fibroblasts, macrophages and cancer cells. At cellular level, it is located in the nucleus,

cytosol and plasma membrane, but is also secreted in the extracellular matrix and present in biological fluids (Desmedt et al., 2016; Xie et al., 2012). Because Gal-3 binds numerous of ligands with β-galactoside motifs by its CRD and is thereby also able to bind natural polysaccharides, the complex nature of its mechanisms remains to be clarified (Ahmed et al., 2023; F.-T. Liu & Stowell, 2023; Mariño et al., 2023). The identification of Gal-3 as a high-affinity receptor for AGE (Vlassara et al., 1995) and its lack of transmembrane sequences led to discussions, if Gal-3 is associated with other potential AGE receptors or impacts on the endocytosis of AGEs (Pricci et al., 2000; W. Zhu et al., 2001).

In general, Gal-3 participates in the initiation and amplification of the acute inflammatory response by recruiting macrophages to sites of injury and maintains a condition of chronic inflammation by activating proinflammatory pathways (Bouffette et al., 2023). Gal-3 has been associated with fibrotic and inflammatory diseases such as myocarditis, nonalcoholic steatohepatitis, chronic kidney disease, pulmonary inflammation and autoinflammatory diseases (Bouffette et al., 2023; Hrynchyshyn et al., 2013). A study of 43 patients with a manifestation of AP showed that serum levels of Gal-3 were significantly higher in AP cases compared to non-AP individuals (Porozan et al., 2021). Deletion of Gal-3 in mice prolonged survival with AP and attenuated tissue damage by affecting the activation of innate inflammatory cells (Stojanovic et al., 2019). In CP, Gal-3 mRNA and protein levels were found to be increased 3.8-fold and 3.0-fold, respectively, compared with non-CP controls. Additionally, *in situ* hybridization analysis and immunohistochemistry indicated the presence of Gal-3 in ductal cells (L. Wang et al., 2000). In tumorigenesis, Gal-3 has been shown to play an essential role in differentiation, transformation and metastasis. For various types of cancer, it was observed that Gal-3 facilitates cell migration (Al Kafri & Hafizi, 2020; K.-L. Wu et al., 2018; Zheng et al., 2017). To date, Gal-3 has been implicated in breast, cervical, colorectal, head and neck, lung, prostate, and thyroid carcinomas (Grazier & Sylvester, 2022; Ko et al., 2023; J. Li et al., 2019). In PDAC, the expression of Gal-3 and the serum levels of Gal-3 were higher compared to those in non-tumorous tissue or in other pancreatic diseases (K. Jiang et al., 2014; Xie et al., 2012). In summary, Gal-3 is a potential biomarker and therapeutic target in many diseases, as elevated levels are associated with

inflammation, fibrosis and cancer development. However, further characterization of Gal-3 is required to elucidate its role in CP and PDAC.

1.11 Aim

Considering that CP is mostly a continuous inflammatory disease, where inflammatory processes prevail even in the absence of clinical symptoms, we aimed to examine whether these can be reflected by changes in serum AGE, sRAGE and Gal-3 levels (Böhme et al., 2020). Additionally, we aimed to identify a possible genetic association with previously described RAGE variants. In PDAC, RAGE and Gal-3 have been discussed for their role in development and progression, however, this is the first time that DDOST and PRKCSH have been investigated for phenotypic effects in pancreatic cancer. Therefore, this thesis aims to further characterize the AGE receptors RAGE, DDOST, PRKCSH and Gal-3 to elucidate their respective influence in CP and PDAC, as there are limited therapeutic options. New insights into the relevant processes of CP and PDAC development may contribute to the understanding of these diseases and thereby open new diagnostic and therapeutic avenues.

The central research questions were: Are the serum levels of AGE and its soluble receptors sRAGE and Gal-3 altered between patients with CP and the control group? What are the expression levels of RAGE, DDOST, PRKCSH and Gal-3 in PDAC tumor tissues and cell lines? And how does the phenotype of PDAC cell lines change after downregulation of each individual protein?

To answer these questions, serum samples from 40 controls and 114 patients with CP were collected and analyzed. In addition, tumor resections from patients suffering from PDAC were evaluated and four human PDAC cell lines were used for various biological assays. To detect the possible influence of KRAS, cell lines with *KRAS* wild-type as well as activated mutant genotypes were included.

2 Results

2.1 Serum Levels of AGEs and their Receptors sRAGE and Gal-3 in CP

Blood samples were collected from CP patients during symptom-free intervals and not during an acute attack. Control samples were collected from blood donors in southwest Germany. A total of 40 control and 114 patient samples were measured, of which 111 samples were classified as NACP and ACP, according to the HaPanEU guideline (Table 2). The etiology of three patients could not be determined and these patients were only used for calculations in the total CP cohort. To elucidate the association between CP and serum levels of AGE, sRAGE and Gal-3, serum concentrations were measured using an enzyme-linked immunosorbent assay (ELISA). To further determine the influence of gender, etiology and age on the overall outcome, all characteristics were also evaluated separately.

Table 2: Characteristics of Patients for Serum Level Analysis

Characteristics of patients for determination of serum levels of AGE, sRAGE and Gal-3. For one patient from Leipzig and two patients from Halle the diagnosis of ACP or NACP could not be made with certainty. These 3 patients were only used for the calculations of the total CP cohort (n = 114), whereas the ACP cohort comprised 85 and the NACP cohort 26 patients.

Cohort	**No.**	**Diabetes (%)**	**Alcohol abuse**	**Mean age (range)**	**Male (%)**
Controls	40	0 (0)	NO	45 (31-60)	20 (50)
Leipzig (total)	49	22 (46)	YES/NO	53 (28-84)	40 (81)
ACP	37	19 (51)	YES	56 (36-84)	33 (89)
NACP	11	3 (27)	NO	43 (28-76)	6 (55)
Munich (total)	43	8 (19)	YES/NO	57 (23-82)	29 (67)
ACP	35	7 (20)	YES	57 (34-77)	25 (71)
NACP	8	1 (13)	NO	58 (23-82)	4 (50)
Halle (total)	22	8 (40)	YES/NO	58 (26-82)	14 (64)
ACP	13	5 (38)	YES	54 (42-67)	11 (85)
NACP	7	2 (29)	NO	64 (26-82)	3 (43)

2.1.1 AGE Serum Levels are Elevated in Patients with CP

AGE levels were significantly increased in CP patients compared to controls across all groups and etiologies (total AGE: Controls: 31.71 ± 2.308 vs. Patients: 56.61 ± 3.043 ng/mL; $P < 0.0001$) (Table 3; Figure 1 A). Correction for gender, as well as analysis of men and women in separate cohorts did not change results (Male: Controls: 28.17 ± 2.804 vs. Patients: 57.48 ± 3.715 ng/mL; $P < 0.0001$; Female: Controls: 35.25 ± 3.563 vs. Patients: 51.67 ± 4.005 ng/mL; $P = 0.0051$) (Figure 1 B; Figure S 1 A). Moreover, etiology of CP (ACP or NACP) had no influence on AGE serum levels. Here, AGE serum levels were increased in ACP and NACP compared to controls, but no differences were detected between these two etiologies. (Controls: 31.71 ± 2.308 vs. ACP: 57.73 ± 3.458; $P = 0.0066$ vs. NACP: 51.51 ± 4.632 ng/mL; $P = 0.0206$) (Table 3; Figure 1 C-D). Furthermore, the results were consistent after correction for age and diabetes mellitus (Figure 1 E-F).

Table 3: Serum Levels AGE, sRAGE and Gal-3

Serum levels of AGE, sRAGE and Gal-3 in controls and patients. The patient cohort is divided in ACP and NACP. Data are given as means and standard deviation in brackets. (Controls: n = 40, Patients: Total n = 114, ACP: n = 85, NACP: n = 26)

Cohort	**AGE [ng/ml]**	***p*-value**	**sRAGE [pg/ml]**	***p*-value**	**Galectin-3 [ng/ml]**	***p*-value**
Control	31.71 ± 2.31		1135 ± 55.74		10.81 ± 0.484	
Patients	56.61 ± 3.04	0.0001	829.7 ± 37.10	0.0001	16.63 ± 0.630	0.0001
ACP	57.73 ± 3.46	0.0066	809.5 ± 44.77	0.0001	16.88 ± 0.718	0.0001
NACP	51.51 ± 4.63	0.0206	885.4 ± 68.73	0.0066	16.07 ± 1.407	0.0001

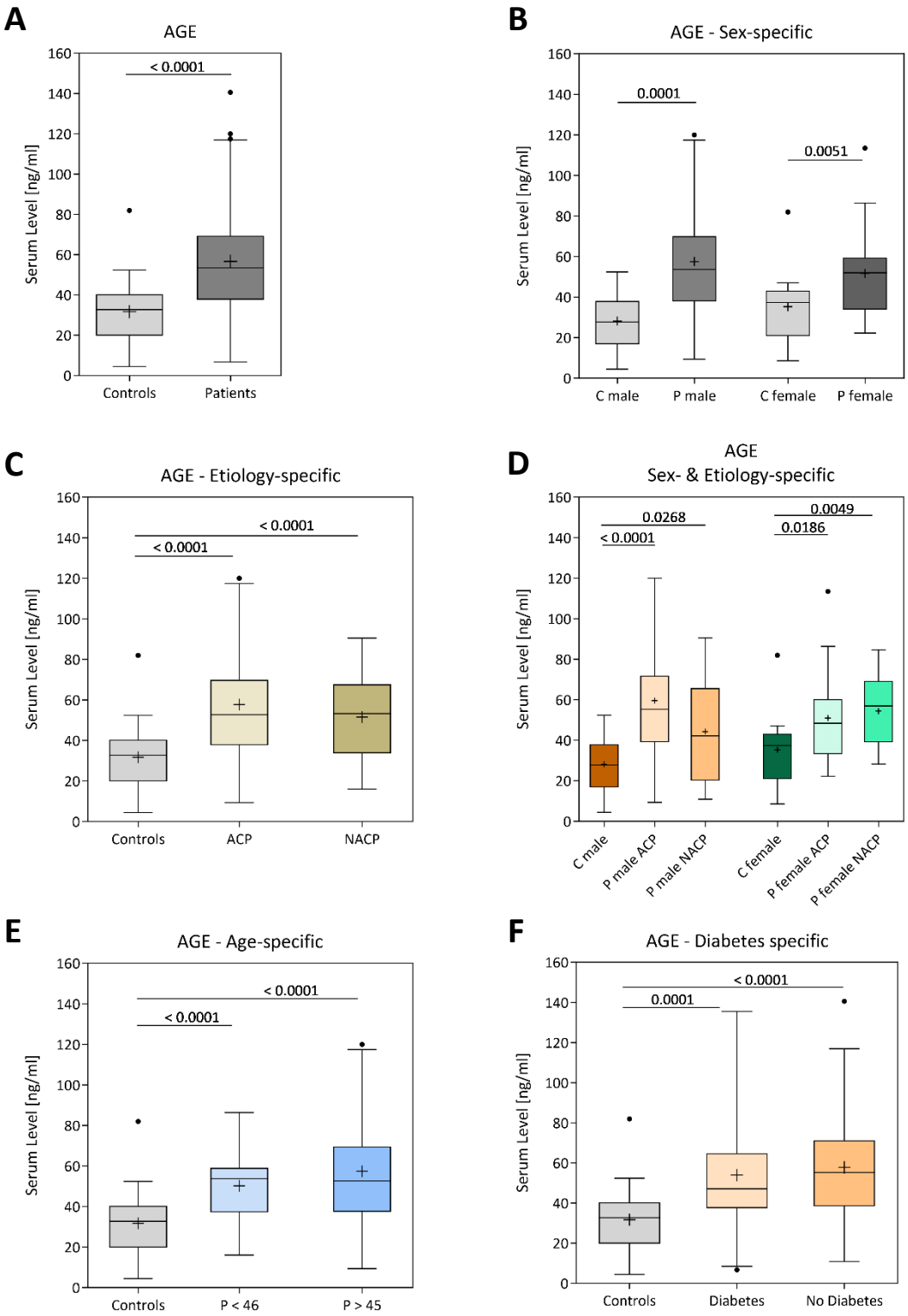

Figure 1: Serum AGE in CP Patients and Controls

A: total AGE serum levels in controls and patients. B: AGE serum levels after correction for gender. C: AGE serum levels after correction for etiology (ACP = alcoholic chronic pancreatitis; NACP = non-alcoholic chronic pancreatitis). D: AGE serum levels after correction for gender and etiology. E: AGE serum levels after correction for age (<46; >45 years of age). F: AGE serum levels after correction for diabetes. (P = patients; controls: n = 40; controls male: n = 20; controls female n = 20; patients: n = 114; patients male: n = 83; patients female: n = 28; ACP: n = 85; NACP: n = 26)

2.1.2 sRAGE Serum Levels are Lower in Patients with CP

In contrast to AGE, serum levels of sRAGE were decreased in patients with CP compared to controls in all groups and etiologies. (sRAGE total cohort: Controls: 1135 ± 55.74 vs. Patients: 829.7 ± 37.10 pg/mL; $P < 0.0001$) (Table 3; Figure 2 A). Again, gender had no effect on sRAGE serum levels, as significant associations were observed for the female and male groups, respectively. (Male: Controls: 1056 ± 76.84 vs. Patients: 787.1 ± 38.46 pg/mL; $P = 0.0025$; Female: Controls: 1215 ± 78.63 vs. Patients: 949.8 ± 92.64 pg/mL; $P = 0.0406$) (Figure 2 B; Figure S 1 B). Furthermore, sRAGE serum levels did not differ between ACP and NACP patients, as both had significantly decreased serum levels in comparison to controls. (Controls: 1135 ± 55.74 vs. ACP: 809.5 ± 44.77; $P < 0.0001$ vs. NACP: 885.4 ± 68.73 pg/mL; $P = 0.0066$) (Table 3; Figure 2 C-D). After correction for age and diabetes mellitus, the difference remained statistically significant. (Figure 2 E-F).

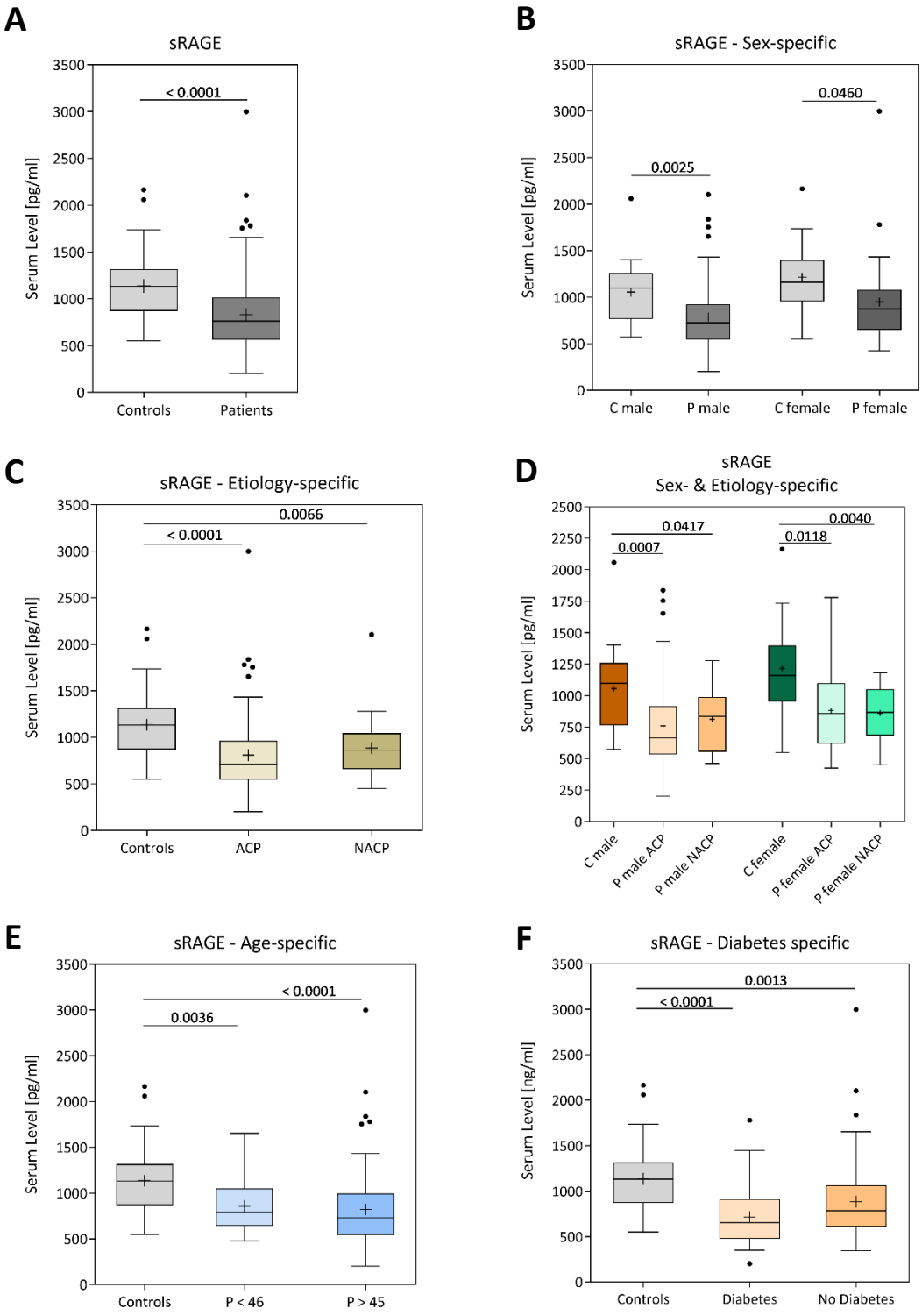

Figure 2: Serum sRAGE in CP Patients and Controls.

A: total sRAGE serum levels in controls and patients. B: sRAGE serum levels after correction for gender. C: sRAGE serum levels after correction for etiology (ACP = alcoholic chronic pancreatitis; NACP = non-alcoholic chronic pancreatitis). D: sRAGE serum levels after correction for gender and etiology. E: sRAGE serum levels after correction for age (<46; >45 years of age). F: sRAGE serum levels after correction for diabetes. (P = patients; controls: n = 40; controls male: n = 20; controls female n = 20; patients: n = 114; patients male: n = 83; patients female: n = 28; ACP: n = 85; NACP: n = 26)

2.1.3 RAGE Gene Variants are not Correlated with sRAGE Serum Levels

To determine the potential effects of *RAGE* gene variants on sRAGE serum levels, four known *RAGE* gene SNPs were genotyped. Therefore, the *RAGE* variants rs2071288, rs2070600, rs1800624 and rs1800625 were analyzed in 378 CP patients (202 ACP; 176 NACP) from our biobank and 338 controls by melting curve analysis (Table 4). Screening of each SNP variant showed no significant difference in genotypes between patients and controls (Table 5).

Table 4: Characteristics of Patients for Genetic Analysis

Age and gender in controls and patients. The patient cohort is divided in NACP and ACP. (Controls: n = 338, Patients: Total n = 378, ACP: n = 202, NACP: n = 176)

Cohort	**No.**	**Age (range)**	**Male (%)**
Controls	338	64 (60-70)	169 (50)
Patients	378	45 (5-82)	281 (74)
NACP	176	41 (5-82)	100 (57)
ACP	202	50 (25-79)	181 (90)

Table 5: Genotypes of Investigated RAGE Single Nucleotide Polymorphisms

Genotypes of RAGE Single Nucleotide Polymorphisms (SNPs) in controls, patients with NACP and ACP. (Controls: n = 338, Patients: Total n = 378, ACP: n = 202, NACP: n = 176)

SNP		**Genotype**			***p*-value**
		GG	GA	AA	
rs2071288	Controls	335/338 (99.1 %)	3/338 (0.9 %)	0/338 (0 %)	
	Patients	377/378 (99.7 %)	1/378 (0.3 %)	0/378 (0 %)	0.2642
	NACP	175/176 (99.4 %)	1/176 (0.6 %)	0/176 (0 %)	0.6958
	ACP	202/202 (100 %)	0/202 (0 %)	0/202 (0 %)	0.1794
		GG	GA	AA	
rs2070600	Controls	314/338 (92.9 %)	22/338 (6.5 %)	2/338 (0.6 %)	
	Patients	347/378 (91.8 %)	31/378 (8.2 %)	0/518 (0 %)	0.2287
	NACP	155/176 (88.1 %)	21/176 (11.9 %)	2/176 (1.1 %)	0.0670
	ACP	192/202 (95 %)	10/202 (5 %)	0/202 (0 %)	0.0670
		TT	TC	CC	
rs1800625	Controls	220/338 (65.1 %)	102/338 (30.2 %)	5/338 (1.5 %)	
	Patients	239/378 (63.2 %)	124/378 (32.8 %)	15/378 (4 %)	0.1188
	NACP	113/176 (64.2 %)	55/176 (31.3 %)	8/176 (4.5 %)	0.9244
	ACP	126/202 (62.4 %)	69/202 (34.2 %)	7/202 (3.5 %)	0.2390

		TT	TA	AA	
rs1800624	Controls	173/338 (51.2 %)	130/338 (38.5 %)	25/338 (7.4 %)	
	Patients	188/378 (49.7 %)	150/378 (39.7 %)	35/378 (9.3 %)	0.6593
	NACP	94/176 (53.4 %)	67/176 (38.1 %)	14/176 (8 %)	0.9540
	ACP	94/202 (46.5 %)	83/202 (41.1 %)	21/202 (10.4 %)	0.3514

2.1.4 Gal-3 Serum Levels are Elevated in Patients with CP

Finally, Gal-3 serum levels were significantly elevated in patients compared to controls for all patient groups and etiologies (Gal-3: Controls: 10.81 ± 0.4835 vs. Patients: 16.63 ± 0.6297 ng/mL; $P < 0.0001$) (Table 3; Figure 3 A). In addition, the significant difference in the elevated serum levels of Gal-3 was maintained when the female and male groups were analyzed separately. (Male: Controls: 10.67 ± 0.6074 vs. Patients: 16.19 ± 0.6467 ng/mL; $P < 0.0001$; Female: Controls: 10.94 ± 0.7674 vs. Patients: 17.97 ± 1.600 ng/mL; $P = 0.0012$) (Figure 3 B; Figure S 1 C). As for AGE and sRAGE, the etiology of CP had no effect on Gal-3 serum levels. (Controls: 10.81 ± 0.4835 vs. ACP: 16.88 ± 0.7176; $P = 0.0001$ vs. NACP: 16.07 ± 1.4070 ng/mL; $P < 0.0001$) (Table 3; Figure 3 C-D). Moreover, the observed correlation between serum Gal-3 levels and CP was not affected by adjustment for age and diabetes mellitus. (Figure 3 E-F).

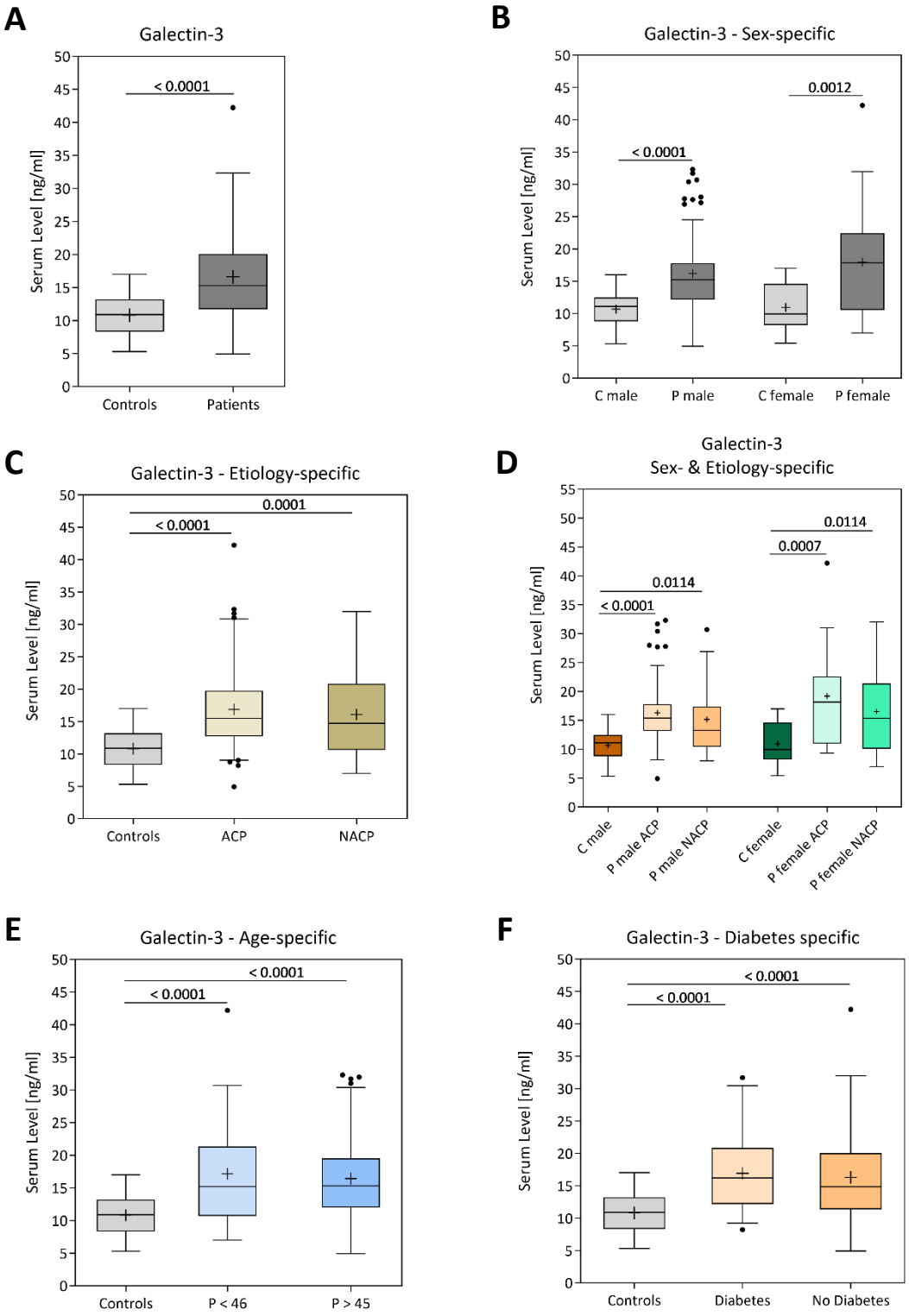

Figure 3: Serum Gal-3 in CP Patients and Controls.

A: total Gal-3 serum levels in controls and patients. B: Gal-3 serum levels after correction for gender. C: Gal-3 serum levels after correction for etiology (ACP = alcoholic chronic pancreatitis; NACP = non-alcoholic chronic pancreatitis). D: Gal-3 serum levels after correction for gender and etiology. E: Gal-3 serum levels after correction for age (<46; >45 years of age). F: Gal-3 serum levels after correction for diabetes. (P = patients; controls: n = 40; controls male: n = 20; controls female n = 20; patients: n = 114; patients male: n = 83; patients female: n = 28; ACP: n = 85; NACP: n = 26)

2.2 Functional Characterization of AGE Receptors RAGE, PRKCSH, Gal-3 and DDOST in Pancreatic Cancer

To characterize RAGE, PRKCSH, Gal-3 and DDOST in PDAC, RNA and protein expression were analyzed in PDAC tissues, followed by phenotypic analysis of PDAC cell lines after knockdown of the respective targets. Since DDOST appeared as the most potential candidate, MS analysis was performed to identify protein-protein interaction partners.

2.2.1 Expression of RAGE in Human PDAC Tissue

To determine the *RAGE* expression and whether it is altered in pancreatic adenocarcinoma (PAAD) tissues compared to normal tissues, the GEPIA2 online tool was used to obtain RNA expression levels based on TCGA and GTEx data. 179 samples from tumors were compared to 171 samples from normal controls (Figure 4). A distinct expression status was shown for both groups. However, RNA expression (log2(TPM+1)) showed no significant differences between tumor and normal tissue.

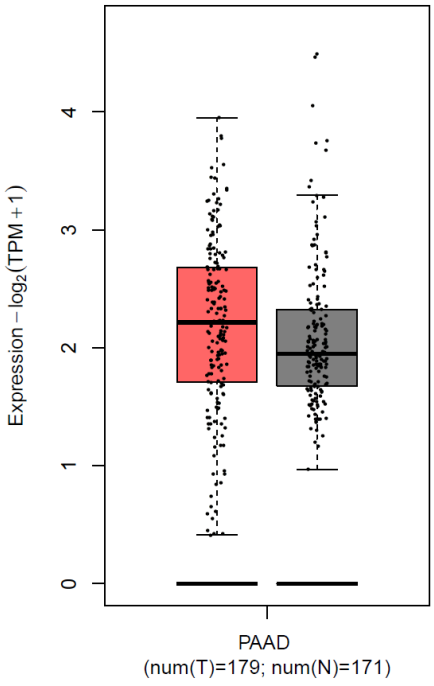

Figure 4: RAGE Expression Levels in Tumor and Normal PAAD Tissue

RAGE RNA expression levels based on TCGA and GTEx data using GEPIA2. (Tumor in red: n = 179; normal in grey: n = 171)

In resected human PDAC tissue, hematoxylin and eosin (H&E) staining revealed high-grade PanIN lesions and ADM (Figure 5 A). Expression of RAGE in PDAC tissues was visualized by RAGE antibody staining and immunohistochemistry (IHC) using a peroxidase assay. Here, RAGE was shown to be expressed in numerous uncharacterized immune cells (arrows, Figure 5 B), but not in PanIN lesions or fibroblast cells. Moreover, RAGE protein expression was detected in ductal-like structure of ADM and muscle cells (Figure S 4 F, H)

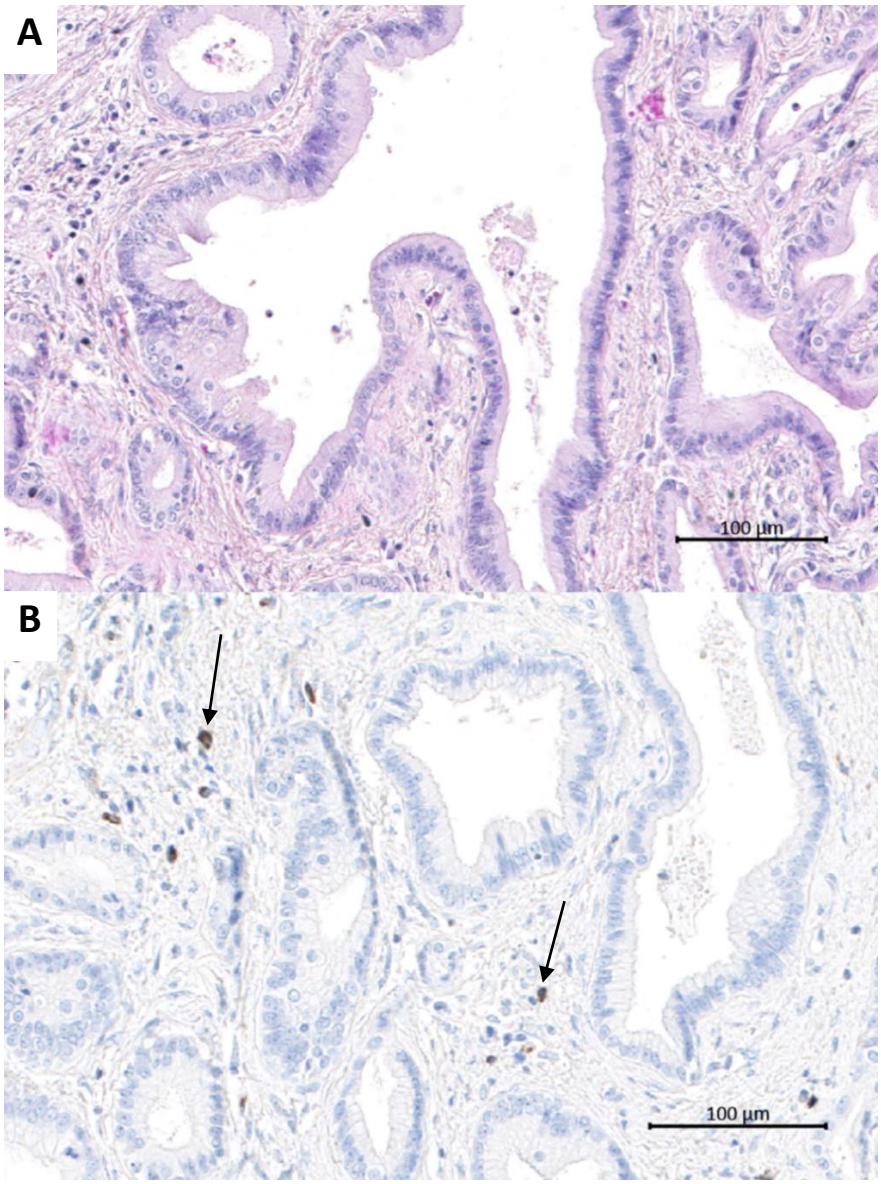

Figure 5: H&E and IHC Staining of RAGE in Human PDAC Tissue

(A) Representative H&E staining of PDAC patient tissue. (B) Representative IHC staining for RAGE expression. Arrows indicate representative RAGE-positive compartments. (Scale bar, 100 µm)

2.2.2 Expression and KD of RAGE in PDAC Cell Lines

In several PDAC tumor cell lines, ranging from PA-TU-8988T and BXPC-3, to PANC-1 and MIA-PACA-2 (Figure 6 A-C), we consistently found RAGE protein and RNA expression by western blot and quantitative real-time polymerase chain reaction (qRT-PCR) analysis. BXPC-3, PA-TU-8988T, PANC-1 and MIA-PACA-2 cell lines were each transiently transfected with homolog-specific siRNA pools to knock down (KD) RAGE expression. KD efficiency was analyzed by both, qRT-PCR and western blot analysis. No reduction in RAGE expression was observed in any of the cell lines compared to a non-targeting control siRNA, except for the *RAGE* RNA level in the PANC-1 cell line, which was significantly reduced by approximately 42 % (Figure 6 A-C).

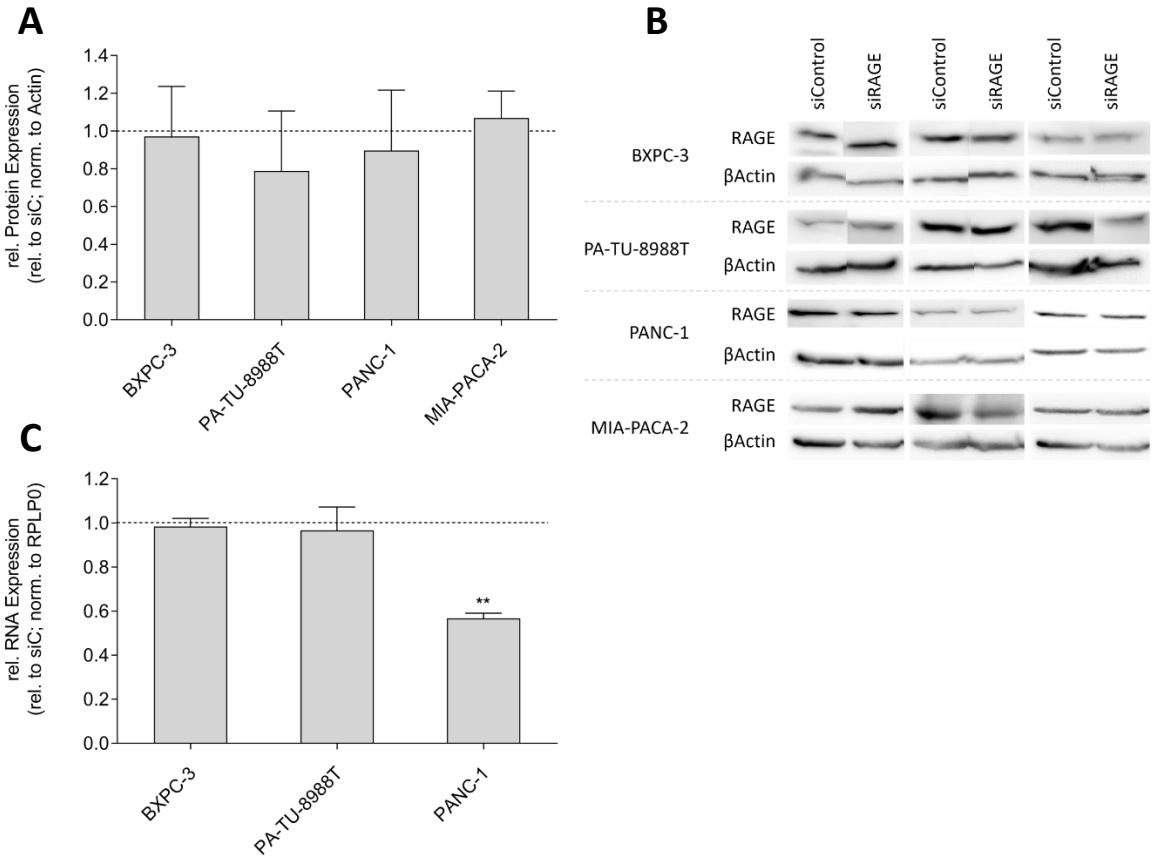

Figure 6: RAGE KD Efficiency on Protein and RNA Expression PDAC Cell Lines

*(A) Quantification of relative RAGE protein expression after RAGE KD. Dotted line indicates siControl. β-Actin was used as loading control. (B) Western blot analysis of RAGE after RAGE KD. β-Actin was used as loading control. (C) Quantification of relative RAGE RNA expression after RAGE KD. Dotted line indicates siControl. RPLP0 was used as housekeeping gene. (n = 3; **P < 0.01; unpaired t-test)*

2.2.3 Expression of PRKCSH in Human PDAC Tissue

To determine the status of *PRKCSH* expression and whether it is altered in PAAD tissues compared to normal tissues, the GEPIA2 online tool was used to obtain RNA expression levels based on TCGA and GTEx data. 179 samples from tumors were compared to 171 samples from normal controls (Figure 7). A distinct expression status was shown for both groups. The RNA expression (log2(TPM+1)) of tumor samples showed a significant increase compared to normal tissue.

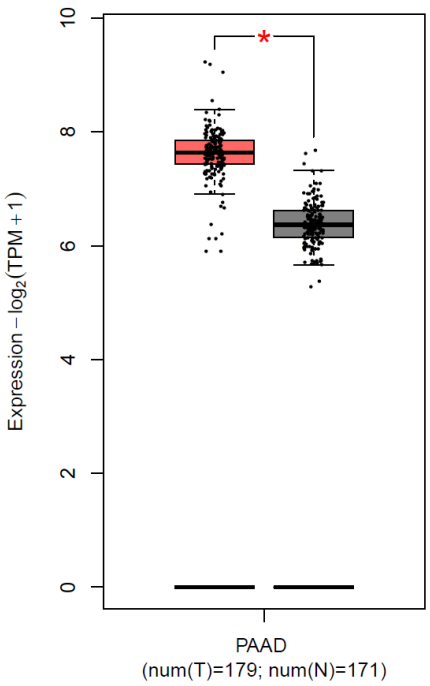

Figure 7: PRKCSH Expression Levels in Tumor and Normal PAAD Tissue

*PRKCSH RNA expression levels based on TCGA and GTEx data using GEPIA2. (Tumor in red: n = 179; normal in grey: n = 171; *P < 0.01)*

2.2.4 PRKCSH KD Reduces Proliferation and Viability in BXPC-3 Cell Line

In several PDAC tumor cell lines, ranging from PA-TU-8988T and BXPC-3, to PANC-1 and MIA-PACA-2 (Figure 8 A-C), we consistently found PRKCSH protein and RNA expression by western blot and qRT-PCR analysis. BXPC-3, PA-TU-8988T, PANC-1 and MIA-PACA-2 cell lines were each transiently transfected with a homolog-specific siRNA pool to KD PRKCSH expression. KD efficiency was analyzed by both, qRT-PCR and western blot

analysis. PRKCSH RNA and protein expression was significantly reduced in all cell lines compared to non-targeting control siRNA (Figure 8 A-C).

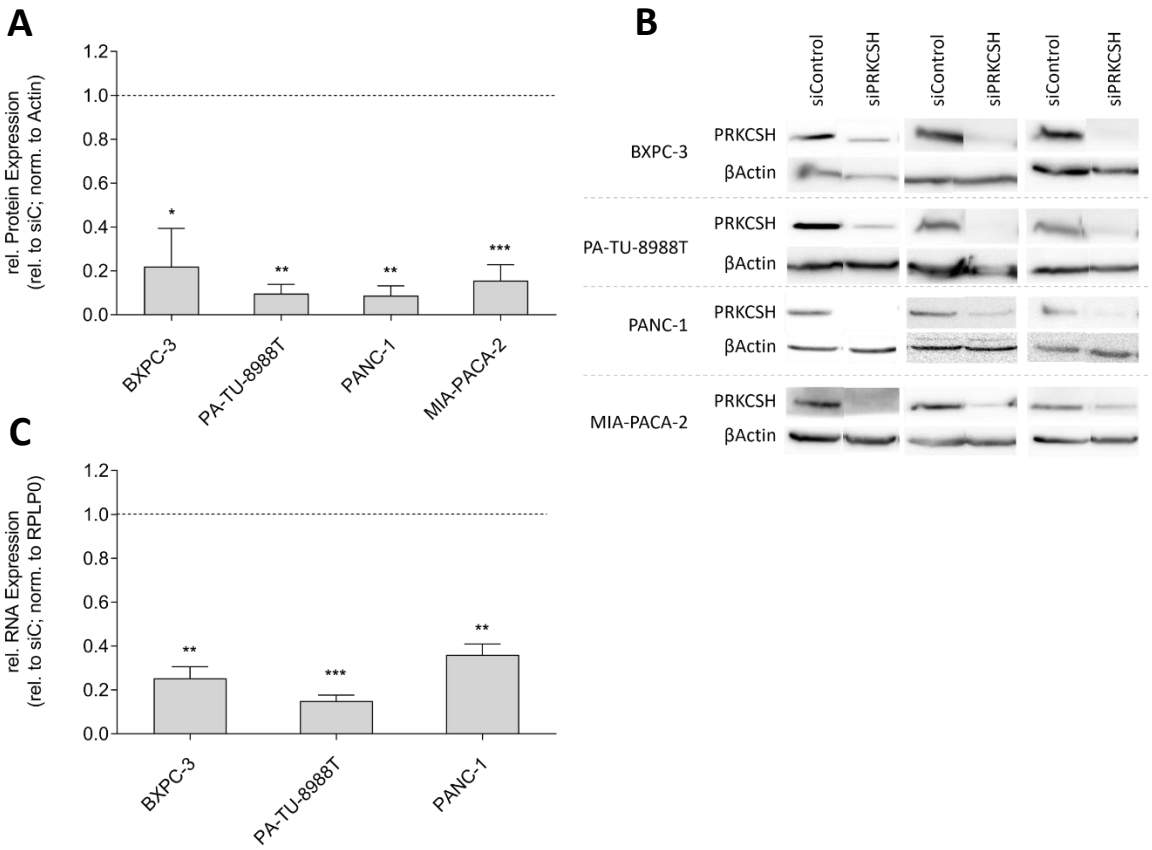

Figure 8: PRKCSH KD Efficiency on Protein and RNA Expression PDAC Cell Lines

*(A) Quantification of relative PRKCSH protein expression after PRKCSH KD. Dotted line indicates siControl. β-Actin was used as loading control. (B) Western blot analysis of PRKCSH after PRKCSH KD. β-Actin was used as loading control. (C) Quantification of relative PRKCSH RNA expression after PRKCSH KD. Dotted line indicates siControl. RPLP0 was used as housekeeping gene. (n = 3; *P < 0.05, **P < 0.01, ***P < 0.001; unpaired t-test)*

PRKCSH KD experiments were performed in the PDAC cell lines BXPC-3 and PA-TU-8988T to assess the effects on proliferation and viability (Figure 9). CML as a model AGE was used as a putative ligand for PRKCSH to demonstrate potential effects of activated AGE receptors. A cell growth assay over 72 hours showed a PRKCSH KD dependent reduction in proliferation in the BXPC-3 cell line of 24 % (P = 0.0163, Figure 9 A-B), but not in PA-TU-8988T, PANC-1 and MIA-PACA-2. Furthermore, detection of the cellular ATP-level indicated a reduced viability of 30 % in BXPC-3 cell line after PRKCSH KD (P = 0.0012,

Figure 9 C-D), but not in PA-TU-8988T, PANC-1 and MIA-PACA-2. Treatment with 250 µM CML had no effect on proliferation or ATP levels (Figure 9 B, D).

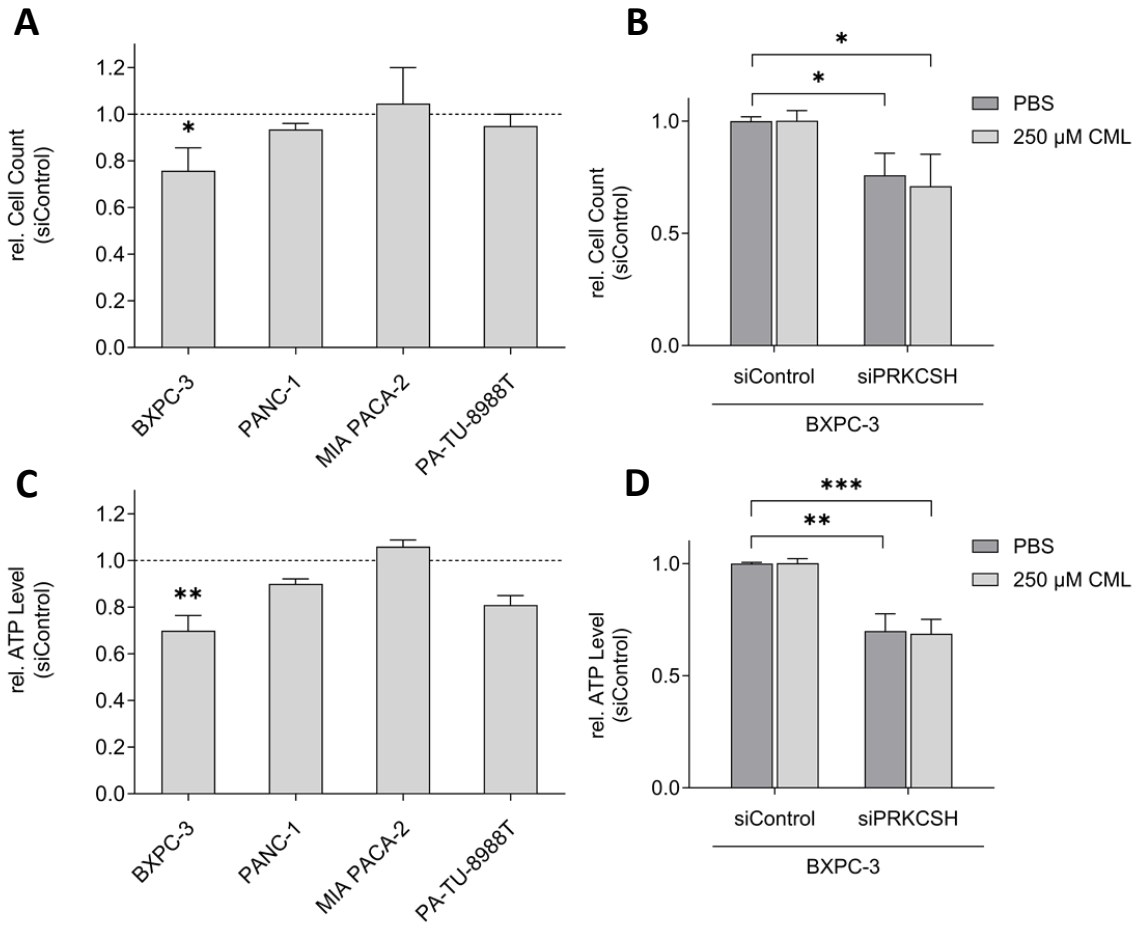

Figure 9: Proliferation and Viability after PRKCSH KD PDAC Cell Lines

*(A) Quantification of proliferation assay 72 hours after PRKCSH KD in different PDAC cell lines. (B) Quantification of proliferation assay 72 hours after PRKCSH KD and CML treatment in BXPC-3 cell line. (C) Quantification of viability assay 72 hours after PRKCSH KD in different PDAC cell lines. (D) Quantification of viability assay 72 hours after PRKCSH KD and CML treatment in BXPC-3 cell line. (n = 3; *P < 0.05, **P < 0.01, ***P < 0.001; unpaired t-test)*

2.2.5 PRKCSH KD has no Effect on Cell Cycle

Based on the potential cell cycle arrest in lung cancer cells caused by PRKCSH deficiency (Lei et al., 2022), the influence of PRKCSH KD on the cell cycle distribution of BXPC-3 and PA-TU-8988T cell lines was investigated. Therefore, flow cytometric analyses were performed on permeabilized and PI-stained cells. Representative flow histograms

depicting the cell cycle distribution of BXPC-3 and PA-TU-8988T cell lines 48 hours after PRKCSH KD are provided in Figure S 5. The quantified results indicated that PRKCSH KD did not cause cell cycle arrest in either the G0/G1 or G2/M phase for both cell lines compared to non-targeting control siRNA (Figure 10 A-D).

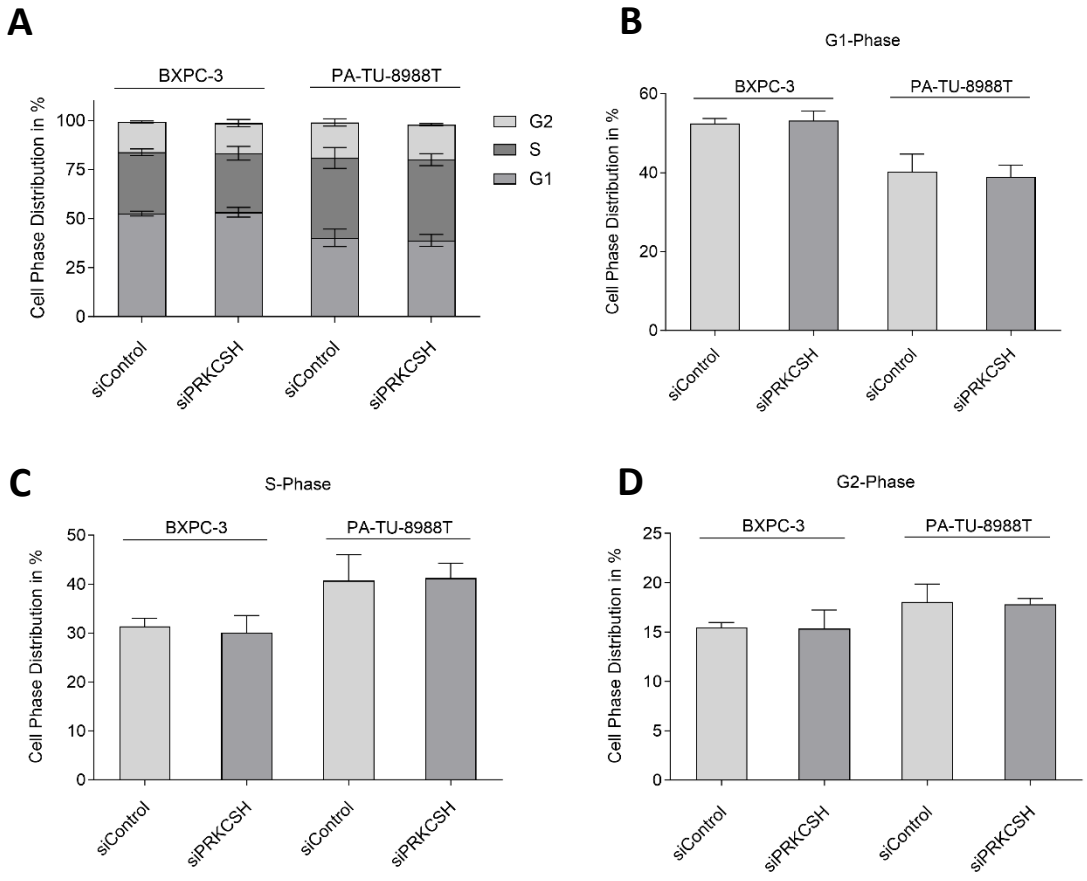

Figure 10: Cell Cycle after PRKCSH KD PDAC Cell Lines

(A) Quantification of cell cycle assay 48 hours after PRKCSH KD in different PDAC cell lines. (B) Quantification of G1 phase 48 hours after PRKCSH KD. (C) Quantification of S phase 48 hours after PRKCSH KD. (D) Quantification of G2 phase 48 hours after PRKCSH KD. (n = 3; unpaired t-test)

2.2.6 Expression of Gal-3 in Human PDAC Tissue

To determine the status of *Gal-3* expression and whether it is altered in PAAD tissues compared to normal tissues, the GEPIA2 online tool was used to obtain RNA expression levels based on TCGA and GTEx data. 179 samples from tumors were compared to 171

samples from normal controls (Figure 11). A distinct expression status was shown for both groups. The RNA expression (log2(TPM+1)) of tumor samples showed a significant increase compared to normal tissue.

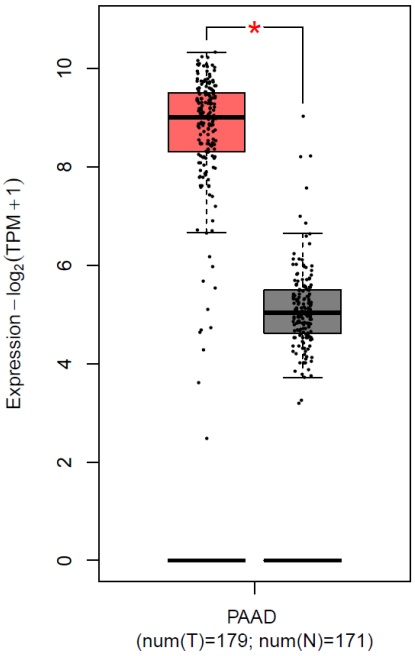

Figure 11: Gal-3 Expression Levels in Tumor and Normal PAAD Tissue

*Gal-3 RNA expression levels based on TCGA and GTEx data using GEPIA2. (Tumor in red: n = 179; normal in grey: n = 171; *P < 0.01)*

2.2.7 Gal-3 KD Reduces Proliferation and Viability in BXPC-3 Cell Line

In several PDAC tumor cell lines, ranging from PA-TU-8988T and BXPC-3, to PANC-1 and MIA-PACA-2 (Figure 12 A-C), Gal-3 protein and RNA expression was consistently found by western blot and qRT-PCR analysis. BXPC-3, PA-TU-8988T, PANC-1 and MIA-PACA-2 cell lines were each transiently transfected with a homolog-specific siRNA pool to KD Gal-3 expression. KD efficiency was analyzed by both, qRT-PCR and western blot analysis. Gal-3 RNA and protein expression was significantly reduced in all cell lines compared to non-targeting control siRNA (Figure 12 A-C).

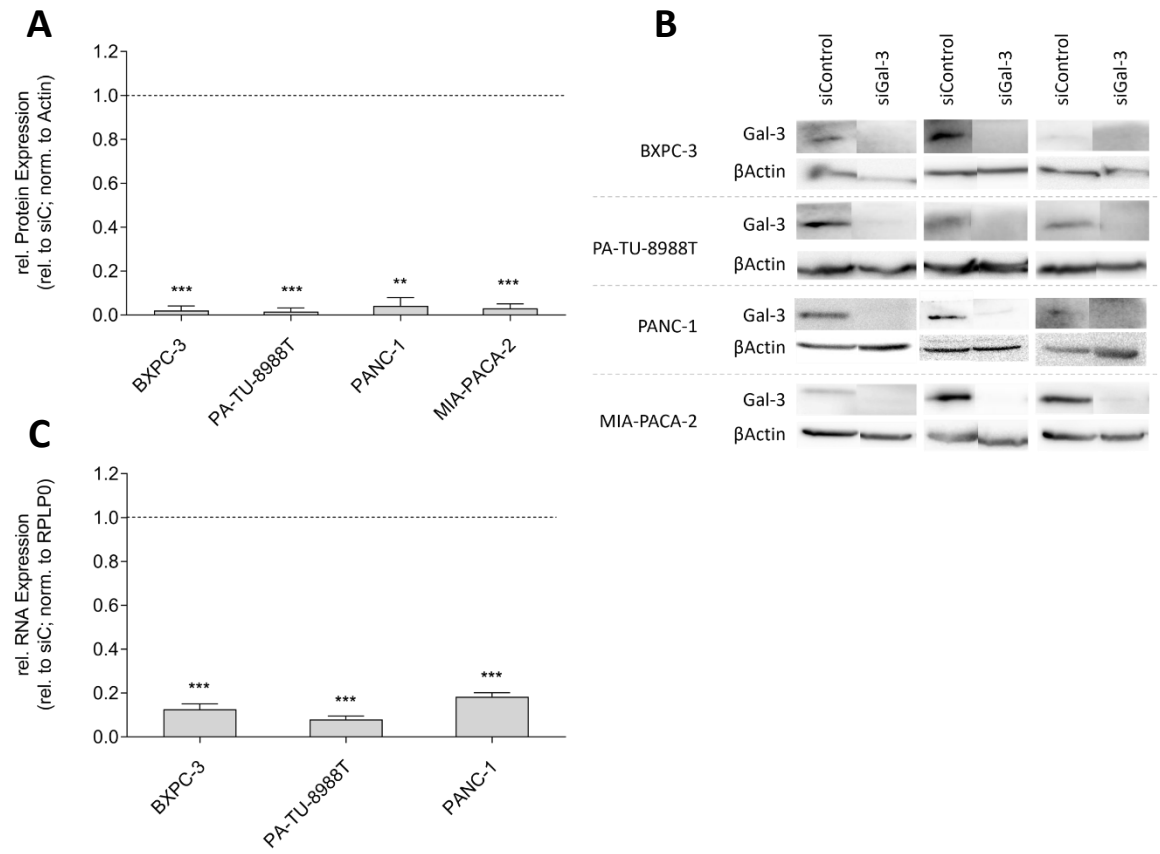

Figure 12: Gal-3 KD Efficiency on Protein and RNA Expression PDAC Cell Lines

*(A) Quantification of relative Gal-3 protein expression after Gal-3 KD. Dotted line indicates siControl. β-Actin was used as loading control. (B) Western blot analysis of Gal-3 after Gal-3 KD. β-Actin was used as loading control. (C) Quantification of relative Gal-3 RNA expression after Gal-3 KD. Dotted line indicates siControl. RPLP0 was used as housekeeping gene. (n = 3; *P < 0.05, **P < 0.01, ***P < 0.001; unpaired t-test)*

Gal-3 KD experiments were performed in the PDAC cell lines BXPC-3 and PA-TU-8988T to assess the effects on proliferation and viability (Figure 13). CML as a model AGE was used as a putative ligand for Gal-3 to demonstrate potential effects of activated AGE receptors. A cell growth assay over 72 hours showed a Gal-3 KD dependent reduction in proliferation in the BXPC-3 cell line of 21 % ($P = 0.0018$, Figure 13 A-B), but not in PA-TU-8988T, PANC-1 and MIA-PACA-2. Furthermore, detection of the cellular ATP-level indicated a reduced viability of 15 % in BXPC-3 ($P = 0.016$, Figure 13 C-D) and 13 % in PA-TU-8988T ($P = 0.013$, Figure 13 C) cell lines after Gal-3 KD, but not in PANC-1 and MIA-PACA-2. Treatment with 250 µM CML had no effect on proliferation or ATP levels (Figure 21 B, D).

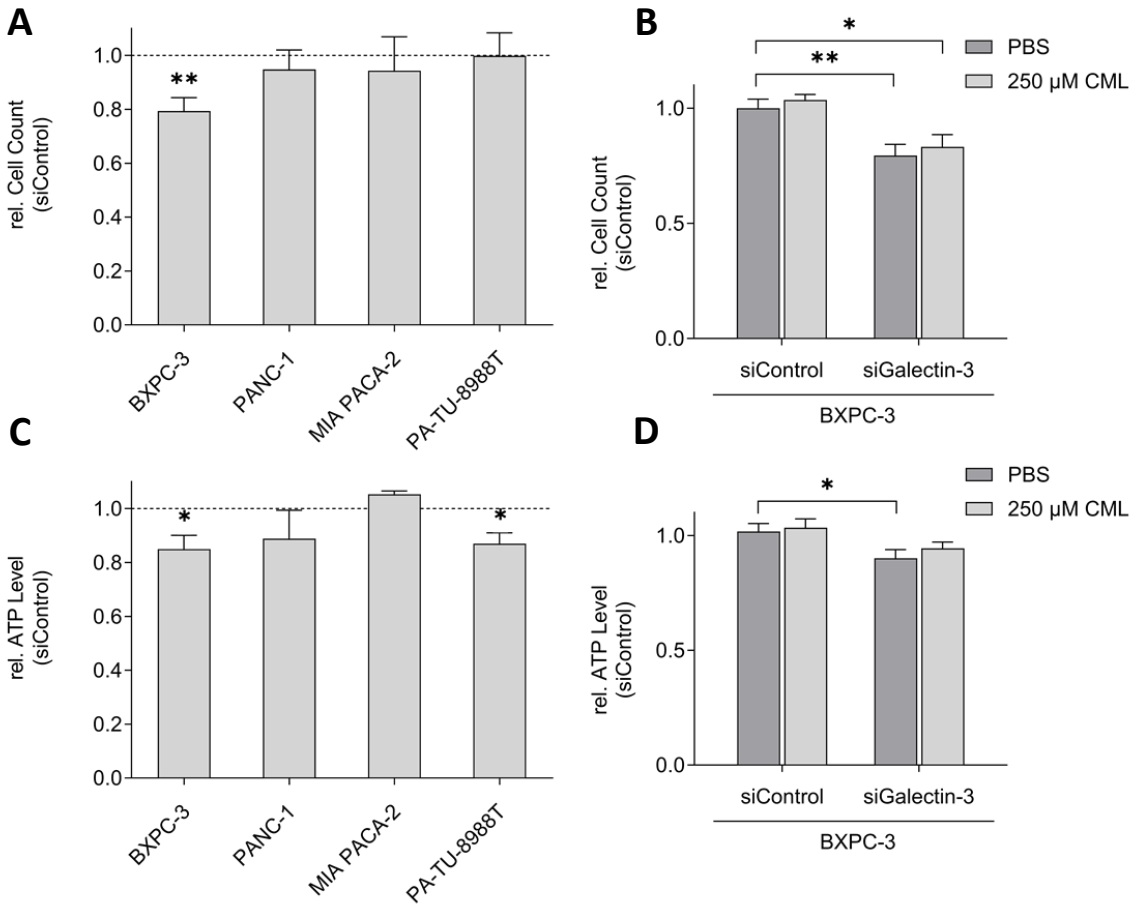

Figure 13: Proliferation and Viability after Gal-3 KD PDAC Cell Lines

*(A) Quantification of proliferation assay 72 hours after Gal-3 KD in different PDAC cell lines. (B) Quantification of proliferation assay 72 hours after Gal-3 KD and CML treatment in BXPC-3 cell line. (C) Quantification of viability assay 72 hours after Gal-3 KD in different PDAC cell lines. (D) Quantification of viability assay 72 hours after Gal-3 KD and CML treatment in BXPC-3 cell line. (n = 3; *P < 0.05, **P < 0.01, ***P < 0.001; unpaired t-test)*

2.2.8 Gal-3 KD Inhibits Cell-Migration in PA-TU-8988T Cell Line

Based on previous studies in which Gal-3 was shown to mediate cell migration in various cancers (Al Kafri & Hafizi, 2020; K.-L. Wu et al., 2018; Zheng et al., 2017), the influence of Gal-3 KD on cell migration of the PA-TU-8988T cell line was investigated. Prepared 12-well plates with attached silicone culture inserts were effective in creating a cell-free gap area of 500 µm in the center of the wells for a confluent monolayer of the PA-TU-8988T cell line. To investigate the influence of Gal-3 KD on the cell migration capacity, cells were photographed at 0 hours and 24 hours after wounding. Representative

images depicting the gap-closure of the PA-TU-8988T cell line 24 hours after wounding are provided in Figure 14 B and Figure S 6. The quantified results show that Gal-3 KD inhibits the cell migration capacity by 55 % compared to non-targeting control siRNA ($P < 0.0001$; Figure 14 A).

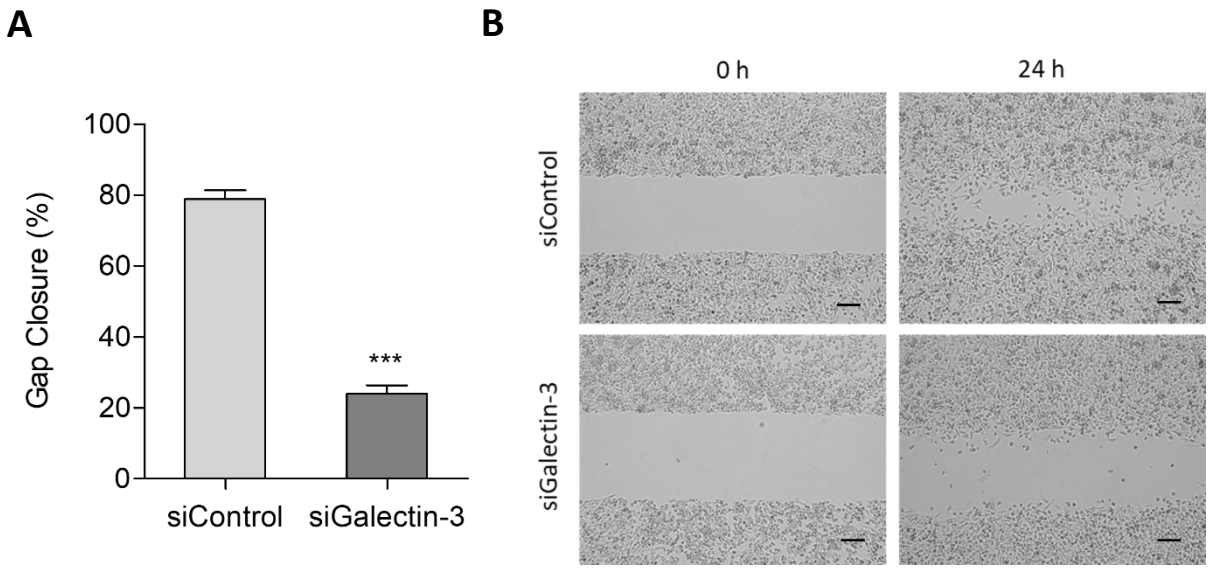

Figure 14: Migration after Gal-3 KD in PA-TU-8988T Cell Line

*(A) Quantification of wound healing assay 72 hours after Gal-3 KD in PA-TU-8988T cell line. (B) Wound healing assay 72 hours after Gal-3 KD in PA-TU-8988T cell line. (n = 3; ***P < 0.001; unpaired t-test; scale bar, 200 µm)*

2.2.9 Expression of DDOST in Human PDAC Tissue

A quantitative proteomic map comparing 32 organs revealed that in healthy human body donors, DDOST is tissue-specifically enriched in the pancreas and stomach (L. Jiang et al., 2020). Furthermore, DDOST is expressed at a significantly higher level in the pancreas than in any of the other organs compared (Figure 15).

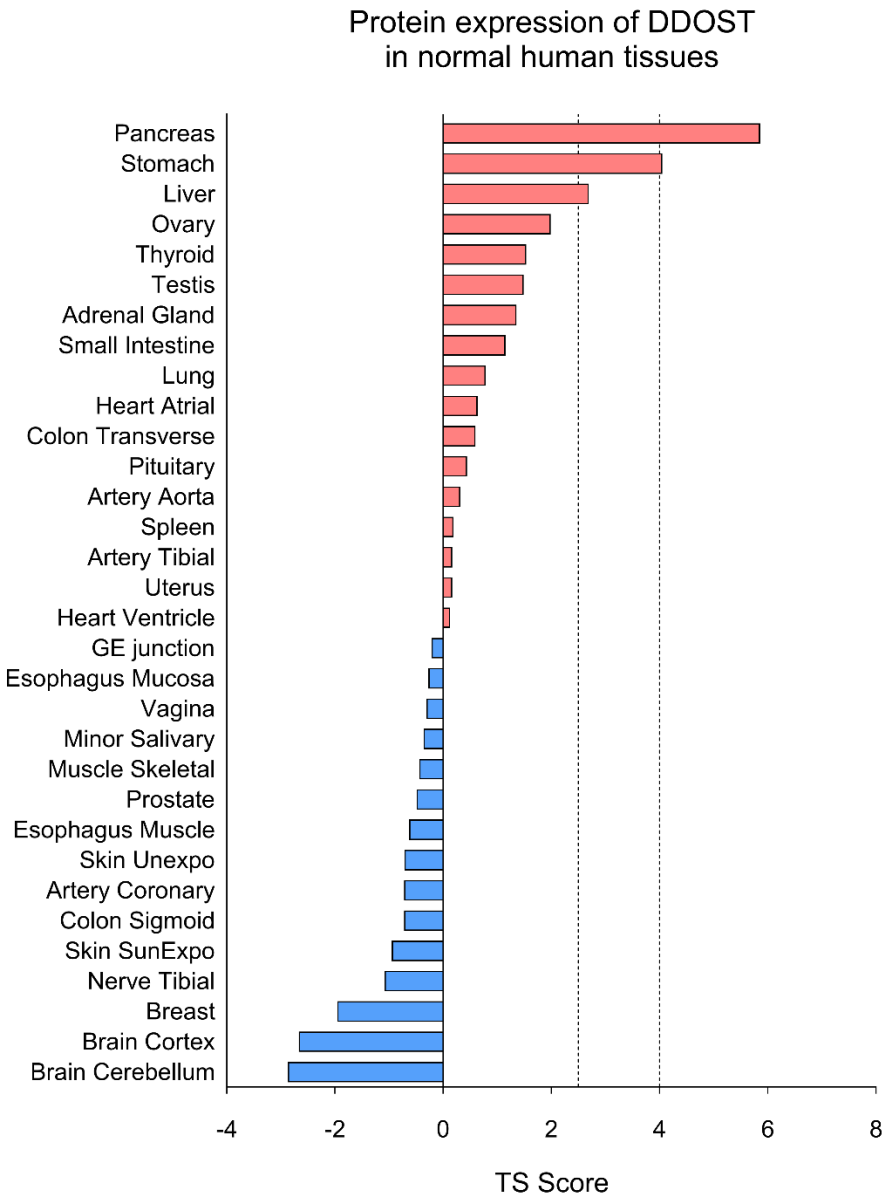

Figure 15: Tissue Specificity Scores of DDOST

DDOST protein expression in human body donors. If a gene has TS (tissue specificity) scores at least in one tissue ≥ 2.5, this gene is called tissue-enriched. Vertical lines indicate the threshold values of 2.5 and 4. Adapted from "A Quantitative Proteome Map of the Human Body" by Jiang et al., 2020.

To determine the status of *DDOST* expression and whether it is altered in PAAD tissues compared to normal tissues, the GEPIA2 online tool was used to obtain RNA expression levels based on TCGA and GTEx data. 179 samples from tumors were compared to 171 samples from controls (Figure 16). A distinct expression status was shown for both groups. However, RNA expression (log2(TPM+1)) showed no significant differences between tumor and normal tissues.

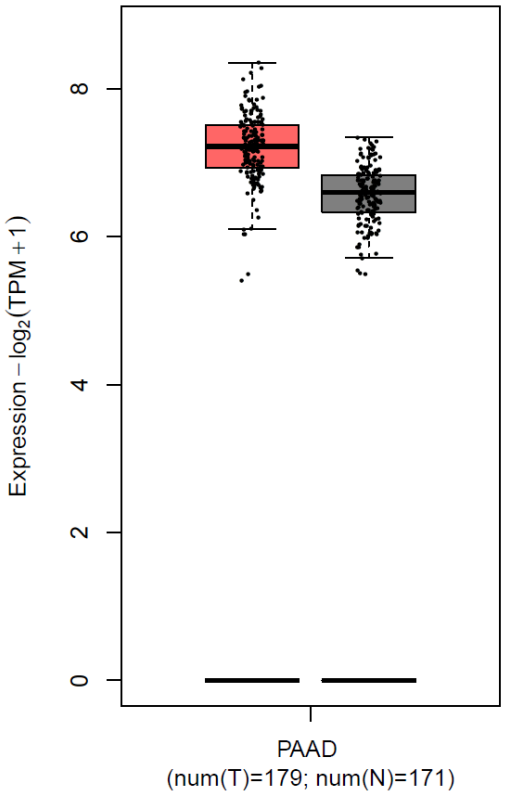

Figure 16: DDOST Expression Levels in Tumor and Normal PAAD Tissue

DDOST RNA expression levels based on TCGA and GTEx data using GEPIA2. (Tumor in red: n = 179; normal in grey: n = 171)

In resected human PDAC tissue, H&E staining revealed high-grade PanIN lesions and ADM (Figure 17 A, C). DDOST protein expression in PDAC tissues was visualized by DDOST antibody staining and IHC using a peroxidase assay. Here, DDOST was shown to be expressed in ductal-like structure of ADM (arrows, Figure 17 D) and uncharacterized immune cells (arrows, Figure 17 B), but less expressed in PanIN lesions (stars, Figure 17 B) and invasive ductal carcinoma (Figure 17; Figure S 8).

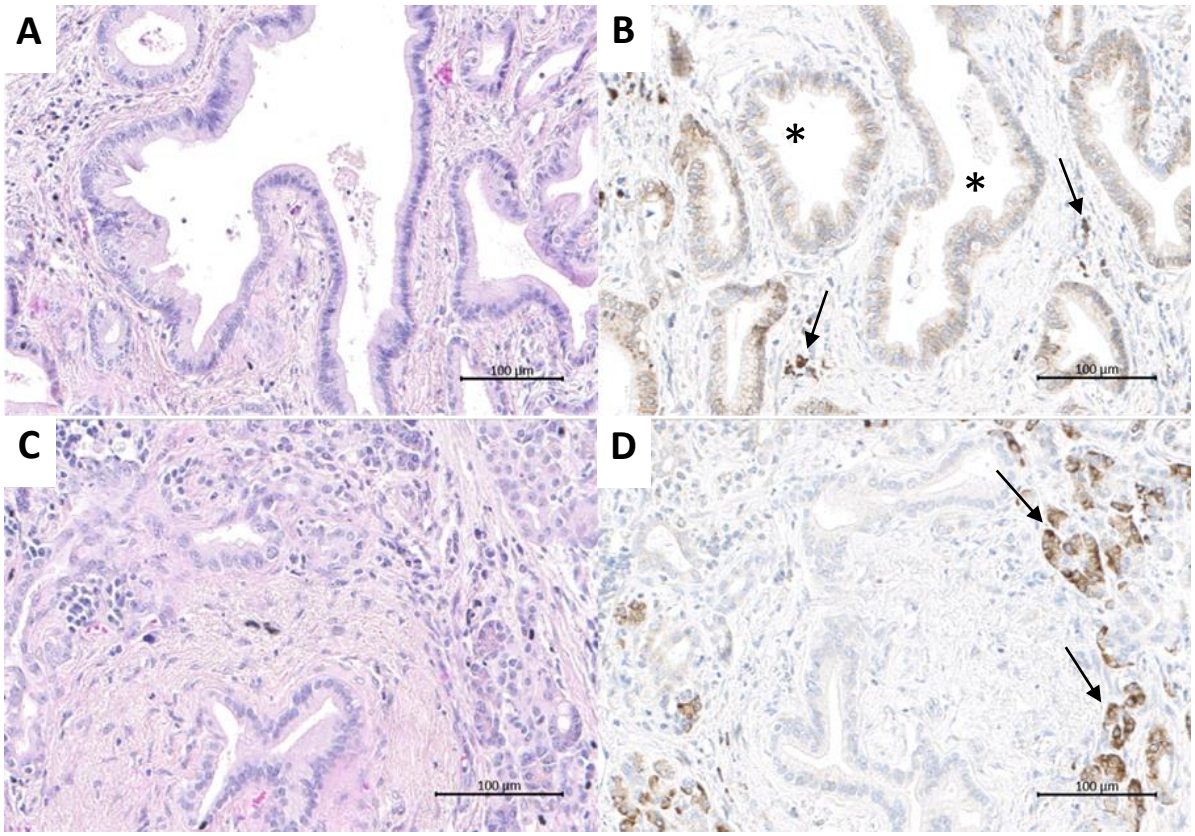

Figure 17: H&E and IHC Staining of DDOST in Human PDAC Tissue

(A, C) Representative H&E staining of PDAC patient tissue. (B, D) Representative IHC staining for DDOST expression. Arrows and stars indicate representative DDOST-positive compartments. (Scale bar, 100 µm)

2.2.10 DDOST KD Reduces Proliferation and Viability in PDAC Cell Lines

In several PDAC tumor cell lines, ranging from PA-TU-8988T and BXPC-3, to PANC-1 and MIA-PACA-2 (Figure 18 A-C), consistent DDOST protein and RNA expression was found by western blot and qRT-PCR analysis. BXPC-3, PA-TU-8988T, PANC-1 and MIA-PACA-2 cell lines were each transiently transfected with a homolog-specific pool of siRNAs to KD DDOST expression. KD efficiency was analyzed by both, qRT-PCR and western blot analysis. DDOST RNA and protein expression was significantly reduced in all cell lines compared to non-targeting control siRNA (Figure 18 A-C).

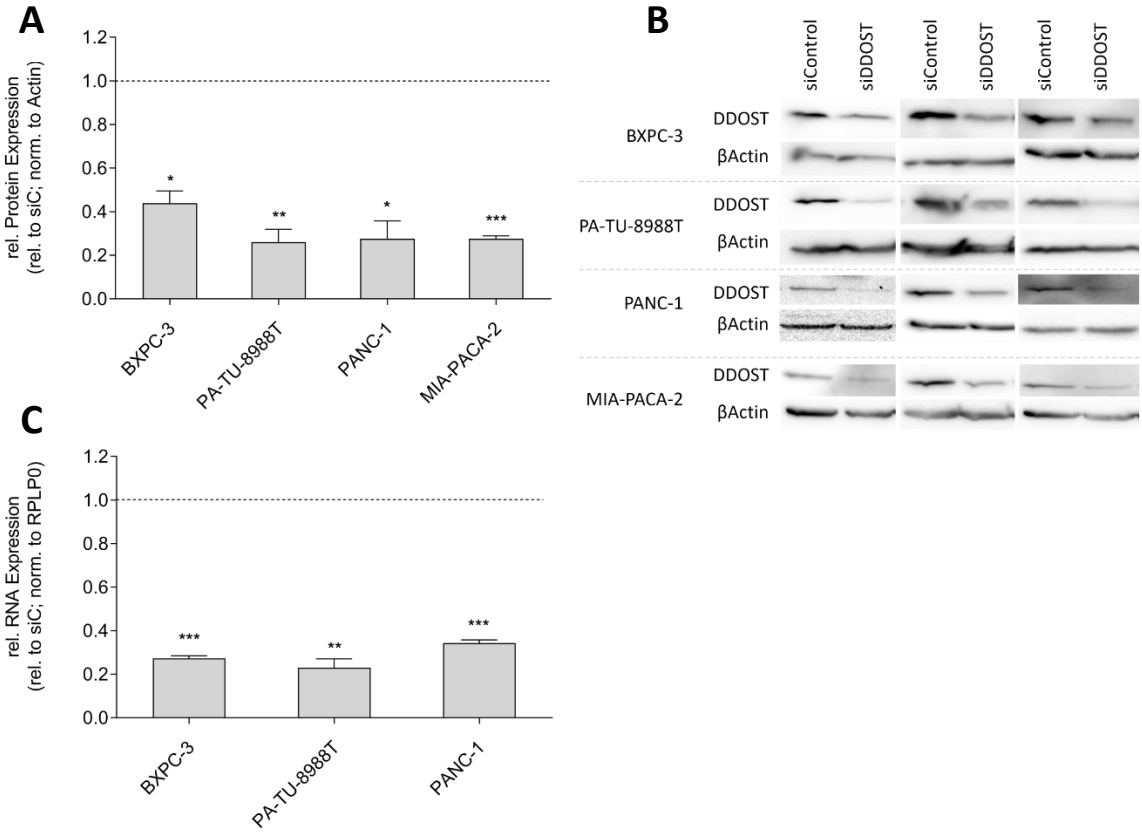

Figure 18: DDOST KD Efficiency on Protein and RNA Expression PDAC Cell Lines

*(A) Quantification of relative DDOST protein expression after DDOST KD. Dotted line indicates siControl. β-Actin was used as loading control. (B) Western blot analysis of DDOST after DDOST KD. β-Actin was used as loading control. (C) Quantification of relative DDOST RNA expression after DDOST KD. Dotted line indicates siControl. RPLP0 was used as housekeeping gene. (n = 3; *P < 0.05, **P < 0.01, ***P < 0.001; unpaired t-test)*

We performed DDOST KD experiments in the PDAC cell lines BXPC-3 and PA-TU-8988T to assess the effects on cell growth and viability. Nε-(1-Carboxymethyl)-L-lysine (CML) as a model AGE was used as a putative ligand for DDOST to demonstrate potential effects of activated AGE receptors. In addition, tunicamycin (TM), an inhibitor of *N*-linked oligosaccharide biosynthesis, was used as a positive control in some experiments to estimate potential effect maxima. A cell growth assay over 72 hours showed a DDOST KD dependent reduction in proliferation in both cell lines, BXPC-3 and PA-TU-8988T, ranging from 20 - 22 % (P = 0.0313 and P = 0.0357, respectively, Figure 19 A-D). Furthermore, detection of the cellular ATP-level indicated a reduced viability of 19 - 22 % in both cell lines after DDOST KD (P = 0.0483 and P = 0.0249, Figure 19 E-F). Treatment

with 250 µM CML had no effect on proliferation or ATP levels (Figure 19 C, E). In contrast, treatment of siControl cells with 1 µM TM as a positive control for OST complex inhibition, led to a decrease in proliferation, ranging from 31 - 71 % (P = 0.0334 and P = 0.0003, respectively, Figure 19 D) and decreased ATP-levels of 37 - 70 % (P = 0.0293 and P < 0.0001, respectively, Figure 19 F). Moreover, treatment of siDDOST cells with 1 µM TM for 24 hours after KD resulted in a 46 - 60 % decrease in cell growth (P = 0.0061 and P = 0.0013, respectively, Figure 19 D) in both, BXPC-3 and PA-TU-8988T. Additionally, treatment of siDDOST cells with 1 µM TM led to 61 % decrease in ATP level in PA-TU-8988T (P = 0.023, respectively, Figure 19 F) but not in BXPC-3. Thus, KD of DDOST reduces proliferation and cell viability in both tested cell lines, which is also observed for the OST complex inhibitor TM.

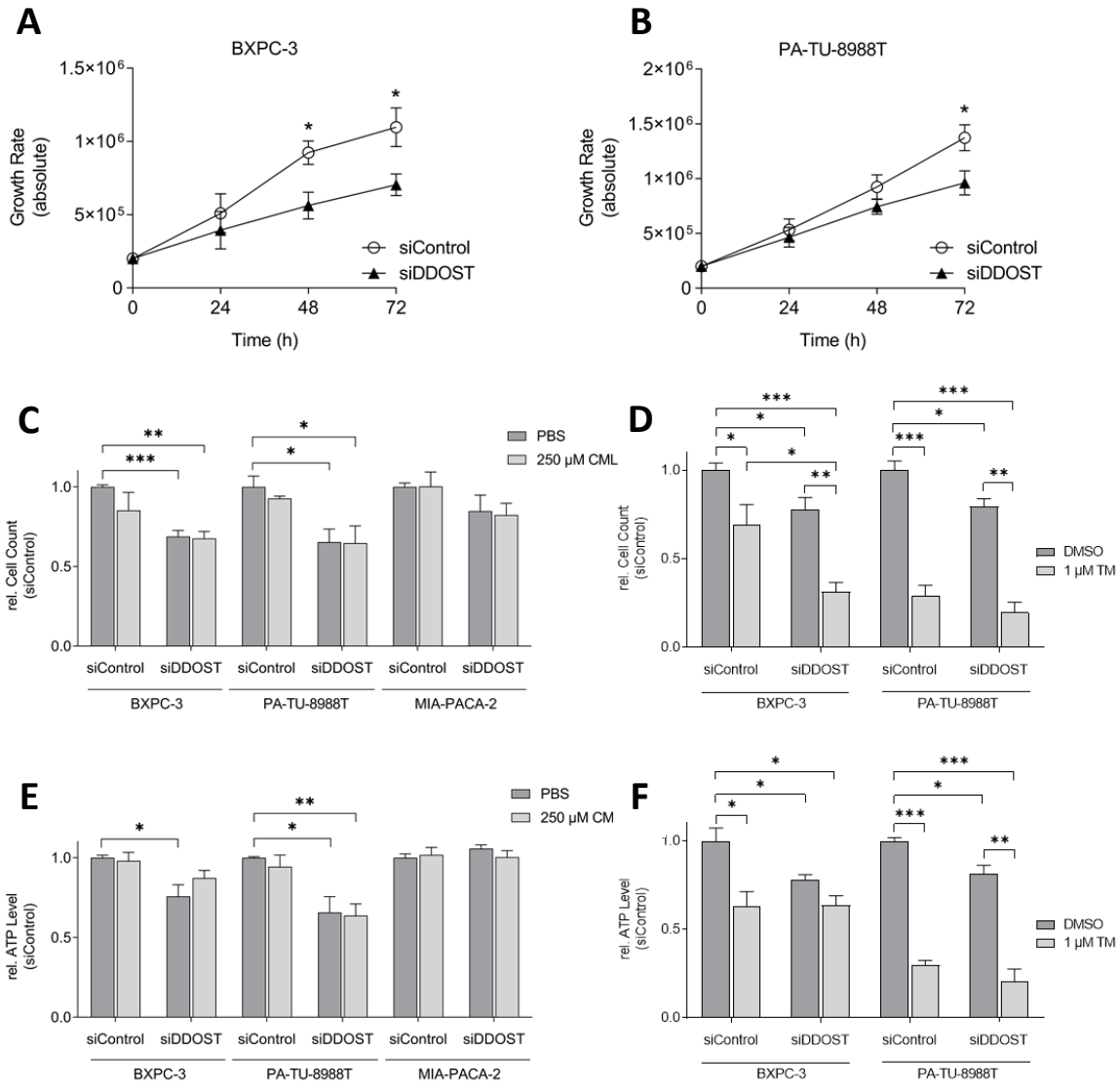

Figure 19: Proliferation and Viability after DDOST KD PDAC Cell Lines

*(A) Growth curve of BXPC-3 cell line after DDOST KD. (B) Growth curve of PA-TU-8988T cell line after DDOST KD. (C) Quantification of proliferation assay 72 hours after DDOST KD and CML treatment. (D) Quantification of proliferation assay 72 hours after DDOST KD and TM treatment. (E) Quantification of viability assay 72 hours after DDOST KD and CML treatment. (F) Quantification of viability assay 72 hours after DDOST KD and TM treatment. (n = 3; *P < 0.05, **P < 0.01, ***P < 0.001; unpaired t-test)*

2.2.11 DDOST KD Induces ER-Stress in PDAC Cell Lines

To examine the effects of DDOST KD on ER-related cell stress, protein level of the ER stress regulator CHOP was detected using an immunofluorescence assay. In BXPC-3, CHOP level was 77 % increased and in PA-TU-8988T 19 % increased after 48 hours of DDOST KD (P = 0.0347, P = 0.0382, respectively, Figure 20). Treatment of siControl cells with 1 µM TM led to a 54 % increase of CHOP level in PA-TU-8988T (P = 0.0057, Figure 20) but not in BXPC-3. Additionally, treatment of siDDOST cells with 1 µM TM led to 34 % increased CHOP level in PA-TU-8988T (P = 0.03, Figure 20) but not in BXPC-3. The ER stress level was increased in both tested cell lines after DDOST KD or TM treatment.

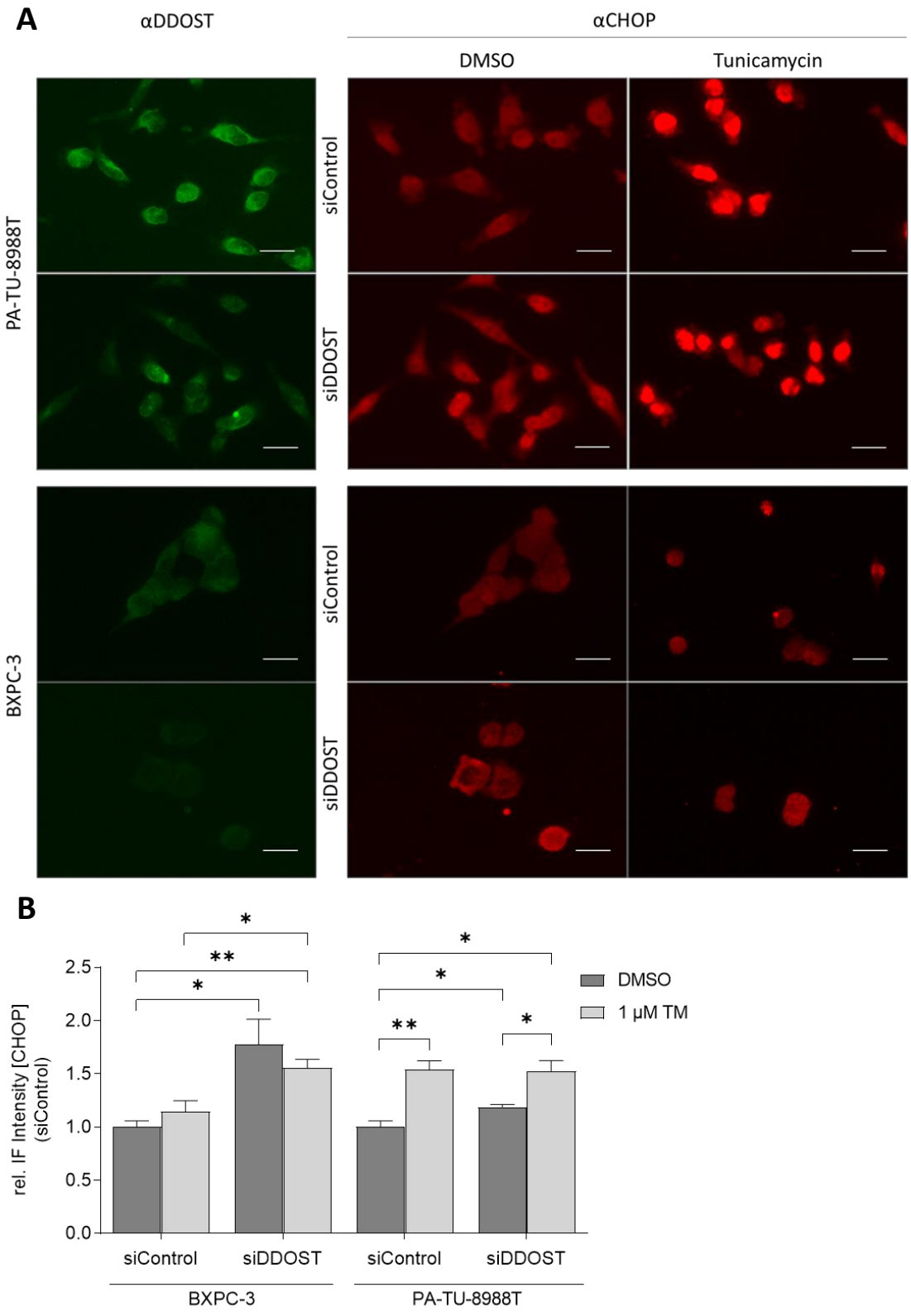

Figure 20: ER-Stress after DDOST KD PDAC Cell Lines

*(A) Immunofluorescence images of DDOST and CHOP after DDOST KD and treatment with TM (scale bar = 50 µm). (B) Quantification of CHOP relative IF intensity after DDOST KD and treatment with TM. (n = 3; *P < 0.05, **P < 0.01; unpaired t-test)*

2.2.12 DDOST KD Induces Oxidative Stress and Apoptosis in PDAC Cell Lines

ROS formation assay was performed to assess the potential effects of DDOST KD on oxidative stress levels in PDAC cell lines. Therefore, cells were incubated with H_2DCFDA, an indicator of intracellular ROS by its oxidated and fluorescent form. After cleavage of the acetate groups by intracellular esterases and oxidation, the non-fluorescent H_2DCFDA is converted to the highly fluorescent 2',7'-dichlorofluorescein (DCF). Fluorescence intensity was determined 48 hours post KD transfection using flow cytometry analysis. DCF intensity was increased 17 % in BXPC-3 and 23 % in PA-TU-8988T cell lines after DDOST KD (P = 0.041, P = 0.0145, respectively, Figure 21). Further, treatment of siControl cells with 1 µM TM led to 28 % increased DCF intensity in PA-TU-8988T (P = 0.0187, Figure 21 B), but not in BXPC-3 cell line. Thus, the oxidative stress level was increased after KD DDOST and partially after TM treatment.

To examine apoptotic effects of DDOST KD, PDAC cell lines were stained with Propidium Iodide (PI) and Annexin V to determine apoptotic activation using flow cytometry analysis 48 hours post transfection. PI is an indicator of cell death by intercalating with cellular DNA through the permeabilized cell membrane, while Annexin V detects the translocation of phosphatidylserine on the outside of apoptotic cells. PI and Annexin V level were significantly increased by 62 % in PA-TU-8988T but not significantly increased in BXPC-3 cell line after DDOST KD (P = 0.0141, P = 0.0546, respectively, Figure 22 A-B). Further, treatment of siControl cells with 1 µM TM led to 3-fold increased PI and Annexin V level in PA-TU-8988T cell line (P = 0.0002, Figure 22 B). To validate the activation of apoptosis, protein level of Caspase 3 and PARP-1 were detected using western blot analysis. Cleavage of PARP-1 was increased in both cell lines after DDOST KD, whereas increased cleavage of Caspase 3 was detected only in PA-TU-8988T cell line after DDOST KD. (Figure 22 C). Thus, apoptosis was increased after DDOST KD or TM treatment in PA-TU-8988T but not in BXPC-3 cell line.

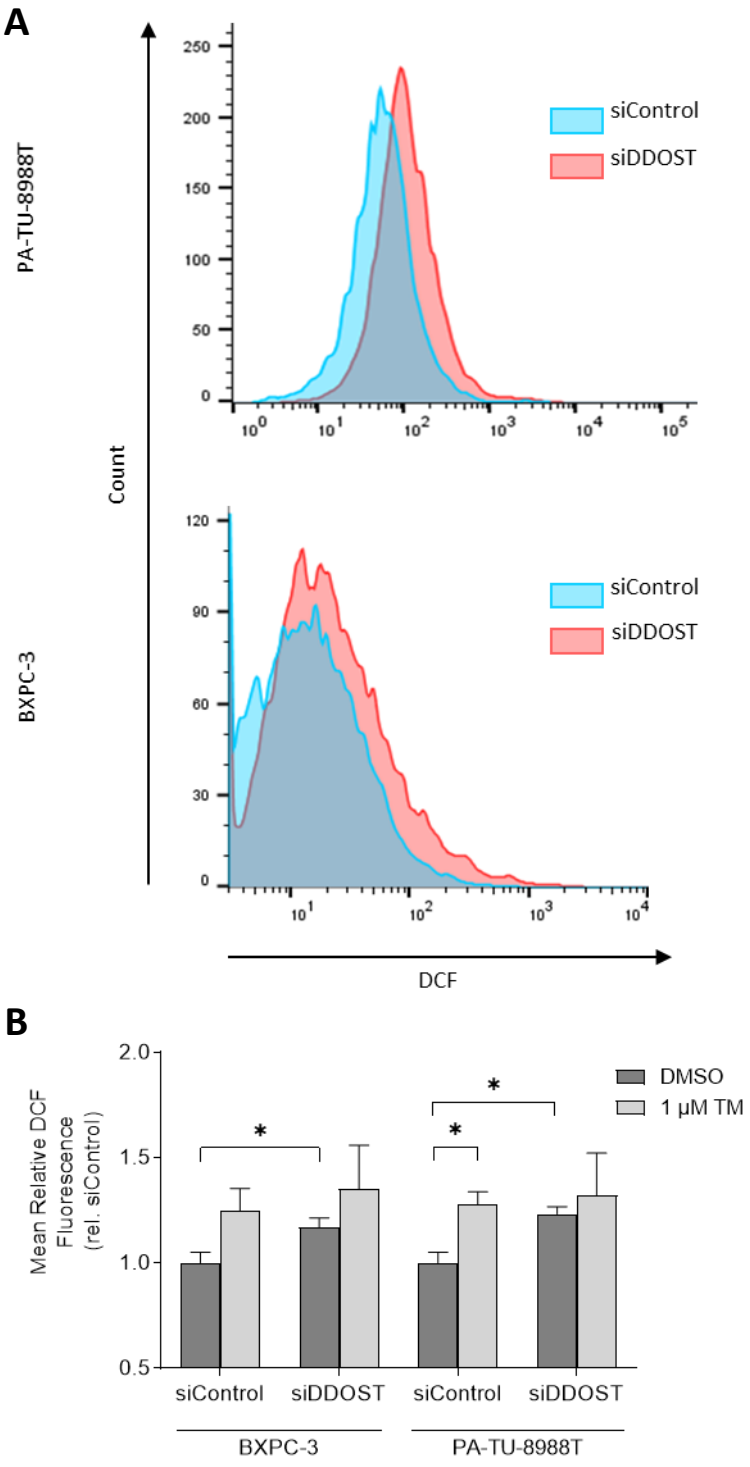

Figure 21: ROS Formation after DDOST KD in PDAC Cell Lines

*(A) Flow cytometry assay of ROS formation by DCF detection after DDOST KD. (B) Quantification of mean relative DCF intensity after DDOST KD and treatment with TM. (n = 3; *P < 0.05; unpaired t-test)*

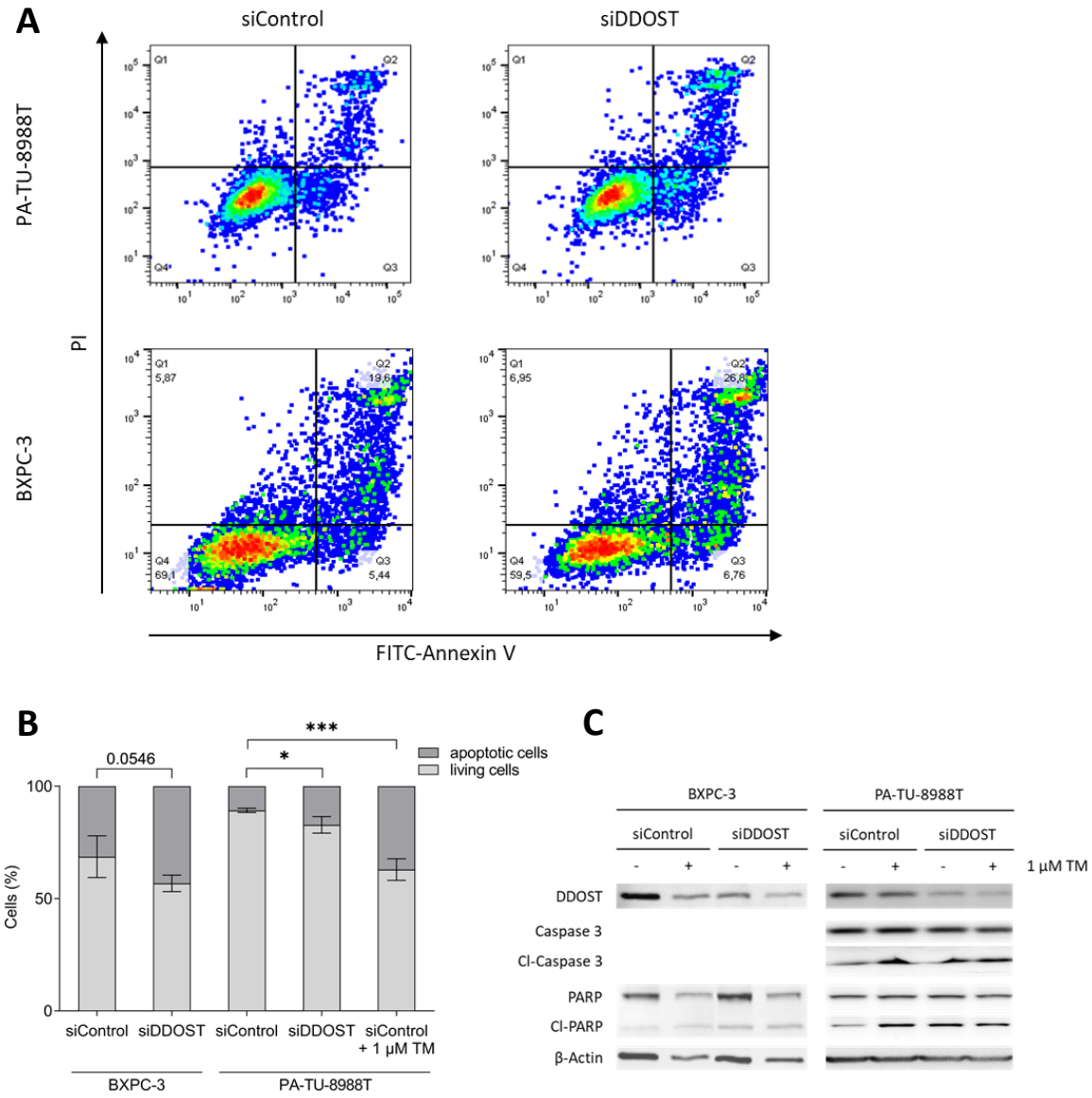

Figure 22: Apoptosis after DDOST KD in PDAC Cell Lines

*(A) Flow cytometry assay of FITC-Annexin V and PI staining after DDOST KD. (B) Quantification of FITC-Annexin V and PI positive cells after DDOST KD and treatment with TM. (C) Western blot analysis of PARP and Caspase 3 after DDOST KD. β-Actin was used as loading control. (n = 4; *P < 0.05, ***P < 0.001; unpaired t-test)*

2.2.13 Proteomic Analysis Reveals that DDOST KD Leads to Fold Change of 22 Proteins and 8 Phosphopeptides in PDAC Cell Lines

To unravel potential regulative effects on the proteome, including the phosphoproteome, DDOST KD experiments in PDAC cell lines were performed, followed by quantitative LC-MS/MS. BXPC-3 and PA-TU-8988T cell lines were each transiently transfected with a pool of homolog-specific siRNAs to KD DDOST expression.

To identify all proteins and phosphopeptides affected by DDOST KD in pancreatic cancer cell lines, a quantitative proteome analysis by TMT-labeling and LC-MS/MS, including an additional phosphopeptide enrichment step, after DDOST KD in PA-TU-8988T cell line was performed. In summary, 1,577 proteins and 2,059 phosphopeptides were identified (Table S 1; Table S 2). Interestingly, the expression levels of only eight proteins (NCEH1 (FDR = 0.05, log2-FC = 0.64), PPME1 (FDR = 0, log2-FC = 0.62), CHORDC1 (FDR = 0, log2-FC = 0.62), HMOX1 (FDR = 0, log2-FC = 0.62), HIBCH (FDR = 0, log2-FC = 0.60), SERBP1 (FDR = 0, log2-FC = 0.54), TFAM (FDR = 0, log2-FC = 0.47), IVD (FDR = 0.05, log2-FC = 0.45)) were significantly increased (FDR < 0.05, Figure 23 A-D). Otherwise, 14 proteins (YWHAZ (FDR = 0.05, log2-FC = -0.42), CAND1 (FDR = 0.05, log2-FC = -0.43), HPCAL1 (FDR = 0.05, log2-FC = -0.49), MAPK1 (FDR = 0, log2-FC = -0.49), MARCKS (FDR = 0.05, log2-FC = -0.51), SERPINH1 (FDR = 0, log2-FC = -0.54), EIF1AX (FDR = 0.05, log2-FC = -0.57), CALU (FDR = 0, log2-FC = -0.66), GRB2 (FDR = 0.05, log2-FC = -0.66), SLC3A2 (FDR = 0, log2-FC = -0.68), TPM4 (FDR = 0, log2-FC = -0.78), RPN2 (FDR = 0, log2-FC = -0.81), DDOST (FDR = 0, log2-FC = -1.36), SLC7A5 (FDR = 0, log2-FC = -2.14)) and eight phosphopeptides (AKAP12$^{[S696;\ S698]}$ (FDR = 0, log2-FC = -0.58), (AKAP12$^{[S697;\ S698]}$ (FDR = 0, log2-FC = -0.65), STT3B$^{[S498]}$ (FDR = 0, log2-FC = -0.66), AKAP12$^{[S696;\ S697;\ S698]}$ (FDR = 0, log2-FC = -0.70), STT3B$^{[S498;\ S499]}$ (FDR = 0, log2-FC = -0.81), ASAP1 (FDR = 0, log2-FC = -0.85), GYS1 (FDR = 0, log2-FC = -1.18), SERBP1 (FDR = 0, log2-FC = -1.2)) were significantly decreased (FDR < 0.05, Figure 23 A-D). In addition to DDOST, two of the downregulated proteins, RPN2 and STT3B, are subunits of the OST complex proteins.

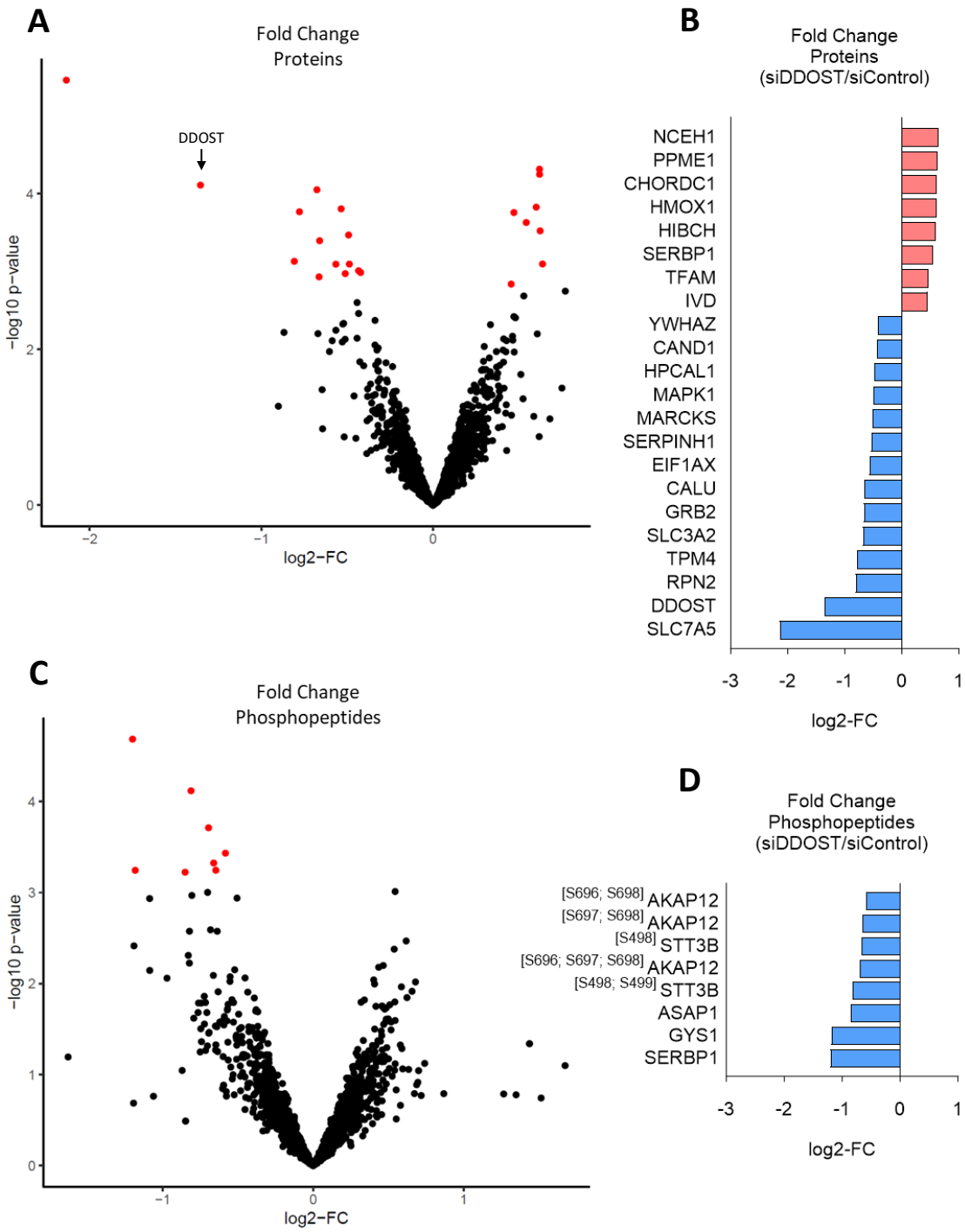

Figure 23: Fold Change of Proteins and Phosphopeptides after DDOST KD in PA-TU-8988T

(A, C) Volcano plot of protein and phosphopeptide log2-FC. Highlighted proteins and phosphopeptides cutoff FDR < 0.05 (n = 5; ROTS-test). Arrow indicates DDOST. (B, D) Bar chart of protein and phosphopeptide log2-FC. Upregulated proteins and phosphopeptides in red, downregulated in blue.

2.2.14 Spearman Correlation Matrix, GO Annotation and Protein-Protein Interaction Analysis Provides Information on Correlations Between DEPs in Public Domain Databases

Based on 179 PAAD tumor tissue samples, a spearman correlation matrix was implemented to analyze the correlation of mRNA expression levels (normalized to *RPLP0*) between all pairs of identified DEPs (Figure 24). Each row and column represents one DEP, independent of their phosphosites, and the value in each cell represents the spearman correlation coefficient (ρ) between the corresponding pair of DEPs. Across all 338 corresponding pairs of identified DEPs, 58 strong correlations ($\rho \geq 0.7$, $P < 0.0001$) and 226 medium correlations ($\rho \geq 0.4$, $P < 0.0001$) were detected (Table S 3). *DDOST* had strong correlations with *RPN2* ($\rho = 0.77$, $P < 0.0001$), *SERBP1* ($\rho = 0.76$, $P < 0.0001$), *CALU* ($\rho = 0.72$, $P < 0.0001$), *STT3B* ($\rho = 0.72$, $P < 0.0001$). Additionally, 20 medium correlations ($\rho \geq 0.4$, $P < 0.0001$) and 1 weak correlation ($\rho \geq 0.1$, $P < 0.0001$) were detected for *DDOST* (Table S 3). The 10 strongest correlations across all DEPs are *MAPK1* with *CAND1* ($\rho \geq 0.89$, $P < 0.0001$), *TFAM* ($\rho \geq 0.87$, $P < 0.0001$), *STT3B* ($\rho \geq 0.85$, $P < 0.0001$), *CAND1* with *TFAM* ($\rho \geq 0.86$, $P < 0.0001$), *STT3B* ($\rho \geq 0.84$, $P < 0.0001$), *ASAP* ($\rho \geq 0.81$, $P < 0.0001$), *STT3B* with *TFAM* ($\rho \geq 0.83$, $P < 0.0001$), *SERBP1* ($\rho \geq 0.82$, $P < 0.0001$) and *CALU* with *TPM4* ($\rho \geq 0.83$, $P < 0.0001$) and *ASAP1* ($\rho \geq 0.8$, $P < 0.0001$) (Table S 3).

To determine the biological processes in which the identified DEPs may participate, the functional enrichment was analyzed for the co-expressed DEPs, using the Gene Ontology (GO) database (Ashburner et al., 2000; The Gene Ontology Consortium et al., 2021). Two functional complexes were found to be enriched (GO – cellular components), including five of the identified DEPs, the OST complex (FDR = 0.0028; included DEPs: RPN2, STT3B, DDOST) and the amino acid transport complex (FDR = 0.0102; included DEPs: SLC7A5, SLC3A2) (Table 6). Assessing the occurrence of all individual DEPs/nodes in 2,120 individual GO annotations, numerous biological processes related to carcinogenesis, such as oxidative stress, proteostasis, apoptosis, cell cycle, and protein glycosylation were found (Table S 4, highlighted in red), suggesting an impact of the deregulated OST complex by DDOST KD on typical phenotypes, that are common for tumor development.

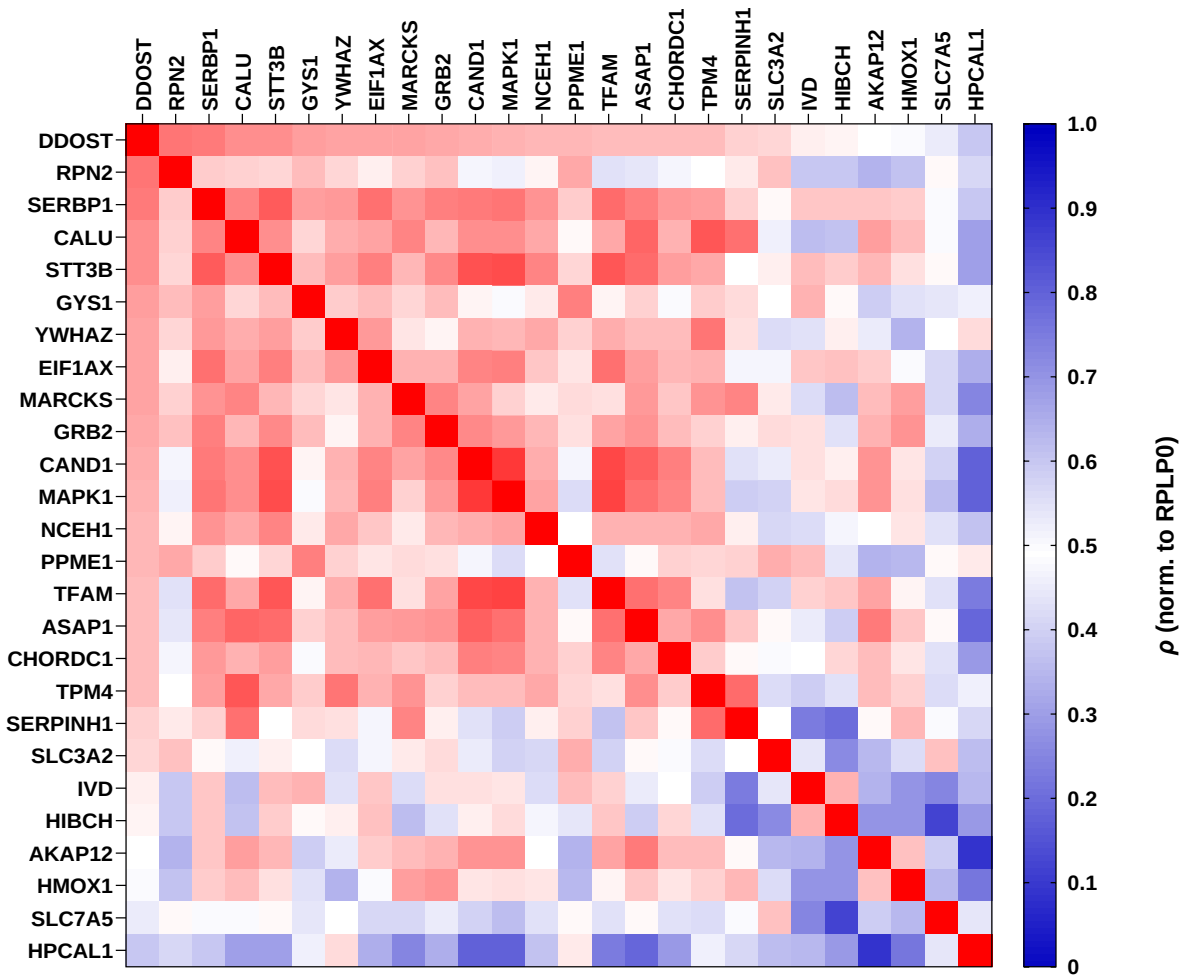

Figure 24: Spearman Correlation Matrix of Identified DEPs

Matrix is computed from Spearman correlation analysis between 26 identified DEPs, colored according to magnitude. Red colors indicate strong positive correlations, blue indicates no empirical relationship between the variables. (All correlations with $\rho \geq 0.4$: $P < 0.0001$; unpaired t-test; normalized to RPLP0; n = 179)

A functional network of differentially expressed proteins and phosphopeptides (DEPs) was constructed from the STRING database to evaluate known and potential protein-protein-interactions (PPI). The resulting PPI network consisted of 26 nodes and 67 edges, with each node representing all splice isoforms or post-translational modifications of each analyzed DEP and each edge representing all predicted or functional associations (PPI enrichment $P = 0.0003$, Figure 25).

Table 6: Functional Enrichment Analysis of co-Expressed DEPs

Term Description	Observed Gene Count	Background Gene Count	Strength	FDR	Matching Proteins
Oligosaccharyl-transferase complex	3	14	2.21	0.0028	RPN2, STT3B, DDOST
Amino acid transport complex	2	2	2.88	0.0102	SLC7A5, SLC3A2

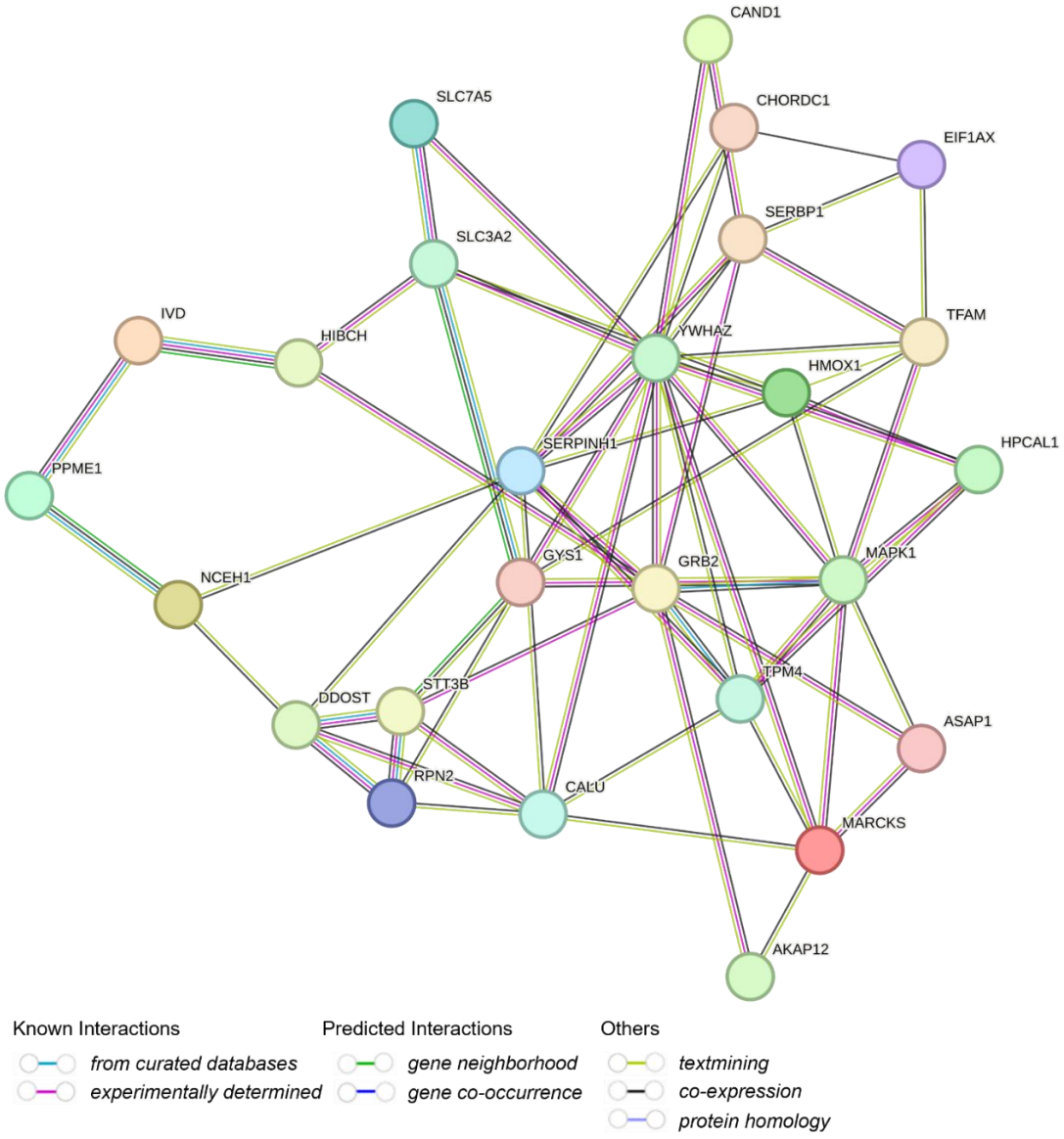

Figure 25: Protein-Protein Interaction (PPI) Network of Identified DEPs

PPI network consisting of 26 nodes and 67 edges from STRING database. Known interactions are edges of pink (experimentally determined) and sky blue (database obtained). Predicted interactions are edges of green (gene neighborhood) and dark blue (gene co-occurrence). Edges of yellowish green are text mining. Edges of black color mean co-expression. Edges of light purple mean protein homology. (PPI enrichment P = 0.0003)

3 Discussion

3.1 Serum Levels of AGEs and their Receptors sRAGE and Gal-3 in CP

Numerous studies have reported that altered serum levels of AGEs, sRAGE, and Gal-3 are associated with pancreatic diseases, including diabetes mellitus, AP, or pancreatic cancer (Gawandi et al., 2018; Kocsis et al., 2009; Lindström et al., 2009; Xie et al., 2012). However, few data are available for CP.

Since serum AGE levels are influenced by several factors, including diet and necrotic and apoptotic cell death (Chaudhuri et al., 2018; Kaczmarek et al., 2013), the inclusion criteria limited patient eligibility to symptom-free intervals in the absence of other inflammatory processes. This study demonstrated elevated serum AGE levels in CP patients (Böhme et al., 2020). AGE are known to induce pro-inflammatory cytokines such as IL-1b and TNF-a, thereby promoting or maintaining inflammatory processes (Rashid et al., 2006; Reznikov et al., 2004). The elevated serum AGE levels found here confirm this role in inflammation, which may also enhance the immune response by stimulating innate immune receptors such as RAGE or Gal-3 (Díaz-Alvarez & Ortega, 2017; Kong et al., 2017). Furthermore, these results indicate that inflammation was detectable even during symptom-free intervals, suggesting that DAMPs released from the injured pancreas might be a main source for this observation.

In contrast to AGEs, sRAGE serum levels were reduced in this analysis (Böhme et al., 2020), confirming the impaired function of sRAGE as a decoy receptor within the AGE-RAGE signaling pathway in CP (Bierhaus et al., 2005; Yan et al., 2010). Previous studies have demonstrated elevated serum levels of RAGE in patients with type 1 and type 2 diabetes mellitus compared to other diseases (Prasad, 2014). Therefore, the serum sRAGE levels in the current CP cohorts were adjusted for a potential influence of diabetes status, but no impact of diabetes was found. This observation may reflect disparities in the pathogenesis of the distinct forms of diabetes. As in patients with type 1 or type 2 diabetes mellitus, increased expression of MMPs possibly underlies the elevation of serum sRAGE levels; this effect may be absent in patients with CP and type 3c diabetes (Prasad, 2014). In conclusion, the observations in CP are consistent with

findings in other inflammatory diseases such as atherosclerosis or chronic obstructive pulmonary disease, suggesting that aging-related mechanisms are generally involved in inflammatory processes. The results presented here are in line with previous studies in distinct forms of pancreatitis, however, these did not have comparable strict inclusion criteria and examined smaller cohorts for sRAGE (Kocsis et al., 2009; Pezzilli et al., 2010). Interestingly, genotypes of *RAGE* SNPs rs2070600 and rs2071288 have been shown to correlate with sRAGE serum levels in an Asian genome-wide association study of type 2 diabetes mellitus patients (Lim et al., 2017), whereas variants rs1800624 and rs1800625 have been associated with diabetic complications (Serveaux-Dancer et al., 2019). A possible influence of these variants on serum sRAGE levels in our cohorts and whether these variants predispose to CP were investigated, but no association was found. This implies that altered sRAGE levels in CP are not genetically determined, but rather represent the contribution of aging-related mechanisms.

Finally, serum Gal-3 levels were found to be elevated in this study, (Böhme et al., 2020), a finding consistent with a previous publication in which Gal-3 expression was overexpressed approximately 3-fold in ductular complexes of CP patients (L. Wang et al., 2000). This indicated an important role of Gal-3 in fibrotic remodeling, as a significant correlation with fibrosis was observed (L. Wang et al., 2000). In addition, Gal-3 is important in the chemoattraction of monocytes and macrophages (Elola et al., 2007; Rabinovich & Gruppi, 2005) and is capable of activating TLR4 (toll-like receptor 4), and thereby prolonging the inflammatory response (Burguillos et al., 2015).

In this comprehensive analysis, increased AGE and Gal-3 and decreased sRAGE serum levels were found in patients with CP. Simultaneous changes in the ligand AGEs and their receptors sRAGE and Gal-3 clearly demonstrated the involvement of aging-related risk molecules in the pathogenesis of CP, independent of gender, age and the presence of diabetes mellitus, even during episodes without active inflammatory processes. Whether these processes are causal or reflect general pathways involved during disease progression remains to be determined. Moreover, no differences between the etiologic groups of CP patients were observed, indicating that the alcoholic and non-alcoholic forms share common pathomechanisms. At this stage, the clinical relevance of the observation cannot be addressed with certainty. The congruence of the three markers in the distinct settings indicates a potential value for diagnosis or monitoring of CP under

predefined circumstances. Therefore, these findings warrant replication in prospective cohorts following a given protocol.

3.2 Functional Characterization of AGE Receptors RAGE, PRKCSH, Gal-3 and DDOST in Pancreatic Cancer

3.2.1 RAGE is Poorly Expressed in PDAC Tissue

RAGE, a multiligand receptor involved in inflammation and proliferation, is a major receptor for AGEs and plays an important role in PDAC progression by promotion of cell survival through increase of ATP production and autophagy and reduction of apoptosis (Hori et al., 1995; Kang et al., 2014; Leclerc & Vetter, 2015). When engaged by its ligands, RAGE activates signaling pathways, including the PI3K/Akt and MAPK pathways, leading to the activation of transcription factors such as NF-κB, AP-1 and STAT-3 (Riehl et al., 2009). In murine models of pancreatic cancer, deletion of the *RAGE* gene inhibited the development and progression of ductal neoplasia and prolonged survival (DiNorcia et al., 2012).

Based on the previous findings, the aim of this study was to unravel the expression levels of RAGE in PDAC tissue and cell lines. Thereby, new insights into the relevant processes of PDAC development should be revealed.

The current study found no change in RNA expression levels in human PAAD tissues between normal and tumor tissues in the TCGA and GTEx data. In addition to the low overall expression rate in the PAAD data, histological staining of human PDAC tissue revealed protein expression primarily in immune cells, but not in PanIN lesions or invasive cancer compartments. To further differentiate the type of RAGE expressing immune cells, IF co-staining may be recommended. Subsequently, RAGE KD was performed in human PDAC cell lines to determine the phenotypic effects of RAGE silencing but no significant downregulation of RNA or protein levels was observed.

Presumably due to the low expression of RAGE in PDAC tissues and cell lines, it is not feasible to implement a KD using a transient RNA interference technique. Future experiments should be performed in homogeneous cell lines with high expression levels

of RAGE or by using stable mutations, such as the CRISPR-Cas9 system. In conclusion, it has been demonstrated that a major part of RAGE protein expression is localized within immune cells.

3.2.2 PRKCSH KD Reduces Proliferation and Viability in a KRAS wild-type PDAC Cell Line

By maintaining cell homeostasis, *N*-linked glycosylation of pivotal proteins has been shown to be essential for tumorigenesis, proliferation and metastasis (Cui et al., 2018; Ding et al., 2021; Guo et al., 2009; X. Liu et al., 2013). Glucosidase II is important in *N*-linked glycosylation. It regulates the folding and maturation of newly synthesized glycoproteins (Ellgaard et al., 1999). One essential subunit of Glucosidase II is PRKCSH (Hirai & Shimizu, 1990). The potential role of PRKCSH in disease has been discussed for PCLD, where loss-of-function mutations, but not large deletions, in the *PRKCSH* gene have been associated with the autosomal dominant form of PCLD (Cnossen et al., 2015; Cornec-Le Gall et al., 2018; Drenth et al., 2003). Bioinformatic analysis and a case study suggested that in patients suffering from lung cancer, higher PRKCSH expression level might be correlated with poorer prognosis (Lei et al., 2022). However, no association with pancreatic cancer has been reported so far.

Based on the TCGA and GTEx gene expression datasets, this study demonstrated that *PRKCSH* RNA expression is elevated in pancreatic cancer tumor samples compared to normal pancreatic tissue. Therefore, the aim of the present study was to determine how PRKCSH may affect the cellular phenotypes of PDAC. Accordingly, a PRKCSH KD was performed in human PDAC cell lines and phenotypic alterations induced by the absence of PRKCSH were subsequently examined. The KD of PRKCSH resulted in reduced proliferation and viability in the PDAC cell line BXPC-3, but not in PA-TU-8988T, PANC-1 or MIA-PACA-2, partially confirming recent findings that KO of PRKCSH in lung cancer cells resulted in reduced growth (Khaodee et al., 2019). Since BXPC-3 is the only *KRAS* wild-type cell line used in this study, the significant reduction in growth rate here may indicate that the *KRAS* genotype is relevant to the effect of PRKCSH. Furthermore, it was demonstrated that the effects on proliferation and viability were independent of potential cell cycle arrests, because neither BXPC-3 nor PA-TU-8988T cell lines showed

G2/M arrest after suppression of PRKCSH, as previously reported in lung cancer cells (Lei et al., 2022).

Based on these data, it can be proposed that PRKCSH has a potential tumor-promoting capacity in PDAC cells containing a wild type *KRAS* genotype. To confirm this suggestion, more cell lines with different genotypes need to be investigated. However, the specific cellular function leading to reduced proliferation rates requires further investigation, such as apoptosis or metabolic assays, as we cannot yet explain the effect of PRKCSH. It could be speculated that the activating mutation of *KRAS* results in the suppression of putative apoptotic effects induced by protein misfolding after PRKCSH KD. However, since >90 % of all PDAC patients carry an activated mutated *KRAS* gene, the clinical relevance is limited. More investigations are necessary to clarify the role of PRKCSH in PDAC.

3.2.3 Gal-3 KD Inhibits Migration in a PDAC Cell Line and Reduces Proliferation and Viability in *KRAS* wild-type Cells

Gal-3 is a member of the lectin family and is involved in a wide variety of functions including cell-cell adhesion, cell-matrix interactions, macrophage activation, angiogenesis, metastasis and apoptosis (Barondes et al., 1994; Dumic et al., 2006; Elola et al., 2007; F.-T. Liu & Rabinovich, 2005; Nakahara & Raz, 2006). As a pattern recognition receptor for the detection of DAMPs, Gal-3 is important for systemic innate immunity in healthy individuals (Díaz-Alvarez & Ortega, 2017). In inflammatory conditions, Gal-3 is implicated in myocarditis, nonalcoholic steatohepatitis, chronic kidney disease, pulmonary inflammation, and autoinflammatory diseases (Bouffette et al., 2023). In tumorigenesis, it has been shown that Gal-3 has a pro-oncogenic role in cancer cells and plays an important role in differentiation, transformation and metastasis. It has been reported that overexpression of Gal-3 increases tumor cell migration and invasion, whereas downregulation of Gal-3 has an opposite effect (Gao et al., 2014; Honjo et al., 2001). So far, Gal-3 has been linked to breast, cervical, colorectal, head and neck, lung, prostate, and thyroid cancers (Grazier & Sylvester, 2022; Ko et al., 2023; J. Li et al., 2019). In PDAC, Gal-3 protein expression was elevated compared to non-tumor tissue or other pancreatic diseases (Xie et al., 2012).

In this study, elevated expression levels of Gal-3 have been confirmed. The *Gal-3* RNA expression was found to be significantly increased in tumor samples from pancreatic cancer patients compared to normal pancreatic tissue. Based on this finding, the aim of the present study was to determine how Gal-3 may contribute to the progression of PDAC. Therefore, a Gal-3 KD was performed in human PDAC cell lines in order to evaluate phenotypic changes. The KD of Gal-3 resulted in reduced proliferation in the PDAC cell line BXPC-3, but not in PA-TU-8988T, PANC-1 or MIA-PACA-2, and reduced viability in BXPC-3 and PA-TU-8988T, partially confirming recent findings that siRNA mediated KD of Gal-3 in human pulmonary artery smooth muscle cells (HPASMC) resulted in reduced proliferation (Barman et al., 2019). Considering that BXPC-3 is the only KRAS wild-type cell line used in this study, the observed reduction in proliferation and viability rate may indicate a role of the activated *KRAS* genotype in the effect of Gal-3. Moreover, KD of Gal-3 resulted in a significant reduction of cell migration in the PA-TU-8988T cell line, which is consistent with the observations that KD of Gal-3 contributed to reduced cell migration in human prostate cancer cells (Y. Wang et al., 2009). To confirm the strong effects on migration in PDAC, additional cell lines need to be investigated.

In conclusion, these data suggest that Gal-3 has a potential tumor-promoting function in PDAC cells, as elevated levels are associated with inflammation and carcinogenesis. As the effect of Gal-3 on proliferation and viability was only observed in the *KRAS* wild-type cell line, the clinical potential of this finding for PDAC patients is limited. However, the relevance of the observed effects on migration in *KRAS* activated cells is of great importance for the metastatic potential of PDAC. Therefore, further studies are needed to elucidate the role of Gal-3 in PDAC cell migration.

3.2.4 DDOST KD Induces Oxidative- and ER-Stress Dependent Cell Apoptosis in PDAC Cell Lines

The pancreatic gland has a high secretory capacity and therefore requires a high level of protein translation, post-translational modification and secretion. The OST complex is essential for *N*-linked glycosylation, one of the most common protein modifications, and has been implicated in ER stress-induced cell death in PDAC (Ishino et al., 2018; Mohorko

et al., 2011). It has been shown that *N*-linked glycosylation of critical proteins is essential for tumorigenesis, proliferation and metastasis through maintenance of cell homeostasis (Cui et al., 2018; Ding et al., 2021; Guo et al., 2009; X. Liu et al., 2013; J. Wu et al., 2018).

The assembly and stability of the OST complex requires the subunit DDOST (Roboti & High, 2012), which has been correlated with immune infiltration, metastasis and prognosis in several types of cancer (Chang et al., 2022; Shapanis et al., 2021; C. Zhu et al., 2021). Data from a proteomic study suggested that DDOST function is particularly relevant in the pancreas, due to its tissue-specific expression (L. Jiang et al., 2020). However, no association with pancreatic cancer has been reported. As there are limited therapeutic options for PDAC, new insights into the relevant processes of PDAC development may contribute to the understanding of tumorigenesis and thereby open novel diagnostic and therapeutic avenues. The present study aims to determine how DDOST may affect the cellular phenotypes of PDAC. Therefore, a DDOST KD was performed in human PDAC cell lines to subsequently examine the phenotypic alterations induced by the reduction of DDOST expression levels. Thereby, regulations in oxidative stress, ER stress and apoptosis were observed. To verify these phenotypic results, a mass-spectrometry based assay was performed to identify relevant DEPs, which were then matched to biological processes. In this way, the involvement of DDOST on key signaling pathways, including stress response and apoptosis could be substantiated.

In this study, siRNA-mediated KD of DDOST resulted in reduced proliferation rates and viability, as well as increased ER stress, ROS formation, and apoptosis in PDAC cell line. This is consistent with the finding that a deletion (c.1265_1286del22) and missense mutation (c.650G>A) in *DDOST* caused a general defect in *N*-linked glycosylation leading to CDG (M. A. Jones et al., 2012), together with the observation that inhibition of *N*-linked glycosylation increased ER stress and apoptosis in gastric cancer cells (J. Wu et al., 2018). A recent review, based on the effects of several therapeutics with the potential to increase ER stress, hypothesized that increased ER stress in pancreatic cancer activates the unfolded protein response and leads to ER-induced apoptosis via CHOP (Botrus et al., 2022). In addition, increased levels of CHOP promoted ROS-induced apoptosis by mediating between ER stress signaling and ROS formation (Lu et al., 2014; Verfaillie et al., 2012). These reports are consistent with the finding that both ROS

formation and apoptosis levels were increased after DDOST downregulation in PDAC cell lines and supported by the increased levels of cleaved Caspase-3 and PARP-1.

To validate the previous findings from *in vitro* experiments, an unbiased mass spectrometry approach was used to identify 30 DEPs, including total proteins and phosphorylated proteins, after DDOST KD. To analyze the relationships among the identified DEPs, the STRING database was used to obtain a PPI network including all significantly regulated DEPs with a wide variety of interactions. One of the clusters identified by functional enrichment analysis was the OST complex, including the three identified DEPs DDOST, RPN2 and STT3B. Interestingly, CALU, which directly interacts with DDOST and RPN2, is known to be highly expressed in tumor cells and may therefore play a crucial role in cancer progression and the induction of epithelial to mesenchymal transition (Du et al., 2021). In addition, the protein with the most edges to other DEPs was YWHAZ, a central hub protein for many signaling pathways that are frequently upregulated in multiple types of cancer and are associated with cell growth, apoptosis, migration and invasion (Gan et al., 2020). Another key regulator identified was MAPK1, which is known to regulate cell functions including proliferation, gene expression, differentiation, mitosis, cell survival and apoptosis (Pearson et al., 2001).

A spearman correlation analysis revealed that all 30 DEPs were significantly correlated with *DDOST* in 179 PAAD tumor tissue samples, among which 24 had strong or medium correlations, including *RPN2*, *SERBP1*, *CALU*, *STT3B*, *YWHAZ* and *MAPK1*. The RNA-binding protein SERBP1 has been shown to play an important role in apoptosis and metabolic processes through post-transcriptional regulation of gene transcription and alternative splicing in HeLa cell line, and to worsen the prognosis for PDAC survival (Zhou et al., 2022). Another cluster identified by functional enrichment analysis was the *amino acid transport complex*, including SLC3A2 and SLC7A5, both of which were downregulated after DDOST KD and both of which correlated with *DDOST*. A recent study reported that the expression level of the *amino acid transport complex* was significantly co-regulated in head and neck squamous cell carcinoma tissues and cell lines (Digomann et al., 2019, p. 98). Upregulation was associated with poor survival in patients with oral squamous cell carcinoma. After KD of SLC3A2, reduced migration, invasion and proliferation, but increased apoptosis was observed in cancer cell lines (Liang & Sun, 2021). The finding that reduced SLC3A2 expression levels together with

decreased proliferation and increased apoptosis after DDOST KD is consistent with this previous study. In addition to functional enrichment analysis, all 30 identified DEPs were annotated with biological processes relevant to tumor development. According to this GO analysis, 16 of the 30 DEPs were found to be related to cellular processes such as oxidative stress, proteostasis, apoptosis, cell cycle, and protein glycosylation. Previously, dysregulation of oxidative stress response and proteostasis have been reported to play important roles in carcinogenesis and tumor progression by exploiting the respective response mechanisms under stress conditions (Hayes et al., 2020; Y. Wang et al., 2019). Based on these data, it can be proposed that DDOST has a potential tumor-promoting capacity in PDAC cells by maintaining ER proteostasis and thereby suppressing ROS generation and apoptosis. The implemented *in vitro* experiments demonstrated that downregulation of DDOST induces ER stress, which leads to enhanced ROS formation and apoptosis as well as to reduced proliferation and cell viability in two human pancreatic cancer cell lines. Further, this study identified DEPs related to DDOST that may be involved in pancreatic carcinogenesis. In total, 29 proteins and phosphopeptides were found to be dependent on DDOST expression. However, the specific effect of DDOST on non-glycosylated proteins requires further investigation. For this reason, the need for a glycosylation assay is a limitation since it could not yet be clarified how DDOST affects non-glycosylated proteins or protein phosphorylation. It could be speculated that the accumulation of unglycosylated proteins induces the UPR, explaining the observed effects. On the other hand, although the MS analysis allowed to relate numerous DEPs to DDOST, it is likely that some regulated proteins remained unidentified by the mass spectrometric approach. Nevertheless, further studies are needed to clarify the exact relationship between DDOST and the candidate interaction partners identified in this study.

3.3 General Discussion and Future Directions

In this study, characterization of the four AGE receptors, RAGE, DDOST, PRKCSH and Gal-3, revealed independent effects on pancreatic inflammation and tumor progression. Since DDOST was the most promising of the four receptors and a partially unknown candidate, it became the main focus of this study.

Interestingly, KD of DDOST and PRKCSH, both involved in protein *N*-linked glycosylation, led to decreased proliferation and viability, with DDOST independent and PRKCSH possibly dependent on *KRAS* genotype. Notably, additional treatment of the receptors DDOST, PRKCSH and Gal-3 with their ligands had no detectable phenotypic effect, suggesting that the observed interaction between AGEs and their corresponding receptors may not be required for functional signaling.

To further characterize the role of RAGE, DDOST, PRKCSH and Gal-3 in PDAC, several aspects need to be addressed. First, in addition to the transient siRNA KD technique, KO and overexpression of target proteins should be performed to reduce methodological shortcomings. Second, the number of cell lines used for phenotypic analysis should be increased. This will help to validate the effects of individual genotypes, such as the *KRAS* status. Methodologically, further high-throughput analysis, such as RNA sequencing, could validate the present results and elucidate possible signaling pathways involved. For the identification of interaction partners, cross-linking mass spectrometry might be a valuable tool. Further, the effect of a DDOST KD on *N*-linked glycosylation should be determined using an appropriate glycosylation assay. Finally, all phenotypic assays should be complemented by protein analysis to verify relevant signaling pathways.

In conclusion, this study demonstrated the diagnostic potential of AGEs and the soluble receptors sRAGE and Gal-3 in CP. Furthermore, the tumor promoting function of DDOST was revealed for the first time in PDAC cell lines, opening new therapeutic opportunities. In addition, PRKCSH and Gal-3 were shown to be valuable targets for further investigation.

4 Methods & Material

4.1 Serum Levels of AGEs and their Receptors sRAGE and Gal-3 in CP

4.1.1 Study Design and Patient Selection

For this study, patients were recruited at the Martin-Luther-University Halle-Wittenberg, the University Leipzig and the Technical University Munich. The study was approved by the Ethics Committee of the Martin-Luther-University Halle-Wittenberg (date: July 21, 2017, processing number: 2017e96, Ethics Committee Medical Faculty, Martin-Luther-University Halle-Wittenberg), by the Ethics Committee of the University of Leipzig (Az.: 107-15-26012015; date: May 14, 2015) and by the Ethics Committee of the Technical University Munich (project number: 104/15; date: April 02, 2015). The study protocol conforms to the ethical guidelines of the 1975 Declaration of Helsinki. Written informed consent was obtained from each patient included in the study.

CP was defined according to the HaPanEU guidelines (Löhr et al., 2017). Patients were classified as having alcoholic CP (ACP) if alcohol consumption was >60 g per day for women and >80 g per day for men for at least 2 years. Patients with no precipitating factor were classified as non-alcoholic CP (NACP). Exclusion criteria have been described in a previous publication (Robinson et al., 2019); an active diagnosis of neoplasia or a disease-free interval of less than five years; patients unable to give informed consent to participate in the study, including those younger than 18 years; patients with Childs-Pugh score B/C liver cirrhosis; patients immunosuppressed either because of disease (e.g. patients who had received antibiotic therapy within the previous month or had an active infectious process; patients who had received systemic steroid therapy within the previous month; patients with chronic kidney disease stage 4 or greater (eGFR <30 mL/min) and those who had received surgical treatment of any type to any site within the previous year. Patient characteristics are summarized in Table 2.

4.1.2 ELISA

AGE, sRAGE, and Gal-3 serum concentrations were measured by enzyme-linked immunosorbent assay (ELISA) using human standards according to the manufacturer's guidelines (Human Advanced Glycation end products (AGE) ELISA Kit; MyBio-Source, San Diego, CA-US; Soluble Receptor of Advanced Glycation End-Products (sRAGE) Human ELISA; BioVendor, Brno, CZE; Galectin-3 Human ELISA Kit; Thermo Fisher Scientific, Waltham, MA-US). Briefly, blood was collected from controls and patients, centrifuged at 524 rcf for 15 min, and serum was immediately stored at -80°C in 200 mL aliquots. Either pure or diluted serum was used for ELISAs according to the manufacturer's instructions. Sample handling was performed as described in the manufacturer's specific protocol. The absorbance of each microwell was read using a spectrophotometer at 450 nm as the primary wavelength. Sample values for each serum parameter were calculated from a standard curve generated in duplicate for each ELISA plate.

4.1.3 Melting Curve Analysis

DNA was isolated from EDTA-anticoagulated blood using a commercially available system (QIAamp Blood DNA Mini Kit; Qiagen, Hilden, Germany). Polymerase chain reaction (PCR) was performed using OneTaq 2X Master Mix (NEB) with 200 µM dNTPs, 1.8 mM $MgCl_2$ and 2 pmol forward primer and 10 pmol reverse primer in a total volume of 25 µL. Cycle conditions were an initial denaturation at 95°C for 5 minutes followed by 45 cycles of 20 seconds denaturation at 95°C, 40 seconds annealing at 60°C, 90 seconds primer extension at 72°C, and a final extension at 72°C for 5 min in an automated thermal cycler. Primers and probes (Table 7) were synthesized by TIB Molbiol (Berlin, Germany). Genotyping was performed using the Light Cycler 480 system (Roche Diagnostics).

4.1.4 Genetics

We analyzed the *RAGE* SNPs rs2071288, rs2070600, rs1800624, and rs1800625 in 378 CP patients (202 ACP; 176 NACP) from our biobank and 338 controls using melting curve

analysis (Table 5). All patients were Caucasian. The used primer sequences are listed in Table 7. Briefly, polymerase chain reaction products were used with 50 nM (final) probe oligomers followed by melting curve analysis using the following protocol: 95°C for 60 seconds, 45°C for 60 seconds and continuous rise to 70°C at 0.19°C/sec. Call rates for all SNPs were > 95 %. For quality control, 5.6 % of all samples were genotyped in duplicate, blinded to the investigator. The resulting concordance rate was 95.3 %. Genotype and allele frequencies were compared between patients and controls using the two-tailed Fisher's exact test. A *p*-value of < 0.0125 (after Bonferroni correction) was considered significant. All data are presented without correction. Calculations were performed for the total group, etiology, and gender subgroups.

Table 7: Sequences of PCR Primers and SimpleProbes

Sequences of PCR primers and SimpleProbes for melting curve analysis of SNPs: rs207128, rs207060, rs1800625, rs1800624.

Name		5'-3' sequence[a]
rs2071288	Forward primer	CAggTgAggggTTTgATAAAgT
	Reverse primer	gCTAgAgTTCCCAgCCCTgAT
	SimpleProbe	TgTCTCC**A**TACAggCTCT XI[b] gTgg--Phosphate
rs2070600	LightSNiP	LightSNiP (TiB Molbiol, Berlin, Germany)
rs1800625	Forward primer	TTTCCCTgggTTTAgTTgAgAAT
	Reverse primer	ACTggAgCCCCATCTTgATT
	SimpleProbe	CACgAAg**C**TCCAA XI ACAggTTTCTC--Phosphate
rs1800624	Forward primer	TTTCCCTgggTTTAgTTgAgAAT
	Reverse primer	gCATCAATAgggTTCAgTCCAgACT
	SimpleProbe	gCCCAA**A**TgCACCCT XI TgCAgA--Phosphate

[a] The position of the SNP in probes is underlined and in bold

[b] XI: the internal SimpleProbe label

4.1.5 Statistical Analysis

SPSS version 24.0 and GraphPad Prism 5.0 software were used for statistical analysis. Data are presented as mean ± standard deviation (SD). Data sets were analyzed for

statistical significance using a two-tailed, unpaired Student t-test. Differences were considered statistically significant at *p* values < 0.05.

4.2 Functional Characterization of RAGE, PRKCSH, Gal-3 and DDOST

4.2.1 Cell Culture

PA-TU-8988T, PANC-1 and MIA-PACA-2 cell lines (Table 16) were maintained in 90 % Dulbecco's MEM (Thermo Fisher Scientific) supplemented with 10 % FBS at 37°C in humidified 5 % CO_2. Prior to treatment, the cells were washed in PBS and incubated in low serum (1 %) media for 5 hours. BXPC-3 cell line (Table 16) was maintained in 90 % RPMI 1640 (Thermo Fisher Scientific) supplemented with 10 % FBS, at 37°C in humidified 5 % CO_2. Prior to treatment, cells were washed in PBS and incubated in low serum (1 %) media for 5 hours. Genotypes of used PDAC cell lines are listed in Table 8.

Table 8: KRAS Genotypes of PDAC Cell Lines

	BXPC-3	**PA-TU-8988T**	**PANC-1**	**MIA-PACA-2**
KRAS	Wild type	G12V	G12D	G12C

4.2.2 Treatment with CML and Tunicamycin

At 24 hours post-transfection, cells were washed in PBS and incubated with low serum (1%) for 5 hours before treatment with 250 µM CML or 1 µM TM for 24 hours. The concentrations used were previously determined by dilution series. Used dose has no cytotoxic effect.

4.2.3 Transfection of siRNA

PA-TU-8988T, BXPC-3, PANC-1 and MIA-PACA-2 cell lines were transfected using Invitrogen Lipofectamine RNAiMAX Transfection Reagent (Thermo Fisher Scientific) according to the manufacturer's instructions. Transfection of Accell non-targeting siRNA (Dharmacon) and custom-designed siRNA (Eurofins) was performed at a final concentration of 50 nM. All sequences used are listed in Table 13.

4.2.4 RNA Quantification

Total RNA was isolated from lysed cells and purified using the NucleoSpin RNA kit (Macherey-Nagel) according to the manufacturer's protocol. Equal amounts of RNA were reverse transcribed into cDNA using the Omniscript RT Kit (Qiagen) according to the manufacturer's protocol. The mRNA expression was detected by qRT-PCR using the Luna Universal SYBR Green Supermix (NEB) via a real-time PCR system (Applied Biosystems), and the corresponding primer sequences, forward and reverse, are listed in Table 12. As housekeeping genes, the ribosomal protein *RPLP0* or human *B2M* was used as an endogenous control. All experiments were performed at least in biological triplicates and are expressed as ± SD.

4.2.5 Western Blot Analysis

Cells were lysed in RIPA lysis buffer (50 mM Tris-HCl (pH 7.5), 150 mM NaCl, 0.1 % SDS, 1 % sodium deoxycholate, and 1 % Triton X-100) supplemented with 4 % complete protease inhibitor cocktail (Roche) and 1 % phosphatase inhibitor mix I (Serva). After brief sonication, equal concentrations of cell protein lysates were mixed with 25 % Laemmli SDS buffer, separated on 10 % SDS-polyacrylamide gels, and transferred to PVDF membranes probed with the appropriate primary antibodies, listed in Table 14, and the appropriate peroxidase-conjugated secondary antibody, listed in Table 15. Target proteins were visualized using WesternBright Chemiluminescence Substrate Sirius system (Biozym). For reprobing, blots were stripped with Restore Western Blot

Stripping Buffer (Thermo Scientific) before adding a new primary antibody. The amount of sample protein was verified using β-Actin as a loading control.

4.2.6 Proliferation Assay

Cell proliferation was determined by cell counting using the CASY counter system (Omni Life Science). For KD-experiments cells were seeded in 24-well plates at a density of 25,000 cells/well in triplicate for each time point. Cells were harvested 24, 48 and 72 hours after seeding and the absolute number of cells was determined. All experiments were performed in biological triplicates and are expressed as ± SD.

4.2.7 ATP Concentration Assay

ATP concentration was measured using the CellTiter-Glo Luminescent Cell Viability Assay (Promega) according to the manufacturer's instructions. Cells were seeded in 96-well plates at a density of 5,000 cells/well with five replicates and incubated at 37°C for 48 hours post-transfection. Finally, the luminescence of each well was measured using Luminoskan Ascent (Thermo Scientific). All experiments were performed in biological triplicates and are expressed as ± SD.

4.2.8 Cell Cycle Analysis

PDAC cells were grown in 12-well plates at a density of 100,000 cells/well and incubated at 37°C in humidified 5 % CO_2 for 48 hours post-transfection. Harvested cells were washed in PBS and resuspended in 0.5 mL PBS. Then, 1.5 mL of ice-cold 100 % ethanol was added dropwise to the cell suspension while vortexing continuously. The cells were stored overnight at -20°C. The cells were then centrifuged and washed with cold PBS. The cells were resuspended in 500 µL PI/RNase staining buffer (BD Biosciences) and incubated at 37°C for 15 min. Finally, the cells were analyzed by flow cytometry (LSRFortessa, BD Bioscience; FlowJo software). All experiments were performed in biological triplicates and are expressed as ± SD.

4.2.9 Immune Fluorescence ER-Stress

PDAC cell lines were grown on polylysine-coated coverslips in 24-well plates at a density of 50,000 cells/well and incubated at 37°C in humidified 5 % CO_2 for 24 hours post-transfection. As a positive control for ER stress, 1 µM TM was added. After incubation, cells were fixed with 4 % paraformaldehyde for 15 min and permeabilized with 0.3 % Triton X-100 (Sigma-Aldrich) in PBS for 10 min. Cells were then blocked with 5 % goat serum (Thermo Fisher Scientific) in PBS for 1 hour, followed by incubation with primary antibodies for DDOST (HPA046841, Atlas Antibodies) and CHOP (2895, Cell Signaling) at 4°C overnight, followed by incubation with Alexa Flour 488 and 594-conjugated secondary antibodies (Thermo Fisher Scientific). Cells were then mounted with ProLong Gold with DAPI (Thermo Fisher Scientific) and visualized using a wide field fluorescence microscope (BZ-X, Keyence). The area of CHOP-positive cells was quantified using ImageJ software. Three randomly selected images from each culture condition were analyzed. Quantification was calculated as the ratio of detected fluorescence emission per cell area relative to siControl.

4.2.10 Immunohistochemistry

Paraffin-embedded PDAC tissue samples were analyzed by immunohistochemistry. Samples were fixed in neutral buffered formalin and embedded in paraffin after surgery. For histopathological examination, tissue sections (3 µm) were deparaffinized in RotiClear (Carl Roth) for 20 min. Slides were rehydrated in a descending gradient of ethanol (100 %, 96 %, 80 % and 70 %) and prepared for epitope retrieval in sodium citrate buffer (0.1 mol/L citric acid, 0.1 mol/L sodium citrate, pH 6.0) for 15 min. After washing in phosphate-buffered saline (PBS), endogenous peroxidase was inactivated with 3 % hydrogen peroxide in methanol and washed again in PBS. Slides were blocked with 2.5 % goat or horse serum (Vector Laboratories) for 1 hour at room temperature (RT). The slides were then incubated with primary antibody (Table 14) diluted in Dako antibody diluent (Agilent Technologies) for 16 hours at 4°C. All slides were washed in PBS after each incubation step. Slides were then incubated with the appropriate secondary antibody and horseradish peroxidase conjugate (Table 15), ImmPRESS

(Vector Laboratories) for 30 min at RT, followed by staining with 3,3'-diaminobenzidine chromogen (DAB; Sigma-Aldrich) and counterstaining with Mayer acidic haematoxylin (Morphisto). After dehydration in an ascending ethanol gradient and Xylol (Carl Roth), the slides were coverslipped with RotiMount (Carl Roth). Corresponding tissue slides were used as positive controls. Images were acquired using a ZEISS Axio Scan.Z1 slide scanner (Carl Zeiss).

4.2.11 Intracellular ROS Assay by Flow Cytometry

PDAC cell lines were grown in 12-well plates at a density of 100,000 cells/well and incubated at 37°C in humidified 5 % CO_2 for 24 hours post-transfection. Intracellular reactive oxygen species (ROS) were detected using H_2DCFDA (HY-D0940, MedChemExpress). Briefly, cells were incubated with H_2DCFDA for 2 hours at 37°C in humidified 5 % CO_2. After washing with PBS, cells were incubated with propidium iodide (PI) solution (P3566, Invitrogen) for a further 15 min and then analysed by flow cytometry (LSRFortessa, BD Bioscience; FlowJo software). All experiments were performed at least in biological triplicates and are expressed as ± SD.

4.2.12 Apoptosis Assay by Flow Cytometry

PDAC cell lines were grown in 12-well plates at a density of 100,000 cells/well and incubated at 37°C in humidified 5 % CO_2 for 48 hours post-transfection. After harvest, cells were resuspended in binding buffer and incubated with BD AnnexinV-FITC (556420, Fisher Scientific) and PI solution (P3566, Invitrogen) according to the manufacturer's instructions. Cells were then analyzed by flow cytometry (LSRFortessa, BD Bioscience; FlowJo software). All experiments were performed at least in biological triplicates and are expressed as ± SD.

4.2.13 Wound Healing Assay

Migration ability was measured using the wound healing assay. Cells were seeded in 12-well plates at 50,000 cells/well and incubated to confluence at 37°C in humidified 5 % CO_2 (triplicates for each time point). The 500 µm wide gaps were created by silicone Culture-Insert (4 Well in µ-Dish 35 mm, high (Ibidi)), which were removed after the cells had formed an optically confluent monolayer, approximately 24 hours after seeding. Cells were photographed at 0 and 24 hours after wounding. The area of gap closure was calculated as: gap closure (%) = (A0-At)/A0 x 100, where A0 is the gap area at 0 hours and At is the remaining gap area at 24 hours. All experiments were performed in biological triplicates and are expressed as ± SD.

4.2.14 Mass Spectrometry

4.2.14.1 Sample Preparation and TMT Labeling

Five biological replicates of cell lysates containing 100 µg total protein were collected and further processed for liquid chromatography-tandem mass spectrometry (LC/MS-MS) analysis following an adapted filter-aided preparation protocol (Wiśniewski et al., 2009). Protein samples were reduced with 10 mM TCEP (8 M urea in 50 mM HEPES, pH 8.5) and centrifuged on 30 kDa cut-off centrifugal filter units. For alkylation, samples were incubated in 50 mM iodoacetamide in 8 M urea, 50 mM HEPES, pH 8.5 under dark conditions, centrifuged and washed before trypsinization with 2 µg trypsin in 50 mM HEPES, pH 8.5 at 37°C overnight. Tryptic peptides were labeled using a tandem mass tag TMT10-plex isobaric labeling reagent kit (Thermo Fisher Scientific) according to the manufacturer's instructions before all labeled samples were pooled for subsequent analysis.

4.2.14.2 Phosphopeptide Enrichment

For phosphopeptide enrichment analysis, the excess portion of the already labeled peptide samples was purified using a high-select TiO2 phosphopeptide enrichment kit (Thermo Fisher Scientific) according to the manufacturer's protocol prior to subsequent analysis.

4.2.14.3 LC-MS/MS Analysis

The prepared peptide solutions were analyzed by LC-MS/MS using the Ultimate 3000 RSLC nano-HPLC system coupled to an Orbitrap Fusion mass spectrometer with an EASY-Spray ion source (Thermo Fisher Scientific). After loading onto a reversed-phase (RP) C18 pre-column (Acclaim PepMap, 300 µm × 5 mm, 5 µm, 100 Å, Thermo Fisher Scientific), samples were washed with 0.1 % TFA prior to elution and separation on a 50 cm µPAC C18 separation column (PharmaFluidics). Peptides were eluted from the column with an increasing gradient of 3-35 % (v/v) ACN, 0.1 % formic acid over 360 min at 300 nL/min. For data-dependent acquisition (DDA), MS/MS experiments were performed for analyzing enriched phosphorylated peptides, while MS^3 experiments were used for TMT-labeled peptides. For MS/MS, high energy collisional dissociation (HCD) normalized collision energies (NCE) at 27 %, 28 % and 38 % and a collision-induced dissociation (CID) at 35 % NCE. High resolution full MS scans were followed by high resolution scans in the orbitrap and low-resolution product ion scans in the linear ion trap. For MS^3 experiments, CID was applied at 35 % NCE. The high-resolution product ion scans were acquired in the orbitrap after simultaneous selection and fragmentation with a HCD NCE at 55 % of the 10 most intense MS/MS fragments in the Orbitrap. For both modes, MS/MS and MS^3, dynamic exclusion was enabled. Data acquisition was performed using Xcalibur version 4.3 software (Thermo Fisher Scientific).

4.2.14.4 MS Data Analysis

For peptide identification and quantification, LC-MS/MS data were searched against the Swissprot database (taxonomy Homo sapiens, 04/23, 20,332 entries) using the

SequestHT database search algorithm with Proteome Discoverer (version 2.4; Thermo Fisher Scientific). A maximum mass deviation of 10 ppm was applied for precursor ions while for product ions, max. 0.6 Da (linear ion trap data) and 0.02 Da (orbitrap data) were allowed. Oxidation of Met, acetylation of protein N-termini, and phosphorylation of Ser, Thr, and Tyr were set as variable modifications. Carbamidomethylation of cysteines and modifications of peptide N-termini and Lys by the TMT label were included as fixed modifications. A maximum of two missed cleavage sites were considered for peptides. Quantification was performed using the TMT reporter ion abundances derived from HCD spectra, reporter ion intensities of protein unique and razor peptides were added to give protein abundances. For both, protein and peptide level analysis, instances with missing quantification for all replicates in both conditions were filtered out. For imputation of missing data, the K-nearest neighbors (kNN) algorithm using the 'impute.knn' function from the 'impute' R package was applied in DDOST KD and control KD experiments separately (Hastie et al., 2023; Troyanskaya et al., 2001). Non-unique phosphopeptides and peptides with ambiguous phosphorylation sites were filtered out before phosphopeptide quantitation was performed. To correct for abundance differences at the protein level, phosphopeptides were normalized after log2 transformation by subtracting the corresponding log2 protein abundance for each replicate/condition, where given. To simplify data analysis, peptides indicating equal phosphorylation sites were merged by summing their reporter ion intensities. Owing to the extensive size of the proteome and phosphoproteome data sets, the supplemental Tables S 1 and S 2 are provided as external Excel files.

4.2.15 Statistical Analysis

Data from Western blot method, PCR and phenotypic assays are expressed as the mean ± SD. Statistical analysis was performed using Graph-Pad Prism (version 9.4.1). Differences were calculated using unpaired, two-tailed Student´s t-test and considered statistically significant if $P \leq 0.05$. *p* values of * $P \leq 0.05$, ** $P \leq 0.01$, or *** $P \leq 0.001$ are indicated in the figures.

LC-MS/MS protein- and peptide-level data were analyzed using the reproducibility-optimized test statistic (ROTS) test implemented in the R package ROTS, a non-

parametric test (Suomi et al., 2017). Before performing the ROTS test, 1 was added to all abundances and the data were log2-transformed.

4.2.16 Differential Expression Analysis in PDAC

The Gepia2 database (http://gepia2.cancer-pku.cn/) (Z. Tang et al., 2019) was used on 03/30/2023, to obtain gene expression information for *RAGE*, *DDOST*, *PRKCSH* and *Gal-3* for PDAC in box plots. In all analyses, the gene symbol was entered in "Gene" and pancreatic adenocarcinoma (PAAD) was selected as the cancer name. "Box Plot" module: [Log2FC] cutoff was 1 and *p*-value cutoff was 0.01, Jitter Size was 0.4, "Multiple Datasets" and "Match TCGA normal and GTEx data" were selected, and log2 (TPM+1) was used for the log scale.

4.2.17 Spearman Correlation Analysis of Identified DEPs

Spearman correlation analysis was performed on 03/27/2023, using GEPIA 2 analysis tool, based on the TCGA Tumor dataset (Z. Tang et al., 2019). In all analyses, the corresponding gene symbols of 30 DEPs were entered and PAAD Tumor dataset was selected as cancer name. The estimates of Spearman ρ are appropriately accompanied by 95 % confidence interval. ρ-results were normalized to *RPLP0* and interpreted according to Schober, Boer, and Schwarte (2018) (Schober et al., 2018). Strong correlation: $\rho \geq 0.7$, medium correlation: $\rho \geq 0.4$, weak correlation: $\rho \geq 0.1$ (n = 179). Due to the size of the spearman correlation dataset, supplemental Table S 3 is provided as external Excel file.

4.2.18 PPI Network Construction

Protein-protein interaction (PPI) clusters were generated on 09/18/2023, using the STRING database (version 12.0; https://string-db.org/cgi/input.pl). Known and predicted protein-protein association data are collected and integrated. Both physical and indirect, functional interactions are associated as long as they are specific and

biologically meaningful (Szklarczyk et al., 2020). The STRING database was used to generate the PPI network of DDOST with a minimum interaction score of 0.15. Interaction predictions were obtained from databases, experiments, gene neighborhood, text mining and co-expression.

In addition, STRING provides a GO analysis, where all identified DEPs are listed individually with their annotations in the category of biological processes (Table S 4). Given the size of the GO annotation dataset, supplemental Table S 4 is provided as external Excel file.

4.3 Material

4.3.1 Equipment & Software

Table 9: Laboratory Equipment

Name	Manufacturer
Applied Biosystems 7500 Real-Time PCR System	Applied Biosystems
Axio Scan Z.1	Zeiss
BioZero BZ-8100E Mikroskop	Keyence
CASY counter system	Omni Life Science
Culture-Insert 4 Well in µ-Dish 35 mm, high	Ibidi
Eppendorf Thermomixer Compact	Sigma-Aldrich
Heraeus Fresco 21 Mikrozentrifuge	ThermoFisher Scientific
Heraeus Megafuge 40	ThermoFisher Scientific
INTAS Advanced Fluorescence Imager	INTAS
LSR II Fortessa	BD Biosciences
Luminoskan Ascent	ThermoFisher Scientific
Master Cycler nexus gradient	Eppendorf
Mini Trans-Blot Cell	Biorad

Mini-PROTEAN Tetra Vertical Electrophoresis Cell	Biorad
Multiskan FC Mikrotiterplatten-Photometer	ThermoFisher Scientific
NanoDrop 2000/2000c Spektralphotometer	ThermoFisher Scientific
Orbitrap Fusion mass spectrometer	Thermo Fisher Scientific
RP C18 precolumn	Thermo Fisher Scientific
Ultimate 3000 RSLC nano-HPLC system	Thermo Fisher Scientific
µPAC C18 separation column (50 cm)	PharmaFluidics

Table 10: Software

Name	**Manufacturer**
ChemoStar	INTAS
Fiji version 2.14.0	ImageJ
FlowJo version 10	FlowJo, LLC
GraphPad Prism version 10.0.2	Graph Pad
'impute' R package version 1.72.3	Bioconductor
MaxQuant version 2.0.3.0	Max-Planck-Institute of Biochemistry
Xcalibur version 4.3 software	Thermo Fisher Scientific
ZEN	Zeiss
7500 Software version 2.3	Thermo Fisher Scientific

4.3.2 Chemicals, Reagents and Enzymes

Table 11: Chemicals, Kits, Reagents and Enzymes

Name	**Manufacturer**
2-(4-(2-Hydroxyethyl)-1-Piperazinyl)-Ethanesulfonic Acid (HEPES)	Roth
3,3'-Diaminobenzidine Chromogen (DAB)	Sigma-Aldrich
Ammonium Chloride (NH_4CL)	Roth
Ammonium Persulfate (APS)	Sigma-Aldrich

BD AnnexinV-FITC	Thermo Fisher Scientific
Calcium Chloride (CaCl)	Sigma-Aldrich
Calf Serum Albumin (BSA)	Serva
CellTiter-Glo Luminescent Cell Viability Assay	Promega
Complete Protease Inhibitor Cocktail	Roche
Dako Antibody Diluent	Agilent
Desoxy-Nucleotide Triphosphates (dNTPs)	Biozym
Dimethyl Sulfoxide (DMSO)	Roth
Disodium Hydrogen Phosphate (Na_2HPO_4)	Roth
Ethanol Absolute	Sigma-Aldrich
Ethanol Absolute (200 Proof)	Thermo Fisher Scientific
Ethylenediaminetetraacetic Acid (EDTA)	Roth
Fetal Calf Serum (FCS)	Capricorn
Glucose	Sigma-Aldrich
Glutamine	Sigma-Aldrich
Glycerol	Roth
Glycine	Roth
Goat Serum	Vector Laboratories
GoTaq G2 DNA Polymerase	Promega
H_2DCFDA	MedChemExpress
HEPES	Roth
High Select TiO2 Phosphopeptide Enrichment Kit	Thermo Fisher Scientific
Horse Serum	Vector Laboratories
Hydrochloric Acid (HCL)	Roth
Hydrogen Peroxide	Roth
Invitrogen Lipofectamine RNAiMAX Transfection Reagent	Thermo Fisher Scientific
Iodoacetamide	Sigma-Aldrich
Isopropanol	Thermo Fisher Scientific
Luna Universal SYBR Green Supermix	NEB
Magnesium Chloride ($MgCl_2$)	Roth

Magnesium Sulfate ($MgSO_4$)	Roth
Mayer Acidic Haematoxylin	Morphisto
Methanesulfonic Acid	Sigma-Aldrich
Methanol	Honeywell
NucleoSpin RNA	Macherey & Nagel
Nε-(1-Carboxymethyl)-L-lysine (CML)	Cayman Chemical
Omniscript RT Kit	Qiagen
Paraformaldehyde (PFA)	Roth
Penicillin	Thermo Fischer Scientific
Phenylmethansulfonylfluorid (PMSF)	Serva
Phosphatase-Inhibitor-Mix I	Th Geyer
PI/RNase Staining Buffer	BD Biosciences
Pierce Coomassie Plus (Bradford) Assay Kit	Thermo Fisher Scientific
Polyethylene Glycol	Roth
Potassium Chloride (KCl)	Roth
Potassium Dihydrogen Phosphate (KH_2PO_4)	Roth
Potassium Hydrogen Carbonate ($KHCO_3$)	Roth
ProLong Gold with DAPI	Thermo Fisher Scientific
Propidium Iodide Solution	Invitrogen
Proteinase K	Applichem
Pyruvat	Sigma-Aldrich
Restore Western Blot Stripping Buffer	Thermo Fisher Scientific
RNase A	Applichem
RNase-Free DNase Set	Qiagen
Rotenone	Roth
RotiClear	Roth
RotiLoad	Roth
RotiMount	Roth
Rotiphorese Gel 30 (37,5:1)	Roth

Rotiphorese Gel 30 Acrylamide, Bisacrylamide Stock Solution	Roth
SERVALight Helios CL HRP WB Substrat-Kit	SERVA
SERVALight Polaris CL HRP WB Substrat-Kit	SERVA
Skim Milk Powder	Roth
Sodium Chloride (NaCl)	Roth
Sodium Deoxycholic Acid (SDS)	Roth
Sodium Hydrogen Carbonate (NaHCO3)	Roth
Sodium Hydroxide Solution (NaOH)	Roth
Streptavidin	Thermo Fisher Scientific
Tetramethylethylendiamine (TEMED)	Merck
TMT10-plex Isobaric Labeling Reagent Kit	Thermo Fisher Scientific
Tris	Serva
Tris-(2-Carboxyethyl)-Phosphin Hydrochlorid (TCEP)	Roth
Triton X-100	Sigma-Aldrich
Trypsin	Thermo Fisher Scientific
Tunicamycin (TM)	Sigma-Aldrich
Tween-20	Sigma-Aldrich
Urea	Roth
WesternBright Chemilumineszenz Substrat Sirius	Biozym
Xylol	Roth

4.3.3 Oligonucleotide Sequences

Table 12: Oligonucleotide Sequences

Gen	Name	Sequence (5'→ 3')
RPLP0	qRT-RPLP0-for	TGGGCAAGAACACCATGATG
	qRT-RPLP0-rev	AGTTTCTCCAGAGCTGGGTTGT
B2M	qRT-B2M-for	TATGCCTGCCGTGTGAAC
	qRT-B2M-rev	GCATCTTCAAACCTCCATGA

RAGE	qRT-RAGE-for	GGGGCAGTAGTAGGTGCTCA
	qRT-RAGE-rev	GCTGGGGTGGTTTCTTGGG
DDOST	qRT-DDOST-for	TTGGTACCCTTCGGCAGGAGGAGGAA
	qRT-DDOST-rev	AAAGGATCCTTTGAGGGCAACATCTCG
PRKCSH	qRT-PRKCSH-for	CAGACAGACGCCACCTCTTT
	qRT-PRKCSH-rev	GAAGGTGTTGGAAGGTCGGT
Gal-3	qRT-Gal3-for	CAGTTTATCTTCTCCCTGCCCA
	qRT-Gal3-rev	TGGAGAGGTGCCTGAAAGGA

Table 13: siRNA Sequences

siRNA	**Sequence**
Non-targeting siRNA#1	UGGUUUACAUGUCGACUAA
RAGE siRNA Pool	GCUGGCACUUGGAUGGGAAtt
	UGUGUCAGAGGGAAGCUACtt
	GCCAGAAGGUGGAGCAGUAtt
	CCACCUUCUCCUGUAGCUUtt
DDOST siRNA Pool	CAACGUGGAGACCAUCAGUGtt
	GACAAGCCUAUCACCCAGUAUtt
	AUACAGUGUUCAGUUCAAGtt
	CAUCAACGUGGAGACCAUCtt
	GUAUGGUGUAUUCCAGUUUAAtt
	GUGAUCCAGCAGCUCUCAAAUtt
PRKCSH siRNA Pool	AUGACUAUUGCGACUGtt
	AAGUUCAGUGCCAUGAAGUAtt
Gal-3 siRNA Pool	UAAAGUGGAAGGCAACAUCAUUCCCtt
	GCUGACCACUUCAAGGUUGCtt

4.3.4 Antibodies

Table 14: Primary Antibodies

Name	Host	Dilution	Order number	Application	Manufacturer
β-Actin	Mouse	1:10,000	A1978	WB	Sigma
Caspase-3	Rabbit	1:1,000	#9662	WB	Cell Signaling
Caspase-3 cleaved	Rabbit	1:1,000	#9661	WB	Cell Signaling
CHOP	Mouse	1:1,000	#2895	IF	Cell Signaling
DDOST	Rabbit	1:1,000	HPA046841	WB, IHC, IF, Flow	Atlas Antibodies
DDOST	Mouse	1:1,000	H00001650-M06	WB, IHC, IF, Flow	Fisher Scientific
Galectin-3	Rabbit	1:1,000	SAB4501746	WB, Flow	Sigma
RAGE	Rabbit	1:1,000	ab37647	WB	Abcam
RAGE	Rabbit	1:1,000	ab3611	WB	Abcam
RAGE	Mouse	1:1,000	sc-365154	WB	Santa Cruz
PARP	Rabbit	1:1,000	#9542	WB	Cell Signaling
PRKCSH	Rabbit	1:1,000	PA5-27551	WB, Flow	Thermo Scientific

Table 15: Secondary Antibodies

Name	Host	Dilution	Order number	Application	Manufacturer
Secondary Antibody, HRP	Goat anti-Rabbit IgG	1: 10,000	# 31460	WB	Invitrogen
Secondary Antibody, HRP	Goat anti-Mouse IgG	1: 10,000	# 31430	WB	Invitrogen
ImmPRESS HRP	Horse anti-Rabbit IgG	ready-to-use	MP-7801	IHC	Vector Laboratories
ImmPRESS HRP	Horse anti-Mouse IgG	ready-to-use	MP-7802	IHC	Vector Laboratories
Alexa Flour 488 Dye	Goat anti-Rabbit IgG	1: 10,000	# A-11029	IF, Flow	Invitrogen

Alexa Flour 488 Dye	Goat anti-Mouse IgG	1: 10,000	# A-11001	IF, Flow	Invitrogen
Alexa Flour 594 Dye	Goat anti-Rabbit IgG	1: 10,000	# A-11012	IF, Flow	Invitrogen
Alexa Flour 594 Dye	Goat anti-Mouse IgG	1: 10,000	# A-11005	IF, Flow	Invitrogen

4.3.5 Cell Lines

Table 16: Cell Lines

Name	**Cell type**	**DSMZ no.:**
BXPC-3	Human, primary pancreatic adenocarcinoma	ACC 760
PA-TU-8988T	Human, liver metastasis of a primary pancreatic adenocarcinoma	ACC 162
PANC-1	Human, ductal cells of a tumor located in the head of the pancreas	ACC 783
MIA-PACA-2	Human, tumor tissue of undifferentiated pancreatic carcinoma	ACC 733

5 References

Aebi, M. (2013). N-linked protein glycosylation in the ER. *Biochimica et Biophysica Acta (BBA) - Molecular Cell Research*, *1833*(11), 2430–2437. https://doi.org/10.1016/j.bbamcr.2013.04.001

Ahmed, R., Anam, K., & Ahmed, H. (2023). Development of Galectin-3 Targeting Drugs for Therapeutic Applications in Various Diseases. *International Journal of Molecular Sciences*, *24*(9), 8116. https://doi.org/10.3390/ijms24098116

Akirav, E. M., Preston-Hurlburt, P., Garyu, J., Henegariu, O., Clynes, R., Schmidt, A. M., & Herold, K. C. (2012). RAGE Expression in Human T Cells: A Link between Environmental Factors and Adaptive Immune Responses. *PLoS ONE*, *7*(4), e34698. https://doi.org/10.1371/journal.pone.0034698

Al Kafri, N., & Hafizi, S. (2020). Galectin-3 Stimulates Tyro3 Receptor Tyrosine Kinase and Erk Signalling, Cell Survival and Migration in Human Cancer Cells. *Biomolecules*, *10*(7), 1035. https://doi.org/10.3390/biom10071035

Aldini, G., Vistoli, G., Stefek, M., Chondrogianni, N., Grune, T., Sereikaite, J., Sadowska-Bartosz, I., & Bartosz, G. (2013). Molecular strategies to prevent, inhibit, and degrade advanced glycoxidation and advanced lipoxidation end products. *Free Radical Research*, *47*(sup1), 93–137. https://doi.org/10.3109/10715762.2013.792926

Andea, A., Sarkar, F., & Adsay, V. N. (2003). Clinicopathological correlates of pancreatic intraepithelial neoplasia: A comparative analysis of 82 cases with and 152 cases without pancreatic ductal adenocarcinoma. *Modern Pathology: An Official Journal of the United States and Canadian Academy of Pathology, Inc*, *16*(10), 996–1006. https://doi.org/10.1097/01.MP.0000087422.24733.62

Apweiler, R., Hermjakob, H., & Sharon, N. (1999). On the frequency of protein glycosylation, as deduced from analysis of the SWISS-PROT database. *Biochimica Et Biophysica Acta*, *1473*(1), 4–8. https://doi.org/10.1016/s0304-4165(99)00165-8

Araki, N., Higashi, T., Mori, T., Shibayama, R., Kawabe, Y., Kodama, T., Takahashi, K., Shichiri, M., & Horiuchi, S. (1995). Macrophage Scavenger Receptor Mediates the Endocytic Uptake and Degradation of Advanced Glycation End Products of the Maillard Reaction. *European Journal of Biochemistry*, *230*(2), 408–415. https://doi.org/10.1111/j.1432-1033.1995.0408h.x

Arendt, C. W., & Ostergaard, H. L. (1997). Identification of the CD45-associated 116-kDa and 80-kDa Proteins as the α- and β-Subunits of α-Glucosidase II *. *Journal of Biological Chemistry*, *272*(20), 13117–13125. https://doi.org/10.1074/jbc.272.20.13117

Arendt, C. W., & Ostergaard, H. L. (2000). Two distinct domains of the β-subunit of glucosidase II interact with the catalytic α-subunit. *Glycobiology*, *10*(5), 487–492. https://doi.org/10.1093/glycob/10.5.487

Arnold, M., Abnet, C. C., Neale, R. E., Vignat, J., Giovannucci, E. L., McGlynn, K. A., & Bray, F. (2020). Global Burden of 5 Major Types of Gastrointestinal Cancer. *Gastroenterology*, *159*(1), 335-349.e15. https://doi.org/10.1053/j.gastro.2020.02.068

Ashburner, M., Ball, C. A., Blake, J. A., Botstein, D., Butler, H., Cherry, J. M., Davis, A. P., Dolinski, K., Dwight, S. S., Eppig, J. T., Harris, M. A., Hill, D. P., Issel-Tarver, L., Kasarskis, A., Lewis, S., Matese, J. C., Richardson, J. E., Ringwald, M., Rubin, G. M., & Sherlock, G. (2000). Gene Ontology: Tool for the unification of biology. *Nature Genetics*, *25*(1), 25–29. https://doi.org/10.1038/75556

Atkinson, M. A., Campbell-Thompson, M., Kusmartseva, I., & Kaestner, K. H. (2020). Organisation of the human pancreas in health and in diabetes. *Diabetologia*, *63*(10), 1966–1973. https://doi.org/10.1007/s00125-020-05203-7

Avery, N. C., & Bailey, A. J. (2006). The effects of the Maillard reaction on the physical properties and cell interactions of collagen. *Pathologie Biologie*, *54*(7), 387–395. https://doi.org/10.1016/j.patbio.2006.07.005

Azizan, N., Suter, M. A., Liu, Y., & Logsdon, C. D. (2017). RAGE maintains high levels of NFκB and oncogenic Kras activity in pancreatic cancer. *Biochemical and Biophysical Research Communications*, *493*(1), 592–597. https://doi.org/10.1016/j.bbrc.2017.08.147

Bai, L., Wang, T., Zhao, G., Kovach, A., & Li, H. (2018). The atomic structure of a eukaryotic oligosaccharyltransferase complex. *Nature*, *555*(7696), 328–333. https://doi.org/10.1038/nature25755

Barman, S. A., Li, X., Haigh, S., Kondrikov, D., Mahboubi, K., Bordan, Z., Stepp, D. W., Zhou, J., Wang, Y., Weintraub, D. S., Traber, P., Snider, W., Jonigk, D., Sullivan, J., Crislip, G. R., Butcher, J. T., Thompson, J., Su, Y., Chen, F., & Fulton, D. J. R. (2019). Galectin-3 is expressed in vascular smooth muscle cells and promotes pulmonary hypertension through changes in proliferation, apoptosis, and fibrosis. *American Journal of Physiology - Lung Cellular and Molecular Physiology*, *316*(5), L784–L797. https://doi.org/10.1152/ajplung.00186.2018

Barondes, S. H., Cooper, D. N., Gitt, M. A., & Leffler, H. (1994). Galectins. Structure and function of a large family of animal lectins. *Journal of Biological Chemistry*, *269*(33), 20807–20810. https://doi.org/10.1016/S0021-9258(17)31891-4

Baumgart, M., Werther, M., Bockholt, A., Scheurer, M., Rüschoff, J., Dietmaier, W., Ghadimi, B. M., & Heinmöller, E. (2010). Genomic Instability at Both the Base Pair Level and the Chromosomal Level Is Detectable in Earliest PanIN Lesions in Tissues of Chronic Pancreatitis. *Pancreas*, *39*(7), 1093. https://doi.org/10.1097/MPA.0b013e3181dc62f6

Bause, E. (1983). Structural requirements of N-glycosylation of proteins. Studies with proline peptides as conformational probes. *The Biochemical Journal*, *209*(2), 331–336. https://doi.org/10.1042/bj2090331

Bazzichetto, C., Conciatori, F., Luchini, C., Simionato, F., Santoro, R., Vaccaro, V., Corbo, V., Falcone, I., Ferretti, G., Cognetti, F., Melisi, D., Scarpa, A., Ciuffreda, L., & Milella, M. (2020). From Genetic Alterations to Tumor Microenvironment: The Ariadne's String in Pancreatic Cancer. *Cells*, *9*(2), 309. https://doi.org/10.3390/cells9020309

Benitz, S., Regel, I., Reinhard, T., Popp, A., Schäffer, I., Raulefs, S., Kong, B., Esposito, I., Michalski, C. W., & Kleeff, J. (2015). Polycomb repressor complex 1 promotes gene silencing through H2AK119 mono-ubiquitination in acinar-to-ductal metaplasia and pancreatic cancer cells. *Oncotarget*, *7*(10), 11424–11433. https://doi.org/10.18632/oncotarget.6717

Bierhaus, A., Humpert, P. M., Morcos, M., Wendt, T., Chavakis, T., Arnold, B., Stern, D. M., & Nawroth, P. P. (2005). Understanding RAGE, the receptor for advanced glycation end products. *Journal of Molecular Medicine (Berlin, Germany)*, *83*(11), 876–886. https://doi.org/10.1007/s00109-005-0688-7

Böhme, R., Becker, C., Keil, B., Damm, M., Rasch, S., Beer, S., Schneider, R., Kovacs, P., Bugert, P., Riedel, J., Griesmann, H., Ruffert, C., Kaune, T., Michl, P., Hesselbarth, N., & Rosendahl, J. (2020). Serum levels of advanced glycation end products and their receptors sRAGE and Galectin-3 in chronic pancreatitis. *Pancreatology*, *20*(2), 187–192. https://doi.org/10.1016/j.pan.2019.12.013

Botrus, G., Miller, R. M., Uson Junior, P. L. S., Kannan, G., Han, H., & Von Hoff, D. D. (2022). Increasing Stress to Induce Apoptosis in Pancreatic Cancer via the Unfolded Protein Response (UPR). *International Journal of Molecular Sciences*, *24*(1), 577. https://doi.org/10.3390/ijms24010577

Bouffette, S., Botez, I., & Ceuninck, F. D. (2023). Targeting galectin-3 in inflammatory and fibrotic diseases. *Trends in Pharmacological Sciences*, *44*(8), 519–531. https://doi.org/10.1016/j.tips.2023.06.001

Braach, N., Frommhold, D., Buschmann, K., Pflaum, J., Koch, L., Hudalla, H., Staudacher, K., Wang, H., Isermann, B., Nawroth, P., & Poeschl, J. (2014). RAGE controls activation and anti-inflammatory signalling of protein C. *PloS One*, *9*(2), e89422. https://doi.org/10.1371/journal.pone.0089422

Bray, F., Ferlay, J., Soerjomataram, I., Siegel, R. L., Torre, L. A., & Jemal, A. (2018). Global cancer statistics 2018: GLOBOCAN estimates of incidence and mortality worldwide for 36 cancers in 185 countries. *CA: A Cancer Journal for Clinicians*, *68*(6), 394–424. https://doi.org/10.3322/caac.21492

Brett, J., Schmidt, A. M., Yan, S. D., Zou, Y. S., Weidman, E., Pinsky, D., Nowygrod, R., Neeper, M., Przysiecki, C., Shaw, A., Migheli, A., & Stern, D. (1993). Survey of the Distribution of a Newly Characterized Receptor for Advanced Glycation End Products in Tissues. *The American Journal of Pathology*, *143*(6), 1699–1712.

Brownlee, M. (1995). Advanced protein glycosylation in diabetes and aging. *Annual Review of Medicine*, *46*, 223–234. https://doi.org/10.1146/annurev.med.46.1.223

Brownlee, M., Vlassara, H., & Cerami, A. (1984). Nonenzymatic Glycosylation and the Pathogenesis of Diabetic Complications. *Annals of Internal Medicine*, *101*(4), 527–537. https://doi.org/10.7326/0003-4819-101-4-527

Burguillos, M. A., Svensson, M., Schulte, T., Boza-Serrano, A., Garcia-Quintanilla, A., Kavanagh, E., Santiago, M., Viceconte, N., Oliva-Martin, M. J., Osman, A. M., Salomonsson, E., Amar, L., Persson, A., Blomgren, K., Achour, A., Englund, E., Leffler, H., Venero, J. L., Joseph, B., & Deierborg, T. (2015). Microglia-Secreted Galectin-3 Acts as a Toll-like Receptor 4 Ligand and Contributes to Microglial Activation. *Cell Reports*, *10*(9), 1626–1638. https://doi.org/10.1016/j.celrep.2015.02.012

Cai, W., He, J. C., Zhu, L., Lu, C., & Vlassara, H. (2006). Advanced glycation end product (AGE) receptor 1 suppresses cell oxidant stress and activation signaling via EGF receptor. *Proceedings of the National Academy of Sciences of the United States of America*, *103*(37), 13801–13806. https://doi.org/10.1073/pnas.0600362103

Cai, W., Torreggiani, M., Zhu, L., Chen, X., He, J. C., Striker, G. E., & Vlassara, H. (2010). AGER1 regulates endothelial cell NADPH oxidase-dependent oxidant stress via PKC-δ: Implications for vascular disease. *American Journal of Physiology - Cell Physiology*, *298*(3), C624–C634. https://doi.org/10.1152/ajpcell.00463.2009

Chang, X., Pan, J., Zhao, R., Yan, T., Wang, X., Guo, C., Yang, Y., & Wang, G. (2022). DDOST Correlated with Malignancies and Immune Microenvironment in Gliomas. *Frontiers in Immunology*, *13*, 917014. https://doi.org/10.3389/fimmu.2022.917014

Chaudhuri, J., Bains, Y., Guha, S., Kahn, A., Hall, D., Bose, N., Gugliucci, A., & Kapahi, P. (2018). The Role of Advanced Glycation End Products in Aging and Metabolic Diseases: Bridging Association and Causality. *Cell Metabolism*, *28*(3), 337–352. https://doi.org/10.1016/j.cmet.2018.08.014

Chen, M.-C., Chen, K.-C., Chang, G.-C., Lin, H., Wu, C.-C., Kao, W.-H., Teng, C.-L. J., Hsu, S.-L., & Yang, T.-Y. (2020). RAGE acts as an oncogenic role and promotes the metastasis of human lung cancer. *Cell Death & Disease*, *11*(4), Article 4. https://doi.org/10.1038/s41419-020-2432-1

Clarke, R. E., Dordevic, A. L., Tan, S. M., Ryan, L., & Coughlan, M. T. (2016). Dietary Advanced Glycation End Products and Risk Factors for Chronic Disease: A Systematic Review of Randomised Controlled Trials. *Nutrients*, *8*(3), 125. https://doi.org/10.3390/nu8030125

Cnossen, W. R., Maurits, J. S. F., Salomon, J., te Morsche, R. H. M., Waanders, E., & Drenth, J. P. H. (2015). Severe Polycystic Liver Disease Is Not Caused by Large Deletions of the PRKCSH Gene. *Journal of Clinical Laboratory Analysis*, *30*(5), 431–436. https://doi.org/10.1002/jcla.21875

Collins, M. A., Yan, W., Sebolt–Leopold, J. S., & di Magliano, M. P. (2014). Mapk Signaling Is Required for Dedifferentiation of Acinar Cells and Development of Pancreatic Intraepithelial Neoplasia in Mice. *Gastroenterology*, *146*(3), 822-834.e7. https://doi.org/10.1053/j.gastro.2013.11.052

Cornec-Le Gall, E., Torres, V. E., & Harris, P. C. (2018). Genetic Complexity of Autosomal Dominant Polycystic Kidney and Liver Diseases. *Journal of the American Society of Nephrology : JASN*, *29*(1), 13–23. https://doi.org/10.1681/ASN.2017050483

Coussens, L. M., & Werb, Z. (2002). Inflammation and cancer. *Nature*, *420*(6917), 860–867. https://doi.org/10.1038/nature01322

Cui, J., Huang, W., Wu, B., Jin, J., Jing, L., Shi, W.-P., Liu, Z.-Y., Yuan, L., Luo, D., Li, L., Chen, Z.-N., & Jiang, J.-L. (2018). N-glycosylation by N-acetylglucosaminyltransferase V enhances the interaction of CD147/basigin with integrin β1 and promotes HCC metastasis. *The Journal of Pathology*, *245*(1), 41–52. https://doi.org/10.1002/path.5054

D'Alessio, C., Fernández, F., Trombetta, E. S., & Parodi, A. J. (1999). Genetic Evidence for the Heterodimeric Structure of Glucosidase II: THE EFFECT OF DISRUPTING THE SUBUNIT-ENCODING GENES ON GLYCOPROTEIN FOLDING *. *Journal of Biological Chemistry*, *274*(36), 25899–25905. https://doi.org/10.1074/jbc.274.36.25899

Desmedt, V., Desmedt, S., Delanghe, J. R., Speeckaert, R., & Speeckaert, M. M. (2016). Galectin-3 in Renal Pathology: More Than Just an Innocent Bystander. *American Journal of Nephrology*, *43*(5), 305–317. https://doi.org/10.1159/000446376

Díaz-Alvarez, L., & Ortega, E. (2017). The Many Roles of Galectin-3, a Multifaceted Molecule, in Innate Immune Responses against Pathogens. *Mediators of Inflammation*, *2017*, 9247574. https://doi.org/10.1155/2017/9247574

Dickinson, M. E., Flenniken, A. M., Ji, X., Teboul, L., Wong, M. D., White, J. K., Meehan, T. F., Weninger, W. J., Westerberg, H., Adissu, H., Baker, C. N., Bower, L., Brown, J. M., Caddle, L. B., Chiani, F., Clary, D., Cleak, J., Daly, M. J., Denegre, J. M., … Murray, S. A. (2016). High-throughput discovery of novel developmental phenotypes. *Nature*, *537*(7621), 508–514. https://doi.org/10.1038/nature19356

Digomann, D., Kurth, I., Tyutyunnykova, A., Chen, O., Löck, S., Gorodetska, I., Peitzsch, C., Skvortsova, I.-I., Negro, G., Aschenbrenner, B., Eisenhofer, G., Richter, S., Heiden, S., Porrmann, J., Klink, B., Schwager, C., Dowle, A. A., Hein, L., Kunz-Schughart, L. A., … Dubrovska, A. (2019). The CD98 Heavy Chain Is a Marker and Regulator of Head and Neck Squamous Cell Carcinoma Radiosensitivity. *Clinical Cancer Research*, *25*(10), 3152–3163. https://doi.org/10.1158/1078-0432.CCR-18-2951

Ding, J., Xu, J., Deng, Q., Ma, W., Zhang, R., He, X., Liu, S., & Zhang, L. (2021). Knockdown of Oligosaccharyltransferase Subunit Ribophorin 1 Induces Endoplasmic-Reticulum-Stress-Dependent Cell Apoptosis in Breast Cancer. *Frontiers in Oncology*, *11*, 722624. https://doi.org/10.3389/fonc.2021.722624

DiNorcia, J., Lee, M. K., Moroziewicz, D. N., Winner, M., Suman, P., Bao, F., Remotti, H. E., Zou, Y. S., Yan, S. F., Qiu, W., Su, G. H., Schmidt, A. M., & Allendorf, J. D. (2012). RAGE Gene Deletion Inhibits the Development and Progression of Ductal Neoplasia and Prolongs Survival in a Murine Model of Pancreatic Cancer. *Journal of Gastrointestinal Surgery*, *16*(1), 104–112. https://doi.org/10.1007/s11605-011-1754-9

Drenth, J. P. H., te Morsche, R. H. M., Smink, R., Bonifacino, J. S., & Jansen, J. B. M. J. (2003). Germline mutations in PRKCSH are associated with autosomal dominant polycystic liver disease. *Nature Genetics*, *33*(3), Article 3. https://doi.org/10.1038/ng1104

Du, Y., Miao, W., Jiang, X., Cao, J., Wang, B., Wang, Y., Yu, J., Wang, X., & Liu, H. (2021). The Epithelial to Mesenchymal Transition Related Gene Calumenin Is an Adverse Prognostic Factor of Bladder Cancer Correlated With Tumor Microenvironment Remodeling, Gene Mutation, and Ferroptosis. *Frontiers in Oncology*, *11*, 683951. https://doi.org/10.3389/fonc.2021.683951

Dumic, J., Dabelic, S., & Flögel, M. (2006). Galectin-3: An open-ended story. *Biochimica et Biophysica Acta (BBA) - General Subjects*, *1760*(4), 616–635. https://doi.org/10.1016/j.bbagen.2005.12.020

Dyer, D. G., Blackledge, J. A., Katz, B. M., Hull, C. J., Adkisson, H. D., Thorpe, S. R., Lyons, T. J., & Baynes, J. W. (1991). The Maillard reaction in vivo. *Zeitschrift Fur Ernahrungswissenschaft*, *30*(1), 29–45. https://doi.org/10.1007/BF01910730

Ellgaard, L., Molinari, M., & Helenius, A. (1999). Setting the standards: Quality control in the secretory pathway. *Science (New York, N.Y.)*, *286*(5446), 1882–1888. https://doi.org/10.1126/science.286.5446.1882

Elola, M. T., Wolfenstein-Todel, C., Troncoso, M. F., Vasta, G. R., & Rabinovich, G. A. (2007). Galectins: Matricellular glycan-binding proteins linking cell adhesion, migration, and survival. *Cellular and Molecular Life Sciences: CMLS*, *64*(13), 1679–1700. https://doi.org/10.1007/s00018-007-7044-8

Eser, S., Reiff, N., Messer, M., Seidler, B., Gottschalk, K., Dobler, M., Hieber, M., Arbeiter, A., Klein, S., Kong, B., Michalski, C. W., Schlitter, A. M., Esposito, I., Kind, A. J., Rad, L., Schnieke, A. E., Baccarini, M., Alessi, D. R., Rad, R., … Saur, D. (2013). Selective Requirement of PI3K/PDK1 Signaling for Kras Oncogene-Driven Pancreatic Cell Plasticity and Cancer. *Cancer Cell*, *23*(3), 406–420. https://doi.org/10.1016/j.ccr.2013.01.023

Esmail, S., & Manolson, M. F. (2021). Advances in understanding N-glycosylation structure, function, and regulation in health and disease. *European Journal of Cell Biology*, *100*(7), 151186. https://doi.org/10.1016/j.ejcb.2021.151186

Falcone, C., Bozzini, S., Guasti, L., D'Angelo, A., Capettini, A. C., Paganini, E. M., Falcone, R., Moia, R., Gazzaruso, C., & Pelissero, G. (2013). Soluble RAGE Plasma Levels in Patients with Coronary Artery Disease and Peripheral Artery Disease. *The Scientific World Journal*, *2013*, 584504. https://doi.org/10.1155/2013/584504

Faruqui, T., Khan, M. S., Akhter, Y., Khan, S., Rafi, Z., Saeed, M., Han, I., Choi, E.-H., & Yadav, D. K. (2022). RAGE Inhibitors for Targeted Therapy of Cancer: A Comprehensive Review. *International Journal of Molecular Sciences*, *24*(1), 266. https://doi.org/10.3390/ijms24010266

Ferlay, J., Partensky, C., & Bray, F. (2016). More deaths from pancreatic cancer than breast cancer in the EU by 2017. *Acta Oncologica (Stockholm, Sweden)*, *55*(9–10), 1158–1160. https://doi.org/10.1080/0284186X.2016.1197419

Freeze, H. H. (1998). Disorders in protein glycosylation and potential therapy: Tip of an iceberg? *The Journal of Pediatrics*, *133*(5), 593–600. https://doi.org/10.1016/s0022-3476(98)70096-4

Gan, Y., Ye, F., & He, X.-X. (2020). The role of YWHAZ in cancer: A maze of opportunities and challenges. *Journal of Cancer*, *11*(8), 2252–2264. https://doi.org/10.7150/jca.41316

Gao, X., Balan, V., Tai, G., & Raz, A. (2014). Galectin-3 induces cell migration via a calcium-sensitive MAPK/ERK1/2 pathway. *Oncotarget*, *5*(8), 2077–2084.

Gautieri, A., Passini, F. S., Silván, U., Guizar-Sicairos, M., Carimati, G., Volpi, P., Moretti, M., Schoenhuber, H., Redaelli, A., Berli, M., & Snedeker, J. G. (2017). Advanced glycation end-products: Mechanics of aged collagen from molecule to tissue. *Matrix Biology: Journal of the International Society for Matrix Biology*, *59*, 95–108. https://doi.org/10.1016/j.matbio.2016.09.001

Gawandi, S., Gangawane, S., Chakrabarti, A., Kedare, S., Bantwal, K., Wadhe, V., Kulkarni, A., Kulkarni, S., & Rajan, M. G. R. (2018). A Study of Microalbuminuria (MAU) and Advanced Glycation End Products (AGEs) Levels in Diabetic and Hypertensive Subjects. *Indian Journal of Clinical Biochemistry: IJCB*, *33*(1), 81–85. https://doi.org/10.1007/s12291-017-0638-5

Grazier, J. J., & Sylvester, P. W. (2022). Role of Galectins in Metastatic Breast Cancer. In H. N. Mayrovitz (Ed.), *Breast Cancer*. Exon Publications. http://www.ncbi.nlm.nih.gov/books/NBK583815/

Guerra, C., Schuhmacher, A. J., Cañamero, M., Grippo, P. J., Verdaguer, L., Pérez-Gallego, L., Dubus, P., Sandgren, E. P., & Barbacid, M. (2007). Chronic Pancreatitis Is Essential for Induction of Pancreatic Ductal Adenocarcinoma by K-Ras Oncogenes in Adult Mice. *Cancer Cell*, *11*(3), 291–302. https://doi.org/10.1016/j.ccr.2007.01.012

Guo, H.-B., Johnson, H., Randolph, M., & Pierce, M. (2009). Regulation of homotypic cell-cell adhesion by branched N-glycosylation of N-cadherin extracellular EC2 and EC3 domains. *The Journal of Biological Chemistry*, *284*(50), 34986–34997. https://doi.org/10.1074/jbc.M109.060806

Habtezion, A., Gukovskaya, A. S., & Pandol, S. J. (2019). Acute Pancreatitis: A Multifaceted Set of Organelle and Cellular Interactions. *Gastroenterology*, *156*(7), 1941–1950. https://doi.org/10.1053/j.gastro.2018.11.082

Hamieh, A., Cartier, D., Abid, H., Calas, A., Burel, C., Bucharles, C., Jehan, C., Grumolato, L., Landry, M., Lerouge, P., Anouar, Y., & Lihrmann, I. (2017). Selenoprotein T is a novel OST subunit that regulates UPR signaling and hormone secretion. *EMBO Reports*, *18*(11), 1935–1946. https://doi.org/10.15252/embr.201643504

Hastie, T., Tibshirani, R., Narasimhan, B., & Chu, G. (2023, April 10). *impute: Imputation for microarray data*. https://www.bioconductor.org/packages/release/bioc/manuals/impute/man/impute.pdf

Hayes, J. D., Dinkova-Kostova, A. T., & Tew, K. D. (2020). Oxidative Stress in Cancer. *Cancer Cell*, *38*(2), 167–197. https://doi.org/10.1016/j.ccell.2020.06.001

Henle, T. (2005). Protein-bound advanced glycation endproducts (AGEs) as bioactive amino acid derivatives in foods. *Amino Acids*, *29*(4), 313–322. https://doi.org/10.1007/s00726-005-0200-2

Herold, K., Moser, B., Chen, Y., Zeng, S., Yan, S. F., Ramasamy, R., Emond, J., Clynes, R., & Schmidt, A. M. (2007). Receptor for advanced glycation end products (RAGE) in a dash to the rescue: Inflammatory signals gone awry in the primal response to stress. *Journal of Leukocyte Biology*, *82*(2), 204–212. https://doi.org/10.1189/jlb.1206751

Hill, R., Calvopina, J. H., Kim, C., Wang, Y., Dawson, D. W., Donahue, T. R., Dry, S., & Wu, H. (2010). PTEN Loss Accelerates K-RASG12D-Induced Pancreatic Cancer Development. *Cancer Research*, *70*(18), 7114–7124. https://doi.org/10.1158/0008-5472.CAN-10-1649

Hirai, M., & Shimizu, N. (1990). Purification of two distinct proteins of approximate Mr 80,000 from human epithelial cells and identification as proper substrates for protein kinase C. *Biochemical Journal*, *270*(3), 583–589.

Honjo, Y., Nangia-Makker, P., Inohara, H., & Raz, A. (2001). Down-regulation of galectin-3 suppresses tumorigenicity of human breast carcinoma cells. *Clinical Cancer Research: An Official Journal of the American Association for Cancer Research*, *7*(3), 661–668.

Hoque, R., Malik, A. F., Gorelick, F., & Mehal, W. Z. (2012). Sterile inflammatory response in acute pancreatitis. *Pancreas*, *41*(3), 353–357. https://doi.org/10.1097/MPA.0b013e3182321500

Hori, O., Brett, J., Slattery, T., Cao, R., Zhang, J., Chen, J. X., Nagashima, M., Lundh, E. R., Vijay, S., Nitecki, D., Morser, J., Stern, D., & Schmidt, A. M. (1995). The Receptor for Advanced Glycation End Products (RAGE) Is a Cellular Binding Site for Amphoterin: MEDIATION OF NEURITE OUTGROWTH AND CO-EXPRESSION OF RAGE AND AMPHOTERIN IN THE DEVELOPING NERVOUS SYSTEM (∗). *Journal of Biological Chemistry*, *270*(43), 25752–25761. https://doi.org/10.1074/jbc.270.43.25752

Hosoda, W., Chianchiano, P., Griffin, J. F., Pittman, M. E., Brosens, L. A., Noë, M., Yu, J., Shindo, K., Suenaga, M., Rezaee, N., Yonescu, R., Ning, Y., Albores-Saavedra, J.,

Yoshizawa, N., Harada, K., Yoshizawa, A., Hanada, K., Yonehara, S., Shimizu, M., … Wood, L. D. (2017). Genetic analyses of isolated high-grade pancreatic intraepithelial neoplasia (HG-PanIN) reveal paucity of alterations in TP53 and SMAD4. *The Journal of Pathology*, *242*(1), 16–23. https://doi.org/10.1002/path.4884

Hrynchyshyn, N., Jourdain, P., Desnos, M., Diebold, B., & Funck, F. (2013). Galectin-3: A new biomarker for the diagnosis, analysis and prognosis of acute and chronic heart failure. *Archives of Cardiovascular Diseases*, *106*(10), 541–546. https://doi.org/10.1016/j.acvd.2013.06.054

Imperiali, B., & O'Connor, S. E. (1999). Effect of N-linked glycosylation on glycopeptide and glycoprotein structure. *Current Opinion in Chemical Biology*, *3*(6), 643–649. https://doi.org/10.1016/s1367-5931(99)00021-6

In't Veld, P., & Marichal, M. (2010). Microscopic Anatomy of the Human Islet of Langerhans. In Md. S. Islam (Ed.), *The Islets of Langerhans* (pp. 1–19). Springer Netherlands. https://doi.org/10.1007/978-90-481-3271-3_1

Ishino, K., Kudo, M., Peng, W.-X., Kure, S., Kawahara, K., Teduka, K., Kawamoto, Y., Kitamura, T., Fujii, T., Yamamoto, T., Wada, R., & Naito, Z. (2018). 2-Deoxy-d-glucose increases GFAT1 phosphorylation resulting in endoplasmic reticulum-related apoptosis via disruption of protein N-glycosylation in pancreatic cancer cells. *Biochemical and Biophysical Research Communications*, *501*(3), 668–673. https://doi.org/10.1016/j.bbrc.2018.05.041

Jakuš, V., & Rietbrock, N. (2004). Advanced glycation end-products and the progress of diabetic vascular complications. *Physiological Research*, 131–142. https://doi.org/10.33549/physiolres.930430

Jiang, K., Lawson, D., Cohen, C., & Siddiqui, M. T. (2014). Galectin-3 and PTEN expression in pancreatic ductal adenocarcinoma, pancreatic neuroendocrine neoplasms and gastrointestinal tumors on fine-needle aspiration cytology. *Acta Cytologica*, *58*(3), 281–287. https://doi.org/10.1159/000362221

Jiang, L., Wang, M., Lin, S., Jian, R., Li, X., Chan, J., Dong, G., Fang, H., Robinson, A. E., GTEx Consortium, & Snyder, M. P. (2020). A Quantitative Proteome Map of the Human Body. *Cell*, *183*(1), 269-283.e19. https://doi.org/10.1016/j.cell.2020.08.036

Jones, M. A., Ng, B. G., Bhide, S., Chin, E., Rhodenizer, D., He, P., Losfeld, M.-E., He, M., Raymond, K., Berry, G., Freeze, H. H., & Hegde, M. R. (2012). DDOST Mutations Identified by Whole-Exome Sequencing Are Implicated in Congenital Disorders of Glycosylation. *American Journal of Human Genetics*, *90*(2), 363–368. https://doi.org/10.1016/j.ajhg.2011.12.024

Jones, S., Zhang, X., Parsons, D. W., Lin, J. C.-H., Leary, R. J., Angenendt, P., Mankoo, P., Carter, H., Kamiyama, H., Jimeno, A., Hong, S.-M., Fu, B., Lin, M.-T., Calhoun, E. S., Kamiyama, M., Walter, K., Nikolskaya, T., Nikolsky, Y., Hartigan, J., … Kinzler, K. W. (2008). Core Signaling Pathways in Human Pancreatic Cancers Revealed by

Global Genomic Analyses. *Science (New York, N.Y.)*, *321*(5897), 1801–1806. https://doi.org/10.1126/science.1164368

Jono, T., Miyazaki, A., Nagai, R., Sawamura, T., Kitamura, T., & Horiuchi, S. (2002). Lectin-like oxidized low density lipoprotein receptor-1 (LOX-1) serves as an endothelial receptor for advanced glycation end products (AGE). *FEBS Letters*, *511*(1–3), 170–174. https://doi.org/10.1016/S0014-5793(01)03325-7

Kaczmarek, A., Vandenabeele, P., & Krysko, D. V. (2013). Necroptosis: The release of damage-associated molecular patterns and its physiological relevance. *Immunity*, *38*(2), 209–223. https://doi.org/10.1016/j.immuni.2013.02.003

Kang, R., Tang, D., Schapiro, N., Loux, T., Livesey, K., Billiar, T., Wang, H., Van Houten, B., Lotze, M., & Zeh, H. (2014). The HMGB1/RAGE inflammatory pathway promotes pancreatic tumor growth by regulating mitochondrial bioenergetics. *Oncogene*, *33*(5), 567–577. https://doi.org/10.1038/onc.2012.631

Katakami, N. (2017). Can soluble receptor for advanced glycation end-product (sRAGE) levels in blood be used as a predictor of cardiovascular diseases? *Atherosclerosis*, *266*, 223–225. https://doi.org/10.1016/j.atherosclerosis.2017.09.007

Khaodee, W., Udomsom, S., Kunnaja, P., & Cressey, R. (2019). Knockout of glucosidase II beta subunit inhibits growth and metastatic potential of lung cancer cells by inhibiting receptor tyrosine kinase activities. *Scientific Reports*, *9*, 10394. https://doi.org/10.1038/s41598-019-46701-y

Ko, F. C. F., Yan, S., Lee, K. W., Lam, S. K., & Ho, J. C. M. (2023). Chimera and Tandem-Repeat Type Galectins: The New Targets for Cancer Immunotherapy. *Biomolecules*, *13*(6), 902. https://doi.org/10.3390/biom13060902

Kocsis, A. K., Szabolcs, A., Hofner, P., Takács, T., Farkas, G., Boda, K., & Mándi, Y. (2009). Plasma concentrations of high-mobility group box protein 1, soluble receptor for advanced glycation end-products and circulating DNA in patients with acute pancreatitis. *Pancreatology: Official Journal of the International Association of Pancreatology (IAP) ... [et Al.]*, *9*(4), 383–391. https://doi.org/10.1159/000181172

Kojima, K., Vickers, S. M., Adsay, N. V., Jhala, N. C., Kim, H.-G., Schoeb, T. R., Grizzle, W. E., & Klug, C. A. (2007). Inactivation of Smad4 Accelerates KrasG12D-Mediated Pancreatic Neoplasia. *Cancer Research*, *67*(17), 8121–8130. https://doi.org/10.1158/0008-5472.CAN-06-4167

Kong, X., Lu, A.-L., Yao, X.-M., Hua, Q., Li, X.-Y., Qin, L., Zhang, H.-M., Meng, G.-X., & Su, Q. (2017). Activation of NLRP3 Inflammasome by Advanced Glycation End Products Promotes Pancreatic Islet Damage. *Oxidative Medicine and Cellular Longevity*, *2017*, 9692546. https://doi.org/10.1155/2017/9692546

Leclerc, E., & Vetter, S. W. (2015). The role of S100 proteins and their receptor RAGE in pancreatic cancer. *Biochimica et Biophysica Acta*, *1852*(12), 2706–2711. https://doi.org/10.1016/j.bbadis.2015.09.022

Lee, E. J., & Park, J. H. (2013). Receptor for Advanced Glycation Endproducts (RAGE), Its Ligands, and Soluble RAGE: Potential Biomarkers for Diagnosis and Therapeutic Targets for Human Renal Diseases. *Genomics & Informatics*, *11*(4), 224–229. https://doi.org/10.5808/GI.2013.11.4.224

Legler, K., Rosprim, R., Karius, T., Eylmann, K., Rossberg, M., Wirtz, R. M., Müller, V., Witzel, I., Schmalfeldt, B., Milde-Langosch, K., & Oliveira-Ferrer, L. (2018). Reduced mannosidase MAN1A1 expression leads to aberrant N-glycosylation and impaired survival in breast cancer. *British Journal of Cancer*, *118*(6), 847–856. https://doi.org/10.1038/bjc.2017.472

Lei, R., Zhou, M., Zhang, S., Luo, J., Qu, C., Wang, Y., Guo, P., & Huang, R. (2022). Potential role of PRKCSH in lung cancer: Bioinformatics analysis and a case study of Nano ZnO. *Nanoscale*, *14*(12), 4495–4510. https://doi.org/10.1039/D1NR08133K

Lévy, P., Domínguez-Muñoz, E., Imrie, C., Löhr, M., & Maisonneuve, P. (2014). Epidemiology of chronic pancreatitis: Burden of the disease and consequences. *United European Gastroenterology Journal*, *2*(5), 345–354. https://doi.org/10.1177/2050640614548208

Li, A., Davila, S., Furu, L., Qian, Q., Tian, X., Kamath, P. S., King, B. F., Torres, V. E., & Somlo, S. (2003). Mutations in PRKCSH Cause Isolated Autosomal Dominant Polycystic Liver Disease. *American Journal of Human Genetics*, *72*(3), 691–703.

Li, J., Vasilyeva, E., & Wiseman, S. M. (2019). Beyond immunohistochemistry and immunocytochemistry: A current perspective on galectin-3 and thyroid cancer. *Expert Review of Anticancer Therapy*, *19*(12), 1017–1027. https://doi.org/10.1080/14737140.2019.1693270

Li, Y. M., Mitsuhashi, T., Wojciechowicz, D., Shimizu, N., Li, J., Stitt, A., He, C., Banerjee, D., & Vlassara, H. (1996). Molecular identity and cellular distribution of advanced glycation endproduct receptors: Relationship of p60 to OST-48 and p90 to 80K-H membrane proteins. *Proceedings of the National Academy of Sciences of the United States of America*, *93*(20), 11047–11052. https://doi.org/10.1073/pnas.93.20.11047

Liang, J., & Sun, Z. (2021). Overexpression of membranal SLC3A2 regulates the proliferation of oral squamous cancer cells and affects the prognosis of oral cancer patients. *Journal of Oral Pathology & Medicine: Official Publication of the International Association of Oral Pathologists and the American Academy of Oral Pathology*, *50*(4), 371–377. https://doi.org/10.1111/jop.13132

Lim, S. C., Dorajoo, R., Zhang, X., Wang, L., Ang, S. F., Tan, C. S. H., Yeoh, L. Y., Ng, X. W., Li, N., Su, C., Liu, S., Wong, M. D. S., Low, K. M. S., Yao, A. O., Babitha, J., Fun, S., Zhou, S., Lee, S. B. M., Tang, W. E., … Liu, J.-J. (2017). Genetic variants in the receptor for advanced glycation end products (RAGE) gene were associated with circulating soluble RAGE level but not with renal function among Asians with type 2 diabetes: A genome-wide association study. *Nephrology, Dialysis, Transplantation: Official Publication of the European Dialysis and Transplant*

Association - European Renal Association, *32*(10), 1697–1704. https://doi.org/10.1093/ndt/gfw263

Lindström, O., Tukiainen, E., Kylänpää, L., Mentula, P., Rouhiainen, A., Puolakkainen, P., Rauvala, H., & Repo, H. (2009). Circulating levels of a soluble form of receptor for advanced glycation end products and high-mobility group box chromosomal protein 1 in patients with acute pancreatitis. *Pancreas*, *38*(8), e215-220. https://doi.org/10.1097/MPA.0b013e3181bb59a7

Liu, F.-T., & Rabinovich, G. A. (2005). Galectins as modulators of tumour progression. *Nature Reviews. Cancer*, *5*(1), 29–41. https://doi.org/10.1038/nrc1527

Liu, F.-T., & Stowell, S. R. (2023). The role of galectins in immunity and infection. *Nature Reviews. Immunology*, 1–16. https://doi.org/10.1038/s41577-022-00829-7

Liu, X., Nie, H., Zhang, Y., Yao, Y., Maitikabili, A., Qu, Y., Shi, S., Chen, C., & Li, Y. (2013). Cell surface-specific N-glycan profiling in breast cancer. *PloS One*, *8*(8), e72704. https://doi.org/10.1371/journal.pone.0072704

Liu, Y., Liang, C., Liu, X., Liao, B., Pan, X., Ren, Y., Fan, M., Li, M., He, Z., Wu, J., & Wu, Z. (2010). AGEs increased migration and inflammatory responses of adventitial fibroblasts via RAGE, MAPK and NF-κB pathways. *Atherosclerosis*, *208*(1), 34–42. https://doi.org/10.1016/j.atherosclerosis.2009.06.007

Löhr, J. M., Dominguez-Munoz, E., Rosendahl, J., Besselink, M., Mayerle, J., Lerch, M. M., Haas, S., Akisik, F., Kartalis, N., Iglesias-Garcia, J., Keller, J., Boermeester, M., Werner, J., Dumonceau, J.-M., Fockens, P., Drewes, A., Ceyhan, G., Lindkvist, B., Drenth, J., … HaPanEU/UEG Working Group. (2017). United European Gastroenterology evidence-based guidelines for the diagnosis and therapy of chronic pancreatitis (HaPanEU). *United European Gastroenterology Journal*, *5*(2), 153–199. https://doi.org/10.1177/2050640616684695

Longnecker, D. S., Gorelick, F., & Thompson, E. D. (2018). Anatomy, Histology, and Fine Structure of the Pancreas. In *The Pancreas* (pp. 10–23). John Wiley & Sons, Ltd. https://doi.org/10.1002/9781119188421.ch2

Lowenfels, A. B., & Maisonneuve, P. (2006). Epidemiology and risk factors for pancreatic cancer. *Best Practice & Research Clinical Gastroenterology*, *20*(2), 197–209. https://doi.org/10.1016/j.bpg.2005.10.001

Lowenfels, A. B., & Maisonneuve, P. (2018). Chronic Pancreatitis. In *The Pancreas* (pp. 417–420). John Wiley & Sons, Ltd. https://doi.org/10.1002/9781119188421.ch50

Lu, T.-H., Tseng, T.-J., Su, C.-C., Tang, F.-C., Yen, C.-C., Liu, Y.-Y., Yang, C.-Y., Wu, C.-C., Chen, K.-L., Hung, D.-Z., & Chen, Y.-W. (2014). Arsenic induces reactive oxygen species-caused neuronal cell apoptosis through JNK/ERK-mediated mitochondria-dependent and GRP 78/CHOP-regulated pathways. *Toxicology Letters*, *224*(1), 130–140. https://doi.org/10.1016/j.toxlet.2013.10.013

Ma, Y., & Hendershot, L. M. (2004). The role of the unfolded protein response in tumour development: Friend or foe? *Nature Reviews. Cancer*, *4*(12), 966–977. https://doi.org/10.1038/nrc1505

Maitra, A., Fukushima, N., Takaori, K., & Hruban, R. H. (2005). Precursors to Invasive Pancreatic Cancer. *Advances in Anatomic Pathology*, *12*(2), 81. https://doi.org/10.1097/01.pap.0000155055.14238.25

Mariño, K. V., Cagnoni, A. J., Croci, D. O., & Rabinovich, G. A. (2023). Targeting galectin-driven regulatory circuits in cancer and fibrosis. *Nature Reviews Drug Discovery*, *22*(4), Article 4. https://doi.org/10.1038/s41573-023-00636-2

Marstrand-Daucé, L., Lorenzo, D., Chassac, A., Nicole, P., Couvelard, A., & Haumaitre, C. (2023). Acinar-to-Ductal Metaplasia (ADM): On the Road to Pancreatic Intraepithelial Neoplasia (PanIN) and Pancreatic Cancer. *International Journal of Molecular Sciences*, *24*(12), 9946. https://doi.org/10.3390/ijms24129946

Masamune, A., & Shimosegawa, T. (2018). Epidemiology and Pathophysiology of Alcoholic Chronic Pancreatitis. In *The Pancreas* (pp. 342–348). John Wiley & Sons, Ltd. https://doi.org/10.1002/9781119188421.ch40

Mills, J. C., Stanger, B. Z., & Sander, M. (2019). Nomenclature for cellular plasticity: Are the terms as plastic as the cells themselves? *The EMBO Journal*, *38*(19), e103148. https://doi.org/10.15252/embj.2019103148

Mocci, E., & Klein, A. P. (2018). Epidemiology of Pancreatic Cancer. In *The Pancreas* (pp. 665–672). John Wiley & Sons, Ltd. https://doi.org/10.1002/9781119188421.ch88

Mohorko, E., Glockshuber, R., & Aebi, M. (2011). Oligosaccharyltransferase: The central enzyme of N-linked protein glycosylation. *Journal of Inherited Metabolic Disease*, *34*(4), 869–878. https://doi.org/10.1007/s10545-011-9337-1

Monnier, V. M. (1990). Nonenzymatic glycosylation, the Maillard reaction and the aging process. *Journal of Gerontology*, *45*(4), B105-111. https://doi.org/10.1093/geronj/45.4.b105

Moremen, K. W., Tiemeyer, M., & Nairn, A. V. (2012). Vertebrate protein glycosylation: Diversity, synthesis and function. *Nature Reviews Molecular Cell Biology*, *13*(7), Article 7. https://doi.org/10.1038/nrm3383

Nakahara, S., & Raz, A. (2006). On the role of galectins in signal transduction. *Methods in Enzymology*, *417*, 273–289. https://doi.org/10.1016/S0076-6879(06)17019-6

Neeper, M., Schmidt, A. M., Brett, J., Yan, S. D., Wang, F., Pan, Y. C., Elliston, K., Stern, D., & Shaw, A. (1992). Cloning and expression of a cell surface receptor for advanced glycosylation end products of proteins. *Journal of Biological Chemistry*, *267*(21), 14998–15004. https://doi.org/10.1016/S0021-9258(18)42138-2

Negre-Salvayre, A., Salvayre, R., Augé, N., Pamplona, R., & Portero-Otín, M. (2009). Hyperglycemia and glycation in diabetic complications. *Antioxidants & Redox Signaling*, *11*(12), 3071–3109. https://doi.org/10.1089/ars.2009.2484

Neoptolemos, J. P., Kleeff, J., Michl, P., Costello, E., Greenhalf, W., & Palmer, D. H. (2018). Therapeutic developments in pancreatic cancer: Current and future perspectives. *Nature Reviews. Gastroenterology & Hepatology*, *15*(6), 333–348. https://doi.org/10.1038/s41575-018-0005-x

Network, T. C. G. A. R. (2017). Integrated Genomic Characterization of Pancreatic Ductal Adenocarcinoma. *Cancer Cell*, *32*(2), 185. https://doi.org/10.1016/j.ccell.2017.07.007

Ohashi, K., Takahashi, H. K., Mori, S., Liu, K., Wake, H., Sadamori, H., Matsuda, H., Yagi, T., Yoshino, T., Nishibori, M., & Tanaka, N. (2010). Advanced glycation end products enhance monocyte activation during human mixed lymphocyte reaction. *Clinical Immunology*, *134*(3), 345–353. https://doi.org/10.1016/j.clim.2009.10.008

Ohgami, N., Nagai, R., Ikemoto, M., Arai, H., Kuniyasu, A., Horiuchi, S., & Nakayama, H. (2001). CD36, a Member of the Class B Scavenger Receptor Family, as a Receptor for Advanced Glycation End Products *. *Journal of Biological Chemistry*, *276*(5), 3195–3202. https://doi.org/10.1074/jbc.M006545200

Ohgami, N., Nagai, R., Miyazaki, A., Ikemoto, M., Arai, H., Horiuchi, S., & Nakayama, H. (2001). Scavenger Receptor Class B Type I-mediated Reverse Cholesterol Transport Is Inhibited by Advanced Glycation End Products *. *Journal of Biological Chemistry*, *276*(16), 13348–13355. https://doi.org/10.1074/jbc.M011613200

Ott, C., Jacobs, K., Haucke, E., Navarrete Santos, A., Grune, T., & Simm, A. (2014). Role of advanced glycation end products in cellular signaling. *Redox Biology*, *2*, 411–429. https://doi.org/10.1016/j.redox.2013.12.016

Park, L., Raman, K. G., Lee, K. J., Lu, Y., Ferran, L. J., Chow, W. S., Stern, D., & Schmidt, A. M. (1998). Suppression of accelerated diabetic atherosclerosis by the soluble receptor for advanced glycation endproducts. *Nature Medicine*, *4*(9), 1025–1031. https://doi.org/10.1038/2012

Pearson, G., Robinson, F., Beers Gibson, T., Xu, B. E., Karandikar, M., Berman, K., & Cobb, M. H. (2001). Mitogen-activated protein (MAP) kinase pathways: Regulation and physiological functions. *Endocrine Reviews*, *22*(2), 153–183. https://doi.org/10.1210/edrv.22.2.0428

Petersen, O. H. (2018). Physiology of Acinar Cell Secretion. In *The Pancreas* (pp. 41–55). John Wiley & Sons, Ltd. https://doi.org/10.1002/9781119188421.ch4

Pezzilli, R., Barassi, A., Corsi, M. M., Morselli-Labate, A. M., Campana, D., Casadei, R., Santini, D., Corinaldesi, R., & D'Eril, G. M. (2010). Serum leptin, but not adiponectin and receptor for advanced glycation end products, is able to distinguish autoimmune pancreatitis from both chronic pancreatitis and pancreatic neoplasms. *Scandinavian Journal of Gastroenterology*, *45*(1), 93–99. https://doi.org/10.3109/00365520903358907

Pinho, S. S., & Reis, C. A. (2015). Glycosylation in cancer: Mechanisms and clinical implications. *Nature Reviews. Cancer*, *15*(9), 540–555. https://doi.org/10.1038/nrc3982

Pollreisz, A., Hudson, B. I., Chang, J. S., Qu, W., Cheng, B., Papapanou, P. N., Schmidt, A. M., & Lalla, E. (2010). Receptor for Advanced Glycation Endproducts mediates proatherogenic responses to periodontal infection in vascular endothelial cells. *Atherosclerosis*, *212*(2), 451–456. https://doi.org/10.1016/j.atherosclerosis.2010.07.011

Porozan, S., Alavinejad, P., Mozafari, J., Kazem Mousavi, H., & Delirrooyfard, A. (2021). Serum Level of Galectin-3 in Early Detection of Acute Pancreatitis. *Middle East Journal of Digestive Diseases*, *13*(4), 350–355. https://doi.org/10.34172/mejdd.2021.246

Prasad, K. (2014). Low levels of serum soluble receptors for advanced glycation end products, biomarkers for disease state: Myth or reality. *The International Journal of Angiology: Official Publication of the International College of Angiology, Inc*, *23*(1), 11–16. https://doi.org/10.1055/s-0033-1363423

Prasad, K. (2019). Is there any evidence that AGE/sRAGE is a universal biomarker/risk marker for diseases? *Molecular and Cellular Biochemistry*, *451*(1–2), 139–144. https://doi.org/10.1007/s11010-018-3400-2

Pricci, F., Leto, G., Amadio, L., Iacobini, C., Romeo, G., Cordone, S., Gradini, R., Barsotti, P., Liu, F.-T., Mario, U. D., & Pugliese, G. (2000). Role of galectin-3 as a receptor for advanced glycosylation end products. *Kidney International*, *58*, S31–S39. https://doi.org/10.1046/j.1523-1755.2000.07706.x

Qian, Z. R., Rubinson, D. A., Nowak, J. A., Morales-Oyarvide, V., Dunne, R. F., Kozak, M. M., Welch, M. W., Brais, L. K., Da Silva, A., Li, T., Li, W., Masuda, A., Yang, J., Shi, Y., Gu, M., Masugi, Y., Bui, J., Zellers, C. L., Yuan, C., … Wolpin, B. M. (2018). Association of Alterations in Main Driver Genes With Outcomes of Patients With Resected Pancreatic Ductal Adenocarcinoma. *JAMA Oncology*, *4*(3), e173420. https://doi.org/10.1001/jamaoncol.2017.3420

Quilichini, E., Fabre, M., Dirami, T., Stedman, A., De Vas, M., Ozguc, O., Pasek, R. C., Cereghini, S., Morillon, L., Guerra, C., Couvelard, A., Gannon, M., & Haumaitre, C. (2019). Pancreatic Ductal Deletion of Hnf1b Disrupts Exocrine Homeostasis, Leads to Pancreatitis, and Facilitates Tumorigenesis. *Cellular and Molecular Gastroenterology and Hepatology*, *8*(3), 487–511. https://doi.org/10.1016/j.jcmgh.2019.06.005

Rabinovich, G. A., & Gruppi, A. (2005). Galectins as immunoregulators during infectious processes: From microbial invasion to the resolution of the disease. *Parasite Immunology*, *27*(4), 103–114. https://doi.org/10.1111/j.1365-3024.2005.00749.x

Ramasamy, R., Yan, S. F., Herold, K., Clynes, R., & Schmidt, A. M. (2008). Receptor for Advanced Glycation End Products. *Annals of the New York Academy of Sciences*, *1126*, 7–13. https://doi.org/10.1196/annals.1433.056

Ramasamy, R., Yan, S. F., & Schmidt, A. M. (2012). Advanced glycation endproducts: From precursors to RAGE: round and round we go. *Amino Acids*, *42*(4), 1151–1161. https://doi.org/10.1007/s00726-010-0773-2

Ramazi, S., & Zahiri, J. (2021). Post-translational modifications in proteins: Resources, tools and prediction methods. *Database: The Journal of Biological Databases and Curation*, *2021*, baab012. https://doi.org/10.1093/database/baab012

Rashid, G., Korzets, Z., & Bernheim, J. (2006). Advanced glycation end products stimulate tumor necrosis factor-alpha and interleukin-1 beta secretion by peritoneal macrophages in patients on continuous ambulatory peritoneal dialysis. *The Israel Medical Association Journal: IMAJ*, *8*(1), 36–39.

Raucci, A., Cugusi, S., Antonelli, A., Barabino, S. M., Monti, L., Bierhaus, A., Reiss, K., Saftig, P., & Bianchi, M. E. (2008). A soluble form of the receptor for advanced glycation endproducts (RAGE) is produced by proteolytic cleavage of the membrane-bound form by the sheddase a disintegrin and metalloprotease 10 (ADAM10). *FASEB Journal: Official Publication of the Federation of American Societies for Experimental Biology*, *22*(10), 3716–3727. https://doi.org/10.1096/fj.08-109033

Rauscher, B., Heigwer, F., Henkel, L., Hielscher, T., Voloshanenko, O., & Boutros, M. (2018). Toward an integrated map of genetic interactions in cancer cells. *Molecular Systems Biology*, *14*(2), e7656. https://doi.org/10.15252/msb.20177656

Reznikov, L. L., Waksman, J., Azam, T., Kim, S. H., Bufler, P., Niwa, T., Werman, A., Zhang, X., Pischetsrieder, M., Shaldon, S., & Dinarello, C. A. (2004). Effect of advanced glycation end products on endotoxin-induced TNF-alpha, IL-1beta and IL-8 in human peripheral blood mononuclear cells. *Clinical Nephrology*, *61*(5), 324–336. https://doi.org/10.5414/cnp61324

Riehl, A., Németh, J., Angel, P., & Hess, J. (2009). The receptor RAGE: Bridging inflammation and cancer. *Cell Communication and Signaling : CCS*, *7*, 12. https://doi.org/10.1186/1478-811X-7-12

Robinson, S. M., Rasch, S., Beer, S., Valantiene, I., Mickevicius, A., Schlaipfer, E., Mann, J., Maisonneuve, P., Charnley, R. M., & Rosendahl, J. (2019). Systemic inflammation contributes to impairment of quality of life in chronic pancreatitis. *Scientific Reports*, *9*(1), 7318. https://doi.org/10.1038/s41598-019-43846-8

Roboti, P., & High, S. (2012). The oligosaccharyltransferase subunits OST48, DAD1 and KCP2 function as ubiquitous and selective modulators of mammalian N-glycosylation. *Journal of Cell Science*, *125*(14), 3474–3484. https://doi.org/10.1242/jcs.103952

Roncero-Ramos, I., Niquet-Léridon, C., Strauch, C., Monnier, V. M., Tessier, F. J., Navarro, M. P., & Delgado-Andrade, C. (2014). An advanced glycation end product (AGE)-rich diet promotes Nε-carboxymethyl-lysine accumulation in the cardiac tissue and tendons of rats. *Journal of Agricultural and Food Chemistry*, *62*(25), 6001–6006. https://doi.org/10.1021/jf501005n

Ruan, D., Wang, H., & Cheng, F. (2018). The Maillard Reaction. In D. Ruan, H. Wang, & F. Cheng (Eds.), *The Maillard Reaction in Food Chemistry: Current Technology and Applications* (pp. 1–21). Springer International Publishing. https://doi.org/10.1007/978-3-030-04777-1_1

Schober, P., Boer, C., & Schwarte, L. A. (2018). Correlation Coefficients: Appropriate Use and Interpretation. *Anesthesia and Analgesia*, *126*(5), 1763–1768. https://doi.org/10.1213/ANE.0000000000002864

Seo, J., & Lee, K.-J. (2004). Post-translational modifications and their biological functions: Proteomic analysis and systematic approaches. *Journal of Biochemistry and Molecular Biology*, *37*(1), 35–44. https://doi.org/10.5483/bmbrep.2004.37.1.035

Serveaux-Dancer, M., Jabaudon, M., Creveaux, I., Belville, C., Blondonnet, R., Gross, C., Constantin, J.-M., Blanchon, L., & Sapin, V. (2019). Pathological Implications of Receptor for Advanced Glycation End-Product (AGER) Gene Polymorphism. *Disease Markers*, *2019*, 2067353. https://doi.org/10.1155/2019/2067353

Shapanis, A., Lai, C., Smith, S., Coltart, G., Sommerlad, M., Schofield, J., Parkinson, E., Skipp, P., & Healy, E. (2021). Identification of proteins associated with development of metastasis from cutaneous squamous cell carcinomas (cSCCs) via proteomic analysis of primary cSCCs*. *British Journal of Dermatology*, *184*(4), 709–721. https://doi.org/10.1111/bjd.19485

Shen, W.-J., Azhar, S., & Kraemer, F. B. (2018). SR-B1: A Unique Multifunctional Receptor for Cholesterol Influx and Efflux. *Annual Review of Physiology*, *80*, 95–116. https://doi.org/10.1146/annurev-physiol-021317-121550

Shi, G., Zhu, L., Sun, Y., Bettencourt, R., Damsz, B., Hruban, R. H., & Konieczny, S. F. (2009). Loss of the Acinar-Restricted Transcription Factor Mist1 Accelerates Kras-Induced Pancreatic Intraepithelial Neoplasia. *Gastroenterology*, *136*(4), 1368–1378. https://doi.org/10.1053/j.gastro.2008.12.066

Shin, G.-C., Moon, S. U., Kang, H. S., Choi, H.-S., Han, H. D., & Kim, K.-H. (2019). PRKCSH contributes to tumorigenesis by selective boosting of IRE1 signaling pathway. *Nature Communications*, *10*, 3185. https://doi.org/10.1038/s41467-019-11019-w

Steward, M. C., Ishiguro, H., & Case, R. M. (2005). Mechanisms of bicarbonate secretion in the pancreatic duct. *Annual Review of Physiology*, *67*, 377–409. https://doi.org/10.1146/annurev.physiol.67.031103.153247

Stojanovic, B., Jovanovic, I., Stojanovic, B. S., Stojanovic, M. D., Gajovic, N., Radosavljevic, G., Pantic, J., Arsenijevic, N., & Lukic, M. L. (2019). Deletion of

Galectin-3 attenuates acute pancreatitis in mice by affecting activation of innate inflammatory cells. *European Journal of Immunology*, *49*(6), 940–946. https://doi.org/10.1002/eji.201847890

Storz, P. (2017). Acinar cell plasticity and development of pancreatic ductal adenocarcinoma. *Nature Reviews. Gastroenterology & Hepatology*, *14*(5), 296–304. https://doi.org/10.1038/nrgastro.2017.12

Stowell, S. R., Ju, T., & Cummings, R. D. (2015). Protein Glycosylation in Cancer. *Annual Review of Pathology*, *10*, 473–510. https://doi.org/10.1146/annurev-pathol-012414-040438

Suomi, T., Seyednasrollah, F., Jaakkola, M. K., Faux, T., & Elo, L. L. (2017). ROTS: An R package for reproducibility-optimized statistical testing. *PLoS Computational Biology*, *13*(5), e1005562. https://doi.org/10.1371/journal.pcbi.1005562

Szklarczyk, D., Gable, A. L., Nastou, K. C., Lyon, D., Kirsch, R., Pyysalo, S., Doncheva, N. T., Legeay, M., Fang, T., Bork, P., Jensen, L. J., & von Mering, C. (2020). The STRING database in 2021: Customizable protein–protein networks, and functional characterization of user-uploaded gene/measurement sets. *Nucleic Acids Research*, *49*(D1), D605–D612. https://doi.org/10.1093/nar/gkaa1074

Tamura, Y., Adachi, H., Osuga, J., Ohashi, K., Yahagi, N., Sekiya, M., Okazaki, H., Tomita, S., Iizuka, Y., Shimano, H., Nagai, R., Kimura, S., Tsujimoto, M., & Ishibashi, S. (2003). FEEL-1 and FEEL-2 Are Endocytic Receptors for Advanced Glycation End Products *. *Journal of Biological Chemistry*, *278*(15), 12613–12617. https://doi.org/10.1074/jbc.M210211200

Tang, L., Chen, X., Zhang, X., Guo, Y., Su, J., Zhang, J., Peng, C., & Chen, X. (2019). N-Glycosylation in progression of skin cancer. *Medical Oncology (Northwood, London, England)*, *36*(6), 50. https://doi.org/10.1007/s12032-019-1270-4

Tang, Z., Kang, B., Li, C., Chen, T., & Zhang, Z. (2019). GEPIA2: An enhanced web server for large-scale expression profiling and interactive analysis. *Nucleic Acids Research*, *47*(W1), W556–W560. https://doi.org/10.1093/nar/gkz430

Teissier, T., & Boulanger, É. (2019). The receptor for advanced glycation end-products (RAGE) is an important pattern recognition receptor (PRR) for inflammaging. *Biogerontology*, *20*(3), 279–301. https://doi.org/10.1007/s10522-019-09808-3

The Gene Ontology Consortium, Carbon, S., Douglass, E., Good, B. M., Unni, D. R., Harris, N. L., Mungall, C. J., Basu, S., Chisholm, R. L., Dodson, R. J., Hartline, E., Fey, P., Thomas, P. D., Albou, L.-P., Ebert, D., Kesling, M. J., Mi, H., Muruganujan, A., Huang, X., … Elser, J. (2021). The Gene Ontology resource: Enriching a GOld mine. *Nucleic Acids Research*, *49*(D1), D325–D334. https://doi.org/10.1093/nar/gkaa1113

Thornalley, P. J. (1998). Cell activation by glycated proteins. AGE receptors, receptor recognition factors and functional classification of AGEs. *Cellular and Molecular Biology (Noisy-Le-Grand, France)*, *44*(7), 1013–1023.

Tolani, P., Gupta, S., Yadav, K., Aggarwal, S., & Yadav, A. K. (2021). Chapter Four—Big data, integrative omics and network biology. In R. Donev & T. Karabencheva-Christova (Eds.), *Advances in Protein Chemistry and Structural Biology* (Vol. 127, pp. 127–160). Academic Press. https://doi.org/10.1016/bs.apcsb.2021.03.006

Tompa, P. (2016). The principle of conformational signaling. *Chemical Society Reviews*, *45*(15), 4252–4284. https://doi.org/10.1039/C6CS00011H

Treml, K., Meimaroglou, D., Hentges, A., & Bause, E. (2000). The α- and β-subunits are required for expression of catalytic activity in the hetero-dimeric glucosidase II complex from human liver. *Glycobiology*, *10*(5), 493–502. https://doi.org/10.1093/glycob/10.5.493

Troyanskaya, O., Cantor, M., Sherlock, G., Brown, P., Hastie, T., Tibshirani, R., Botstein, D., & Altman, R. B. (2001). Missing value estimation methods for DNA microarrays. *Bioinformatics*, *17*(6), 520–525. https://doi.org/10.1093/bioinformatics/17.6.520

Tu, Y., Yin, X.-J., Liu, Q., Zhang, S., Wang, J., Ji, B.-Z., Zhang, J., Sun, M.-S., Yang, Y., Wang, C.-H., Yin, L., & Liu, Y. (2022). MITA oligomerization upon viral infection is dependent on its N-glycosylation mediated by DDOST. *PLOS Pathogens*, *18*(11), e1010989. https://doi.org/10.1371/journal.ppat.1010989

Uribarri, J., del Castillo, M. D., de la Maza, M. P., Filip, R., Gugliucci, A., Luevano-Contreras, C., Macías-Cervantes, M. H., Markowicz Bastos, D. H., Medrano, A., Menini, T., Portero-Otin, M., Rojas, A., Sampaio, G. R., Wrobel, K., Wrobel, K., & Garay-Sevilla, M. E. (2015). Dietary Advanced Glycation End Products and Their Role in Health and Disease12. *Advances in Nutrition*, *6*(4), 461–473. https://doi.org/10.3945/an.115.008433

Urra, H., Dufey, E., Avril, T., Chevet, E., & Hetz, C. (2016). Endoplasmic Reticulum Stress and the Hallmarks of Cancer. *Trends in Cancer*, *2*(5), 252–262. https://doi.org/10.1016/j.trecan.2016.03.007

Vazzana, N., Santilli, F., Cuccurullo, C., & Davì, G. (2009). Soluble forms of RAGE in internal medicine. *Internal and Emergency Medicine*, *4*(5), 389–401. https://doi.org/10.1007/s11739-009-0300-1

Verfaillie, T., Rubio, N., Garg, A. D., Bultynck, G., Rizzuto, R., Decuypere, J.-P., Piette, J., Linehan, C., Gupta, S., Samali, A., & Agostinis, P. (2012). PERK is required at the ER-mitochondrial contact sites to convey apoptosis after ROS-based ER stress. *Cell Death and Differentiation*, *19*(11), 1880–1891. https://doi.org/10.1038/cdd.2012.74

Verkerke, H., Dias-Baruffi, M., Cummings, R. D., Arthur, C. M., & Stowell, S. R. (2022). Galectins: An Ancient Family of Carbohydrate Binding ProteinsCarbohydrate binding proteins (CBPs) with Modern Functions. In S. R. Stowell, C. M. Arthur, & R. D. Cummings (Eds.), *Galectins: Methods and Protocols* (pp. 1–40). Springer US. https://doi.org/10.1007/978-1-0716-2055-7_1

Very, N., Lefebvre, T., & El Yazidi-Belkoura, I. (2018). Drug resistance related to aberrant glycosylation in colorectal cancer. *Oncotarget*, *9*(1), 1380–1402. https://doi.org/10.18632/oncotarget.22377

Vicente Miranda, H., El-Agnaf, O. M. A., & Outeiro, T. F. (2016). Glycation in Parkinson's disease and Alzheimer's disease. *Movement Disorders*, *31*(6), 782–790. https://doi.org/10.1002/mds.26566

Vistoli, G., De Maddis, D., Cipak, A., Zarkovic, N., Carini, M., & Aldini, G. (2013). Advanced glycoxidation and lipoxidation end products (AGEs and ALEs): An overview of their mechanisms of formation. *Free Radical Research*, *47*(sup1), 3–27. https://doi.org/10.3109/10715762.2013.815348

Vlassara, H., Li, Y. M., Imani, F., Wojciechowicz, D., Yang, Z., Liu, F. T., & Cerami, A. (1995). Identification of galectin-3 as a high-affinity binding protein for advanced glycation end products (AGE): A new member of the AGE-receptor complex. *Molecular Medicine*, *1*(6), 634–646.

Walsh, C. T., Garneau-Tsodikova, S., & Gatto Jr., G. J. (2005). Protein Posttranslational Modifications: The Chemistry of Proteome Diversifications. *Angewandte Chemie International Edition*, *44*(45), 7342–7372. https://doi.org/10.1002/anie.200501023

Wang, L., Friess, H., Zhu, Z., Frigeri, L., Zimmermann, A., Korc, M., Berberat, P. O., & Büchler, M. W. (2000). Galectin-1 and galectin-3 in chronic pancreatitis. *Laboratory Investigation; a Journal of Technical Methods and Pathology*, *80*(8), 1233–1241. https://doi.org/10.1038/labinvest.3780131

Wang, S., Osgood, A. O., & Chatterjee, A. (2022). Uncovering Post-Translational Modification-Associated Protein-Protein Interactions. *Current Opinion in Structural Biology*, *74*, 102352. https://doi.org/10.1016/j.sbi.2022.102352

Wang, Y., Nangia-Makker, P., Tait, L., Balan, V., Hogan, V., Pienta, K. J., & Raz, A. (2009). Regulation of Prostate Cancer Progression by Galectin-3. *The American Journal of Pathology*, *174*(4), 1515–1523. https://doi.org/10.2353/ajpath.2009.080816

Wang, Y., Wang, H., Piper, M. G., McMaken, S., Mo, X., Opalek, J., Schmidt, A. M., & Marsh, C. B. (2010). sRAGE Induces Human Monocyte Survival and Differentiation. *Journal of Immunology (Baltimore, Md. : 1950)*, *185*(3), 1822–1835. https://doi.org/10.4049/jimmunol.0903398

Wang, Y., Wang, K., Jin, Y., & Sheng, X. (2019). Endoplasmic reticulum proteostasis control and gastric cancer. *Cancer Letters*, *449*, 263–271. https://doi.org/10.1016/j.canlet.2019.01.034

Wang, Y.-C., Peterson, S. E., & Loring, J. F. (2014). Protein post-translational modifications and regulation of pluripotency in human stem cells. *Cell Research*, *24*(2), 143–160. https://doi.org/10.1038/cr.2013.151

Wetzels, S., Wouters, K., Schalkwijk, C. G., Vanmierlo, T., & Hendriks, J. J. A. (2017). Methylglyoxal-Derived Advanced Glycation Endproducts in Multiple Sclerosis.

International Journal of Molecular Sciences, *18*(2), 421. https://doi.org/10.3390/ijms18020421

Wiśniewski, J. R., Zougman, A., Nagaraj, N., & Mann, M. (2009). Universal sample preparation method for proteome analysis. *Nature Methods*, *6*(5), 359–362. https://doi.org/10.1038/nmeth.1322

Wu, J., Chen, S., Liu, H., Zhang, Z., Ni, Z., Chen, J., Yang, Z., Nie, Y., & Fan, D. (2018). Tunicamycin specifically aggravates ER stress and overcomes chemoresistance in multidrug-resistant gastric cancer cells by inhibiting N-glycosylation. *Journal of Experimental & Clinical Cancer Research: CR*, *37*(1), 272. https://doi.org/10.1186/s13046-018-0935-8

Wu, K.-L., Kuo, C.-M., Huang, E.-Y., Pan, H.-M., Huang, C.-C., Chen, Y.-F., Hsiao, C.-C., & Yang, K. D. (2018). Extracellular galectin-3 facilitates colon cancer cell migration and is related to the epidermal growth factor receptor. *American Journal of Translational Research*, *10*(8), 2402–2412.

Xie, L., Ni, W.-K., Chen, X.-D., Xiao, M.-B., Chen, B.-Y., He, S., Lu, C.-H., Li, X.-Y., Jiang, F., & Ni, R.-Z. (2012). The expressions and clinical significances of tissue and serum galectin-3 in pancreatic carcinoma. *Journal of Cancer Research and Clinical Oncology*, *138*(6), 1035–1043. https://doi.org/10.1007/s00432-012-1178-2

Yadav, D., & Lowenfels, A. B. (2013). The epidemiology of pancreatitis and pancreatic cancer. *Gastroenterology*, *144*(6), 1252–1261. https://doi.org/10.1053/j.gastro.2013.01.068

Yamagata, T., Tsuru, T., Momoi, M. Y., Suwa, K., Nozaki, Y., Mukasa, T., Ohashi, H., Fukushima, Y., & Momoi, T. (1997). Genome Organization of Human 48-kDa Oligosaccharyltransferase (DDOST). *Genomics*, *45*(3), 535–540. https://doi.org/10.1006/geno.1997.4966

Yamagishi, S., & Matsui, T. (2011). Advanced Glycation End Products (AGEs), Oxidative Stress and Diabetic Retinopathy. *Current Pharmaceutical Biotechnology*, *12*(3), 362–368.

Yan, S. F., Ramasamy, R., & Schmidt, A. M. (2010). Soluble RAGE: Therapy and biomarker in unraveling the RAGE axis in chronic disease and aging. *Biochemical Pharmacology*, *79*(10), 1379–1386. https://doi.org/10.1016/j.bcp.2010.01.013

Yasuda, T., Ueda, T., Takeyama, Y., Shinzeki, M., Sawa, H., Nakajima, T., Ajiki, T., Fujino, Y., Suzuki, Y., & Kuroda, Y. (2006). Significant increase of serum high-mobility group box chromosomal protein 1 levels in patients with severe acute pancreatitis. *Pancreas*, *33*(4), 359–363. https://doi.org/10.1097/01.mpa.0000236741.15477.8b

Yonekura, H., Yamamoto, Y., Sakurai, S., Petrova, R. G., Abedin, M. J., Li, H., Yasui, K., Takeuchi, M., Makita, Z., Takasawa, S., Okamoto, H., Watanabe, T., & Yamamoto, H. (2003). Novel splice variants of the receptor for advanced glycation end-products expressed in human vascular endothelial cells and pericytes, and their

putative roles in diabetes-induced vascular injury. *Biochemical Journal*, *370*(Pt 3), 1097–1109. https://doi.org/10.1042/BJ20021371

Zeng, M., Vachel, L., & Muallem, S. (2018). Physiology of Duct Cell Secretion. In *The Pancreas* (pp. 56–62). John Wiley & Sons, Ltd. https://doi.org/10.1002/9781119188421.ch5

Zhang, L., Bukulin, M., Kojro, E., Roth, A., Metz, V. V., Fahrenholz, F., Nawroth, P. P., Bierhaus, A., & Postina, R. (2008). Receptor for advanced glycation end products is subjected to protein ectodomain shedding by metalloproteinases. *The Journal of Biological Chemistry*, *283*(51), 35507–35516. https://doi.org/10.1074/jbc.M806948200

Zhang, Y., Cui, C., & Lai, Z.-C. (2016). The defender against apoptotic cell death 1 gene is required for tissue growth and efficient N-glycosylation in Drosophila melanogaster. *Developmental Biology*, *420*(1), 186–195. https://doi.org/10.1016/j.ydbio.2016.09.021

Zheng, J., Lu, W., Wang, C., Xing, Y., Chen, X., & Ai, Z. (2017). Galectin-3 induced by hypoxia promotes cell migration in thyroid cancer cells. *Oncotarget*, *8*(60), 101475–101488. https://doi.org/10.18632/oncotarget.21135

Zhou, J., Chen, W., He, Q., Chen, D., Li, C., Jiang, C., Ding, Z., & Qian, Q. (2022). SERBP1 affects the apoptotic level by regulating the expression and alternative splicing of cellular and metabolic process genes in HeLa cells. *PeerJ*, *10*, e14084. https://doi.org/10.7717/peerj.14084

Zhu, C., Xiao, H., Jiang, X., Tong, R., & Guan, J. (2021). Prognostic Biomarker DDOST and Its Correlation With Immune Infiltrates in Hepatocellular Carcinoma. *Frontiers in Genetics*, *12*, 819520. https://doi.org/10.3389/fgene.2021.819520

Zhu, L., Shi, G., Schmidt, C. Max., Hruban, R. H., & Konieczny, S. F. (2007). Acinar Cells Contribute to the Molecular Heterogeneity of Pancreatic Intraepithelial Neoplasia. *The American Journal of Pathology*, *171*(1), 263–273. https://doi.org/10.2353/ajpath.2007.061176

Zhu, W., Sano, H., Nagai, R., Fukuhara, K., Miyazaki, A., & Horiuchi, S. (2001). The Role of Galectin-3 in Endocytosis of Advanced Glycation End Products and Modified Low Density Lipoproteins. *Biochemical and Biophysical Research Communications*, *280*(4), 1183–1188. https://doi.org/10.1006/bbrc.2001.4256

6 Appendices

6.1 Supplemental Results

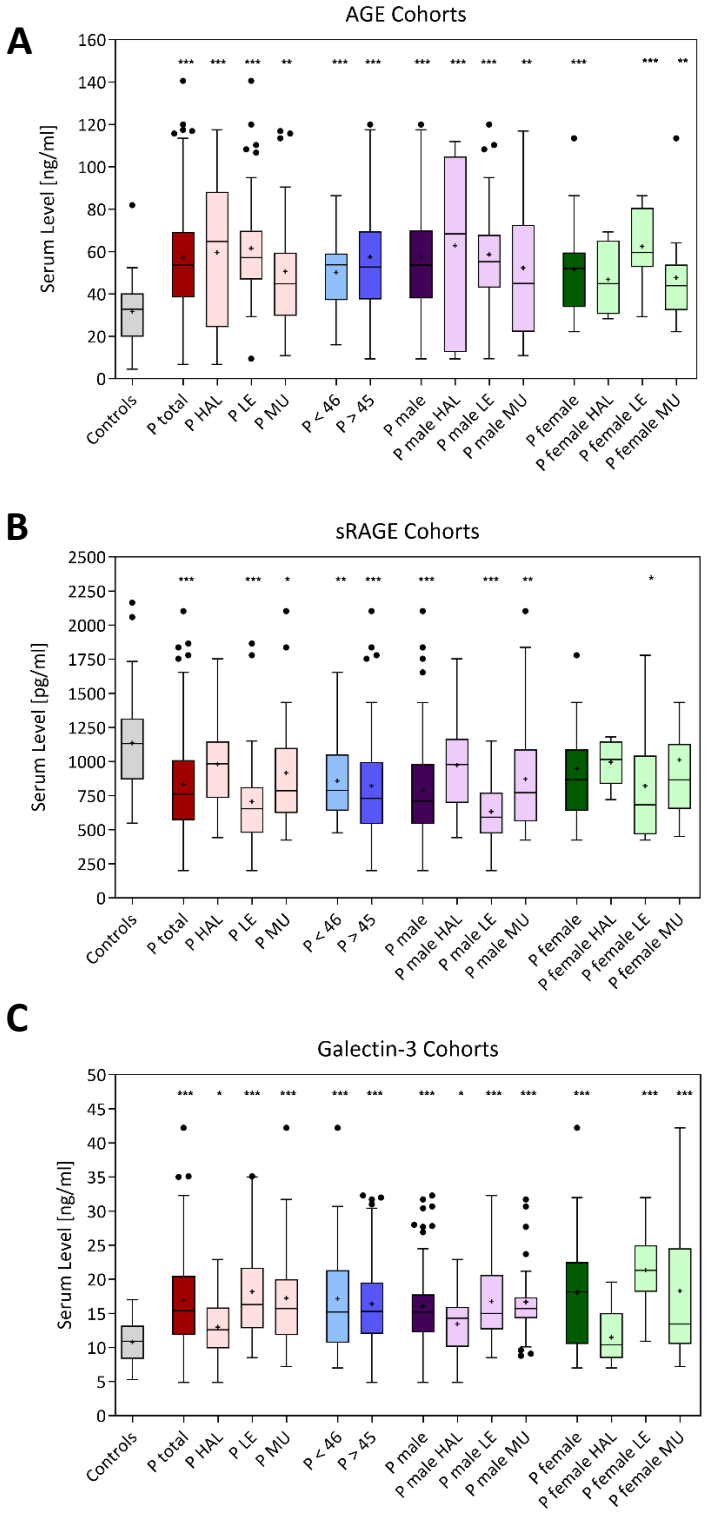

Figure S 1: Serum Levels of AGE, sRAGE and Gal-3 after Correction for Cohorts

*A: Serum levels of AGE after correction for cohorts; B: Serum levels of sRAGE after correction for cohorts; C: Serum levels of Gal-3 after correction for cohorts. (*P < 0.05, **P < 0.01, ***P < 0.001; unpaired t-test)*

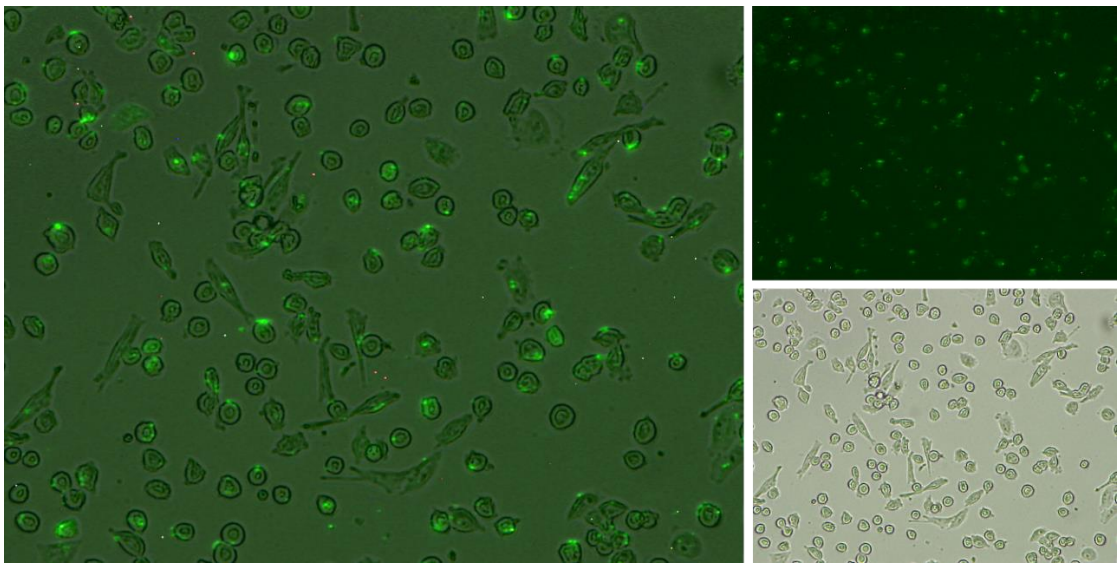

Figure S 2: Transfection Efficiency in PA-TU-8988T Cell Line

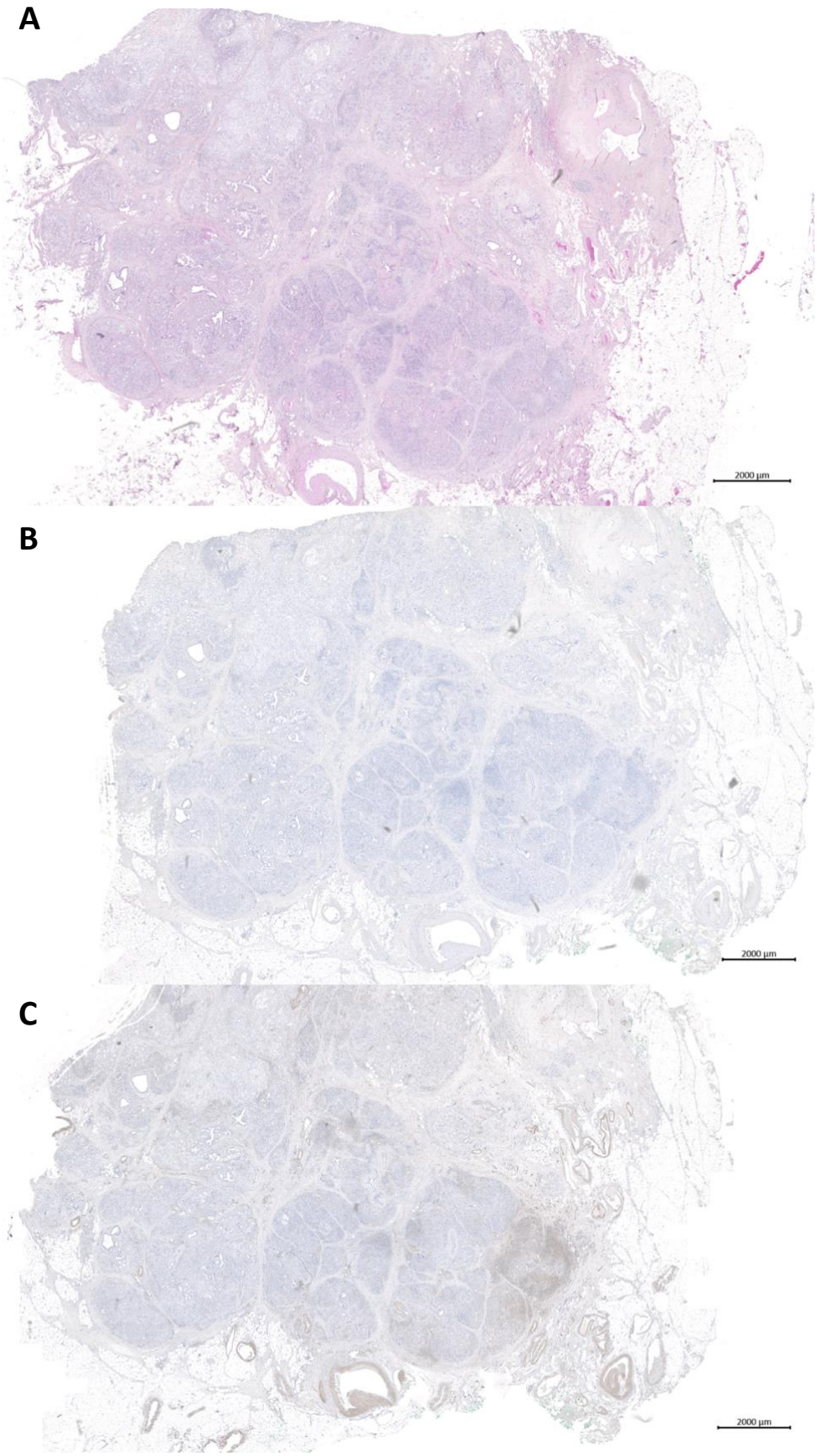

Figure S 3: H&E/IHC Overview Image RAGE

A: H&E; B: Control; C: RAGE (scale bar, 2000 µm)

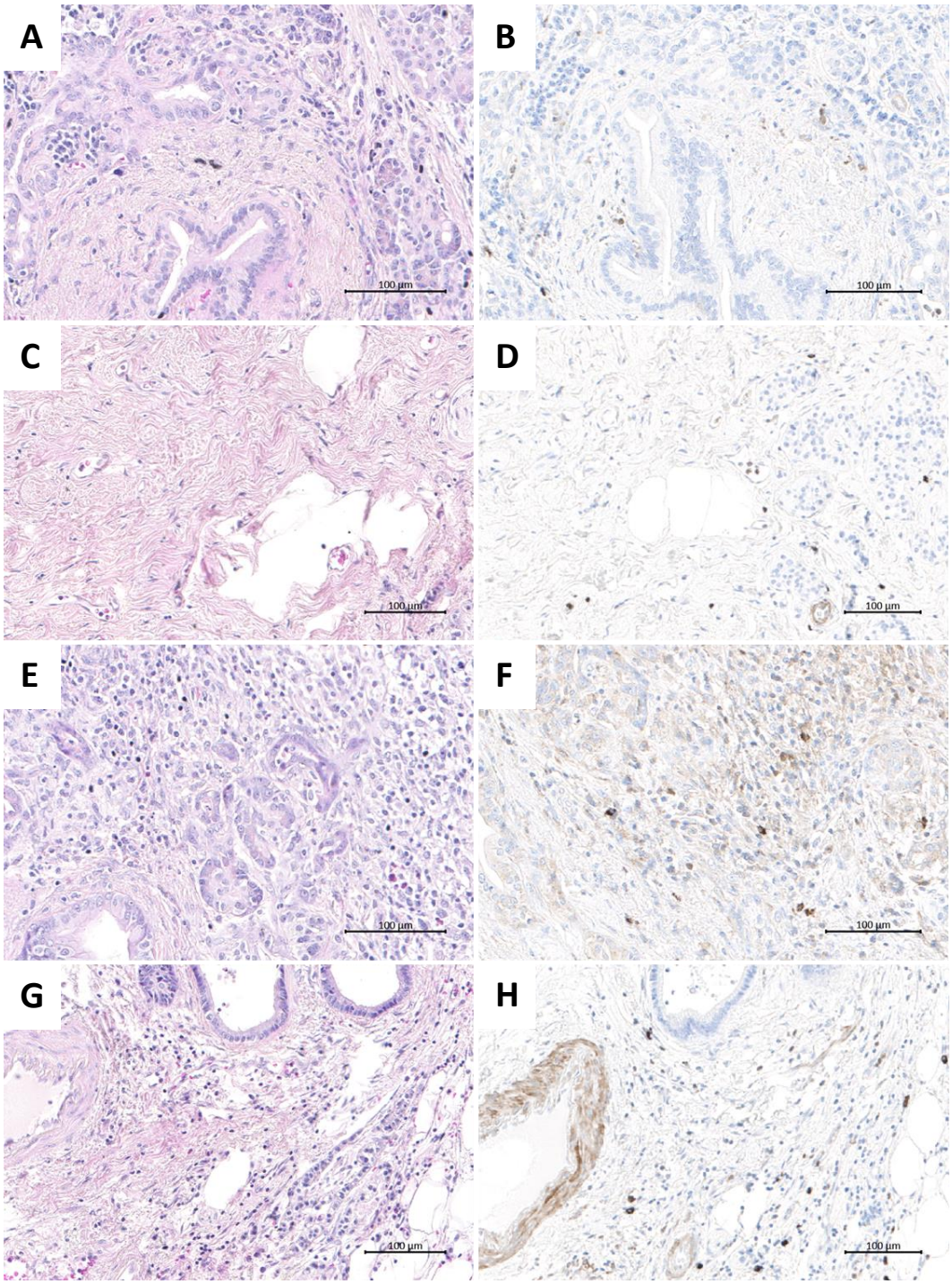

Figure S 4: H&E/IHC Image RAGE

A, C, E, G: H&E Image; B, D, F, H: IHC Image RAGE (scale bar, 100 µm)

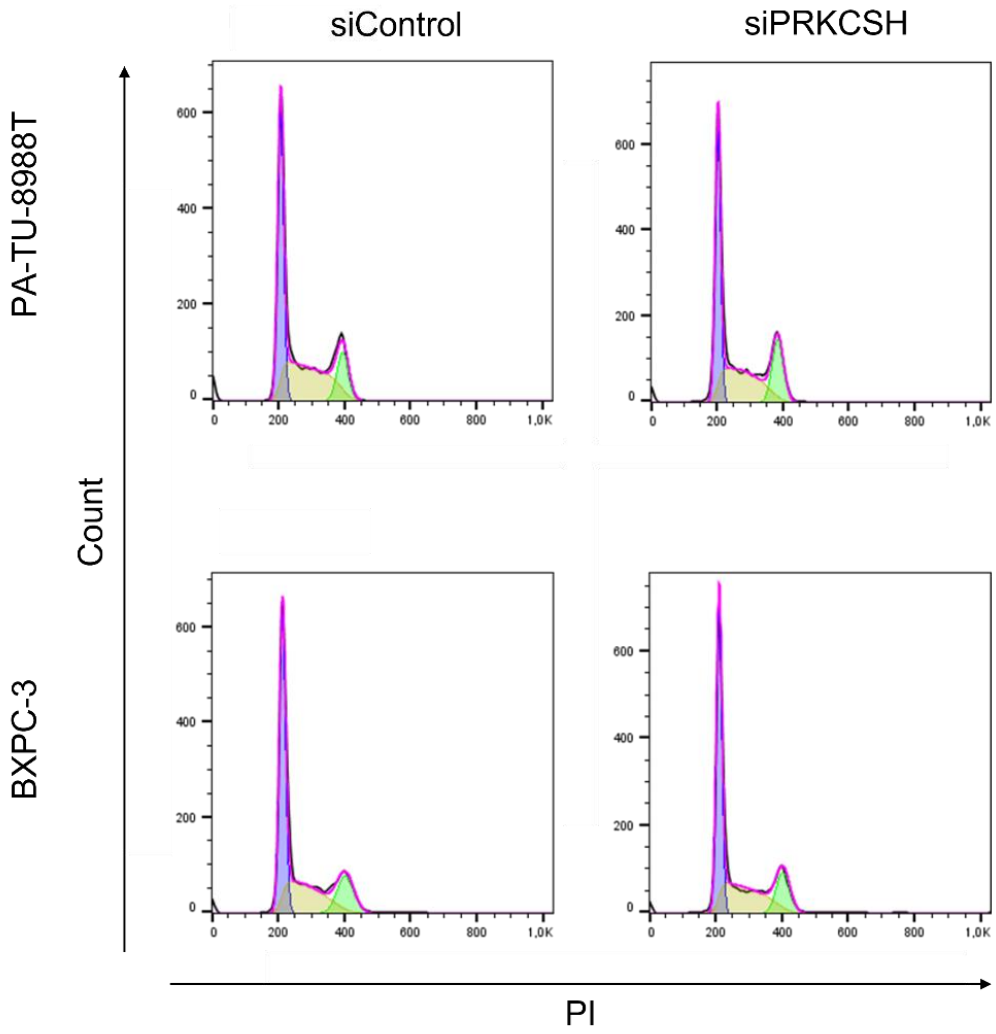

Figure S 5: Cell Cycle after PRKCSH KD in PDAC Cell Lines

Flow cytometry assay of PI staining 48 hours after PRKCSH KD in BXPC-3 and in PA-TU-8988T cell lines. G1 phase is colored in purple, S phase in yellow and G2 phase in green.

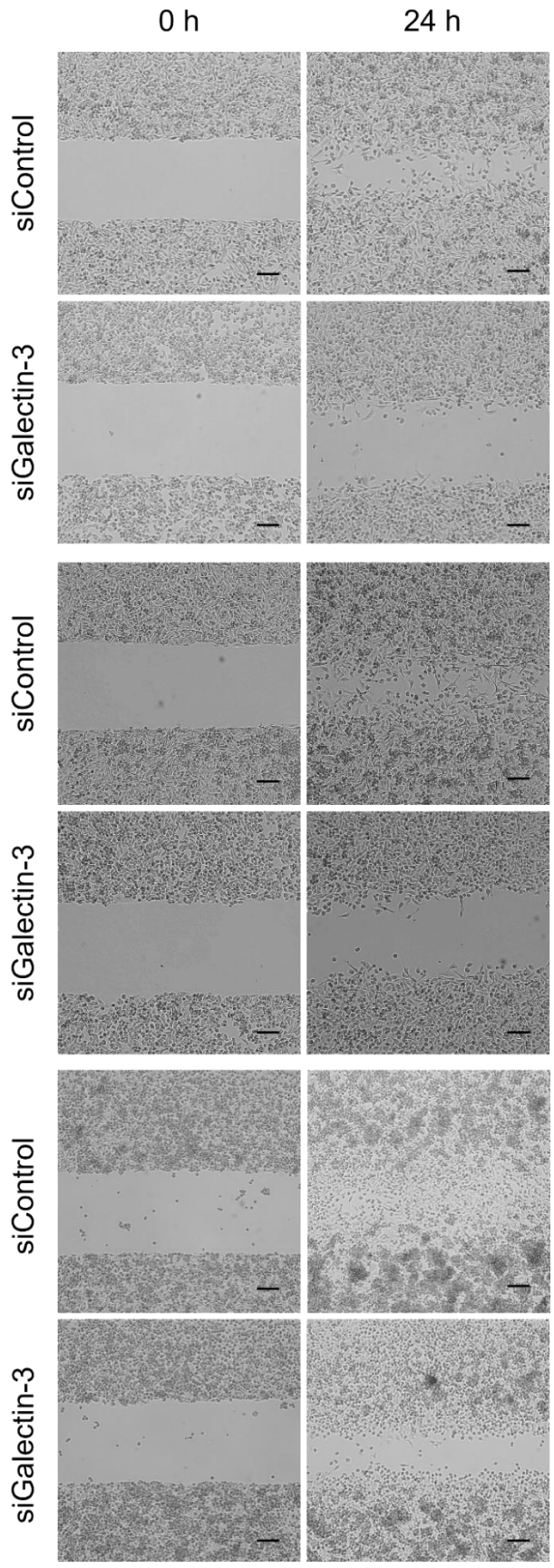

Figure S 6: Migration after Gal-3 KD in PA-TU-8988T Cell Line

Wound healing assay after Gal-3 KD in PA-TU-8988T cell line. (scale bar, 200 µm)

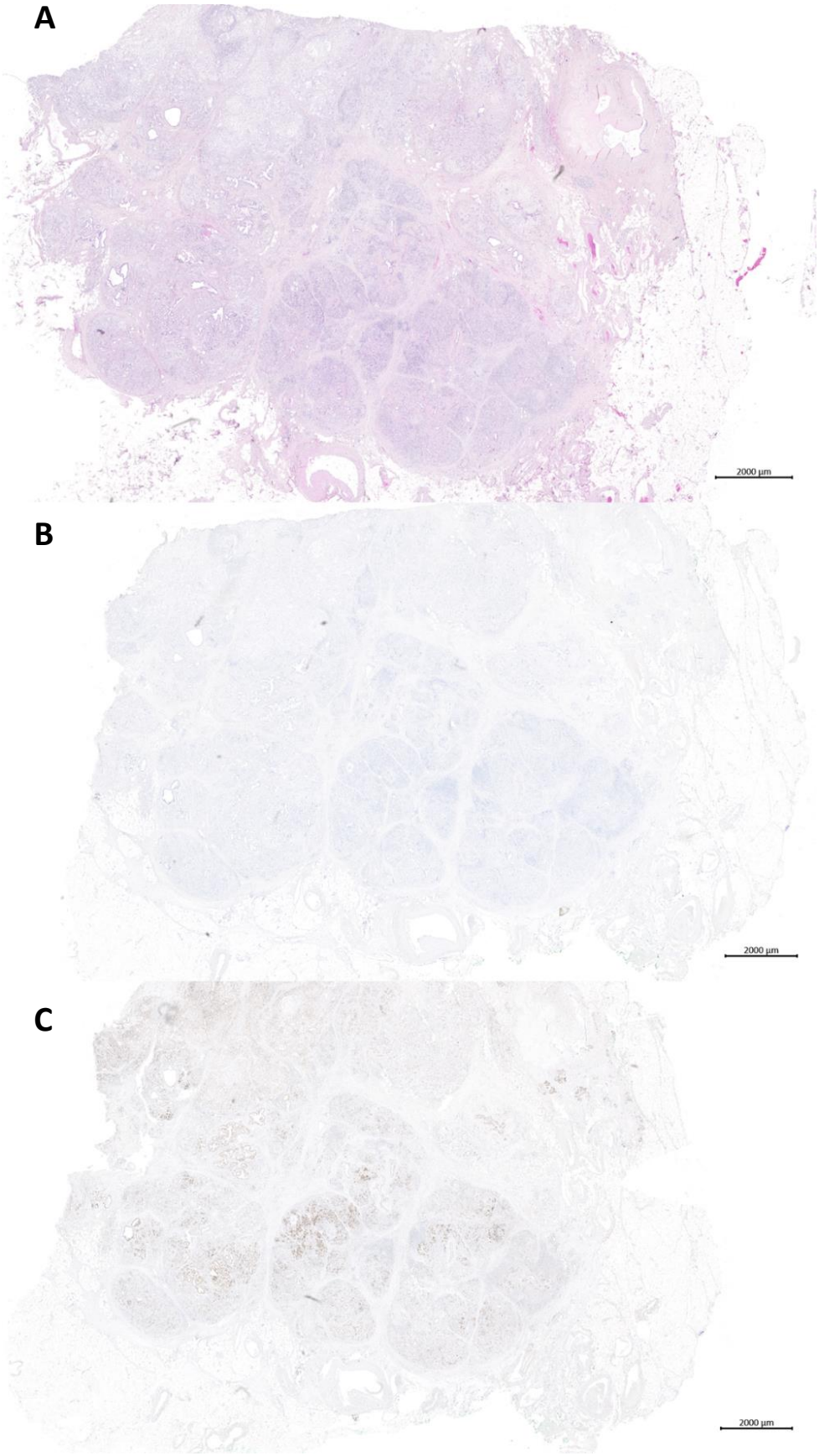

Figure S 7: H&E/IHC Overview Image DDOST

A: H&E; B: Control; C: DDOST (scale bar, 2000 µm)

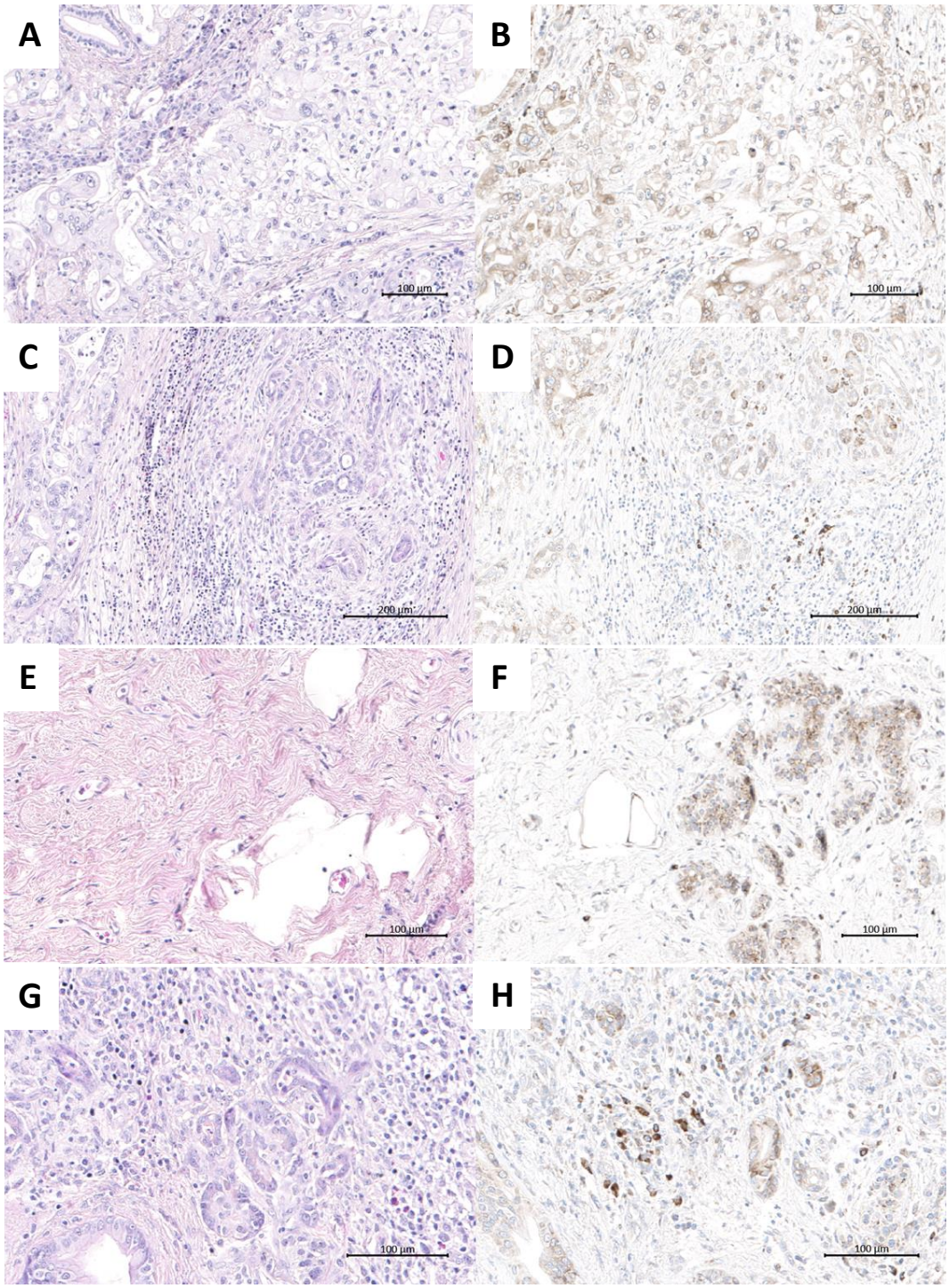

Figure S 8: H&E/IHC Image DDOST

A, C, E, G: H&E Image; B, D, F, H: IHC Image DDOST (scale bar, 100 µm)

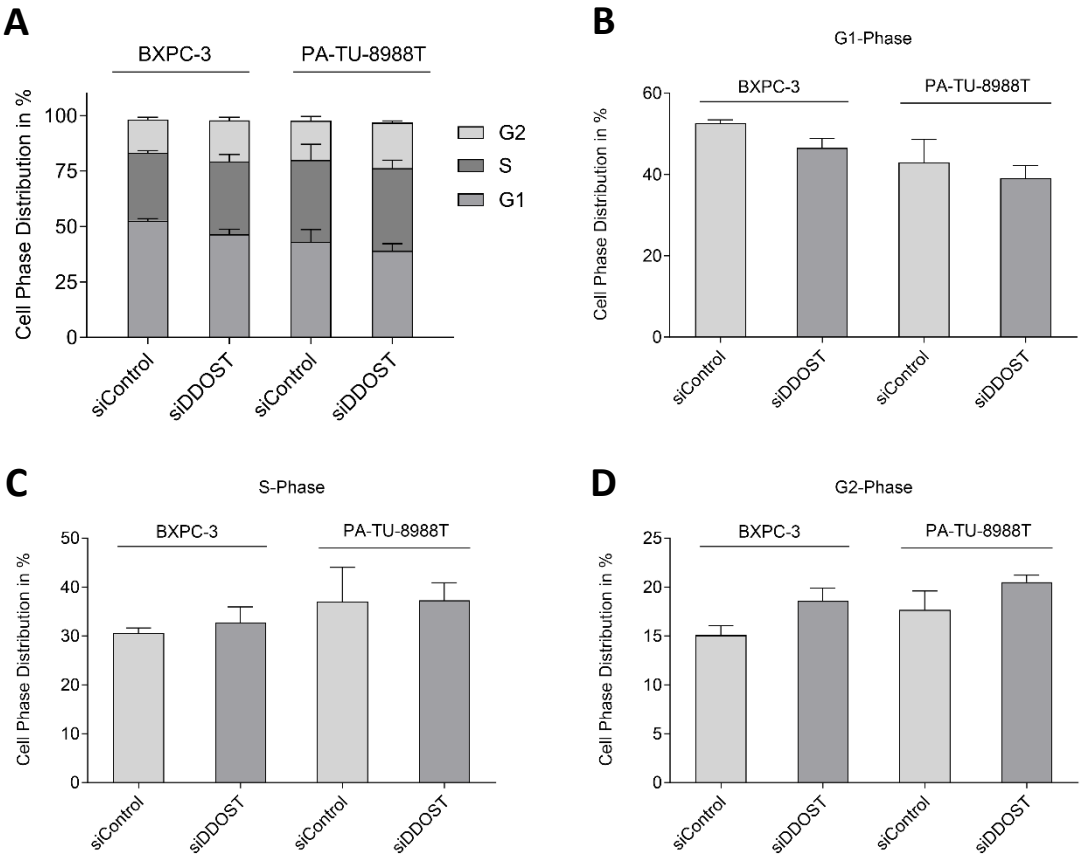

Figure S 9: Cell Cycle after DDOST KD PDAC Cell Lines

(A) Quantification of cell cycle assay 72 hours after DDOST KD in different PDAC cell lines. (B) Quantification of G1 phase 72 hours after DDOST KD. (C) Quantification of S phase 72 hours after DDOST KD. (D) Quantification of G2 phase 72 hours after DDOST KD. (Unpaired t-test)

6.2 Uncropped Western Blots

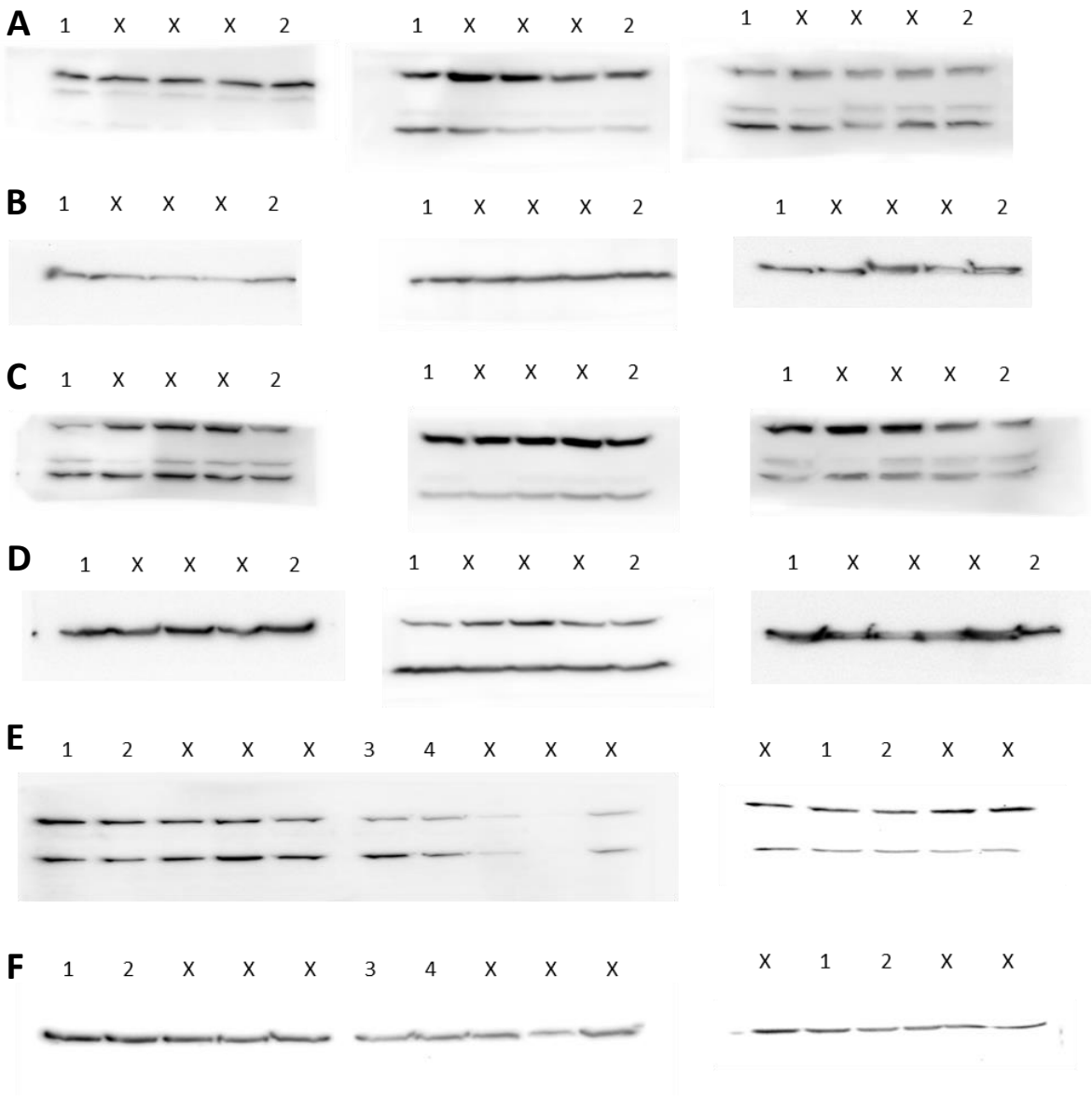

Figure S 10: Raw WB Images Related to Fig. 6 B

Expression of RAGE in BXPC-3, PA-TU-8988T, PANC-1 and MIA-PACA-2 cell lines. (A) Lanes 1-2: BXPC-3 cell protein extract incubated with the RAGE Antibody. (B) Lanes 1-2: BXPC-3 cell protein extract incubated with the βActin Antibody. (C) Lanes 1-2: PA-TU-8988T cell protein extract incubated with the RAGE Antibody. (D) Lanes 1-2: PA-TU-8988T cell protein extract incubated with the βActin Antibody. (E) Lanes 1-4: PANC-1 cell protein extract incubated with the RAGE Antibody. (F) Lanes 1-4: PANC-1 cell protein extract incubated with the βActin Antibody. Lanes X: Not included in figure.

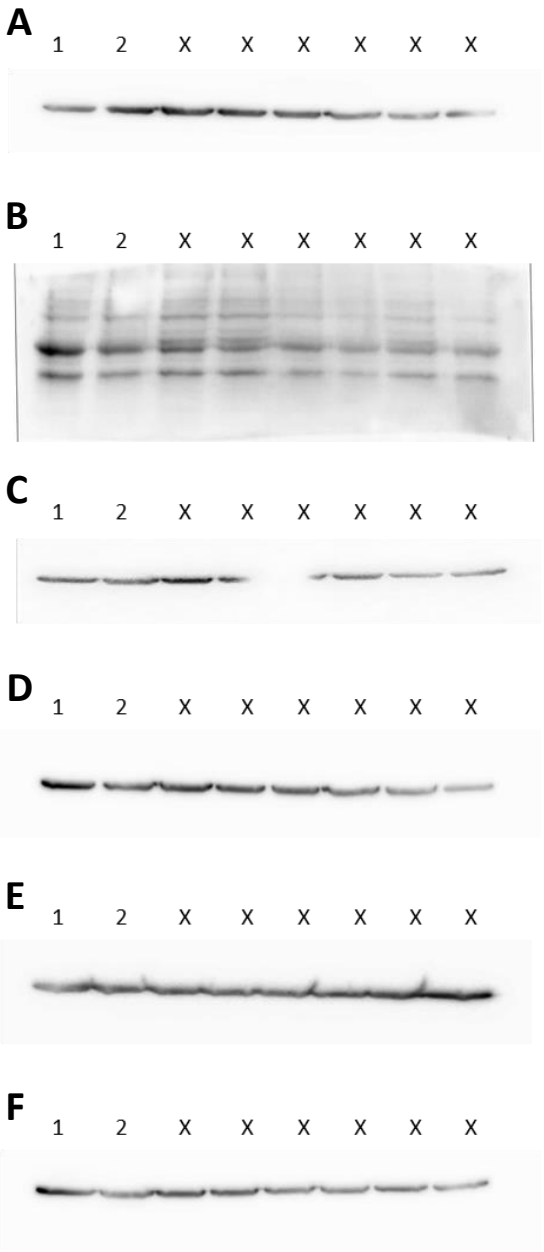

Figure S 11: Raw WB Images Related to Fig. 6 B

Expression of RAGE in MIA-PACA-2 cell line. (A) Lanes 1-2: MIA-PACA-2 cell protein extract incubated with the RAGE Antibody. (B) Lanes 1-2: MIA-PACA-2 cell protein extract incubated with the βActin Antibody. (C) Lanes 1-2: MIA-PACA-2 cell protein extract incubated with the RAGE Antibody. (D) Lanes 1-2: MIA-PACA-2 cell protein extract incubated with the βActin Antibody indicated in Fig 10 B. (E) Lanes 1-2: MIA-PACA-2 cell protein extract incubated with the RAGE Antibody. (F) Lanes 1-2: MIA-PACA-2 cell protein extract incubated with the βActin Antibody. Lanes X: Not included in figure.

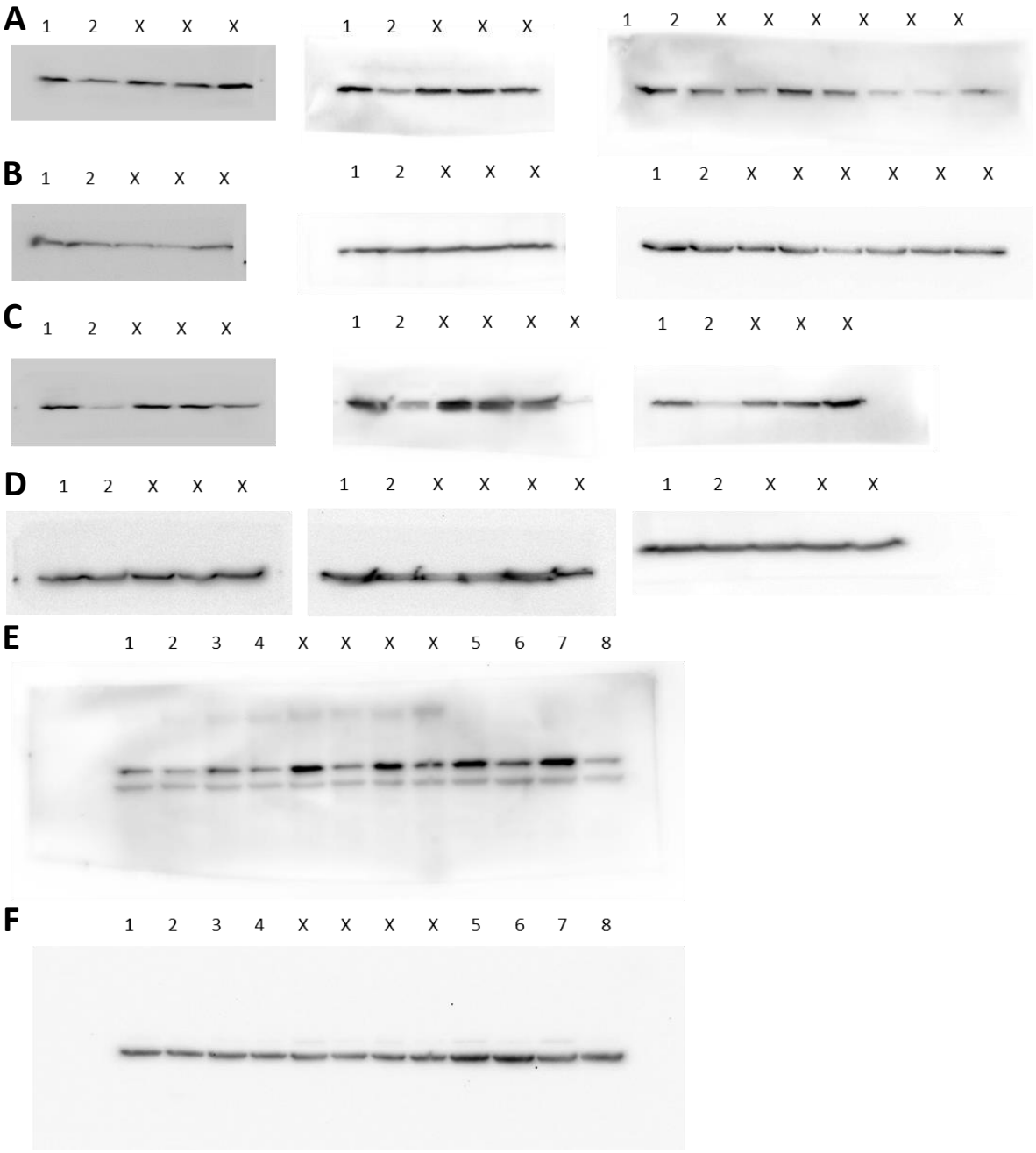

Figure S 12: Raw WB Images Related to Fig. 10 B

Expression of DDOST in BXPC-3, PA-TU-8988T, PANC-1 and MIA-PACA-2 cell lines. (A) Lanes 1-2: BXPC-3 cell protein extract incubated with the DDOST Antibody. (B) Lanes 1-2: BXPC-3 cell protein extract incubated with the βActin Antibody. (C) Lanes 1-2: PA-TU-8988T cell protein extract incubated with the DDOST Antibody. (D) Lanes 1-2: PA-TU-8988T cell protein extract incubated with the βActin Antibody indicated in Fig 10 B. (E) Lanes 1-4: MIA-PACA-2 cell protein extract incubated with the DDOST Antibody. Lanes 5-8: PANC1 cell protein extract incubated with the DDOST Antibody. (F) Lanes 1-2: MIA-PACA-2 cell protein extract incubated with the βActin Antibody. Lanes 5-8: PANC1 cell protein extract incubated with the βActin Antibody. Lanes X: Not included in figure.

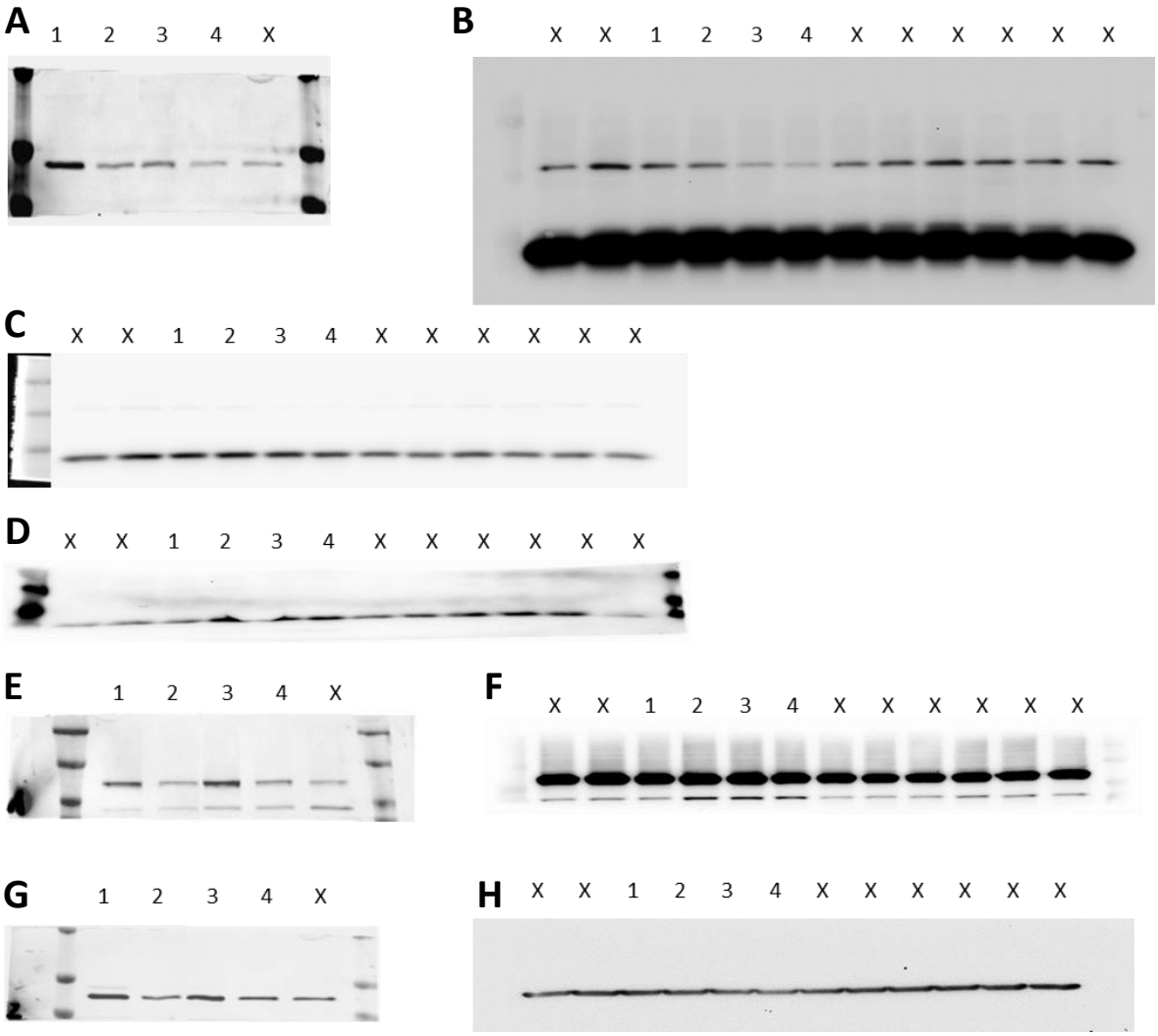

Figure S 13: Raw WB Images Related to Fig. 14 C

Expression of DDOST, PARP and Caspase 3 in BXPC-3, PA-TU-8988T cell lines. (A) Lanes 1-4: BXPC-3 cell protein extract incubated with the DDOST Antibody. (B) Lanes 1-4: PA-TU-8988T cell protein extract incubated with the DDOST Antibody. (C) Lanes 1-4: PA-TU-8988T cell protein extract incubated with the Caspase-3 Antibody. (D) Lanes 1-4: PA-TU-8988T cell protein extract incubated with the Cleaved-Caspase-3 Antibody. (E) Lanes 1-4: BXPC-3 cell protein extract incubated with the PARP Antibody. (F) Lanes 1-4: PA-TU-8988T cell protein extract incubated with the PARP Antibody. (G) Lanes 1-4: BXPC-3 cell protein extract incubated with the β-Actin Antibody. (H) Lanes 1-4: PA-TU-8988T cell protein extract incubated with the β-Actin Antibody. Lanes X: Not included in figure.

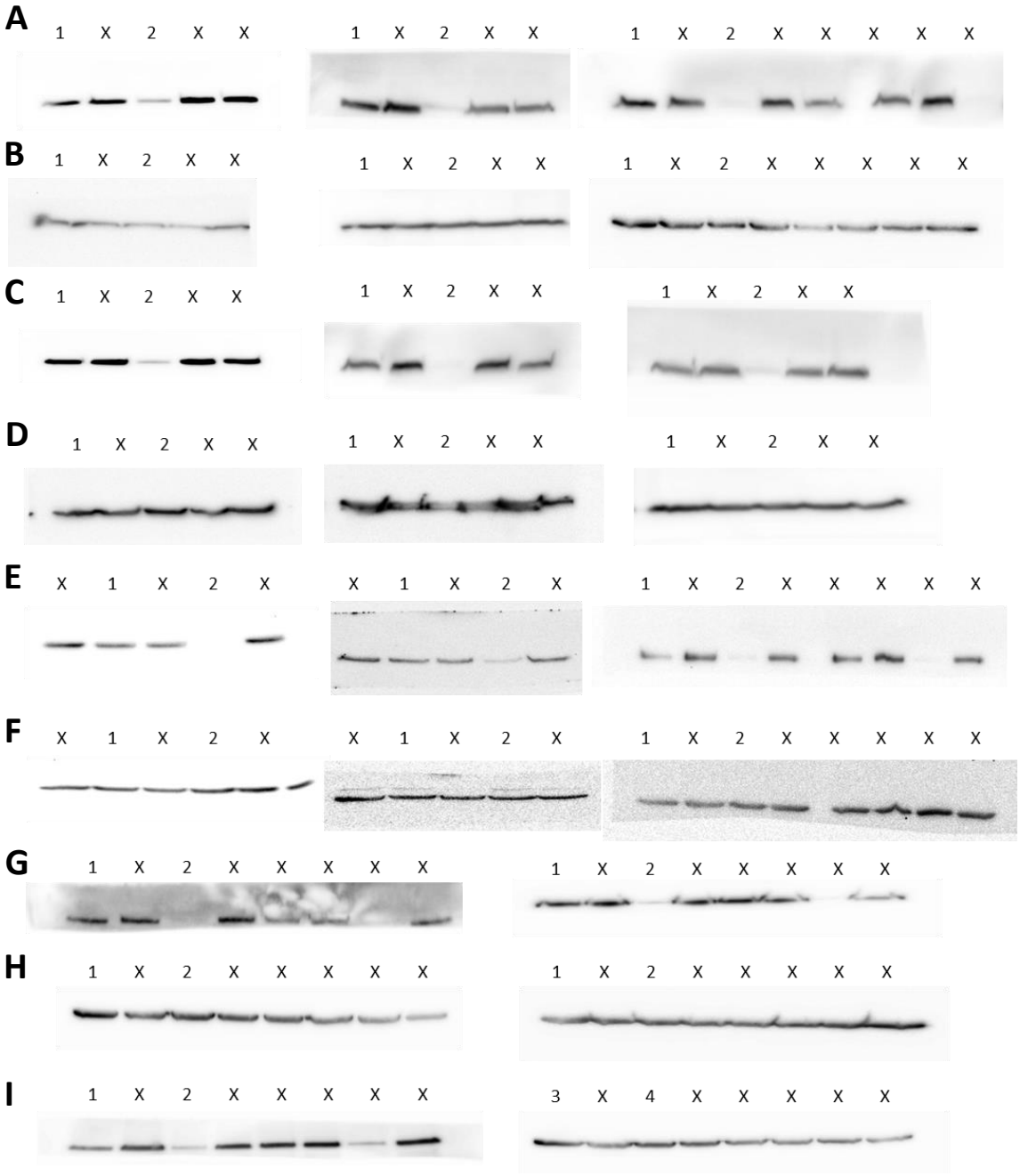

Figure S 14: Raw WB Images Related to Fig. 20 B

Expression of PRKCSH in BXPC-3, PA-TU-8988T, PANC-1 and MIA-PACA-2 cell lines. (A) Lanes 1-2: BXPC-3 cell protein extract incubated with the PRKCSH Antibody. (B) Lanes 1-2: BXPC-3 cell protein extract incubated with the βActin Antibody. (C) Lanes 1-2: PA-TU-8988T cell protein extract incubated with the PRKCSH Antibody. (D) Lanes 1-2: PA-TU-8988T cell protein extract incubated with the βActin Antibody. (E) Lanes 1-2: PANC-1 cell protein extract incubated with the PRKCSH Antibody. (F) Lanes 1-2: PANC-1 cell protein extract incubated with the βActin Antibody. (G) Lanes 1-2: MIA-PACA-2 cell protein extract incubated with the PRKCSH Antibody. (H) Lanes 1-2: MIA-PACA-2 cell protein extract incubated with the βActin Antibody. (I) Lanes 1-2: MIA-PACA-2 cell protein extract incubated with the PRKCSH Antibody and lanes 3-4 incubated with the βActin Antibody. Lanes X: Not included in figure.

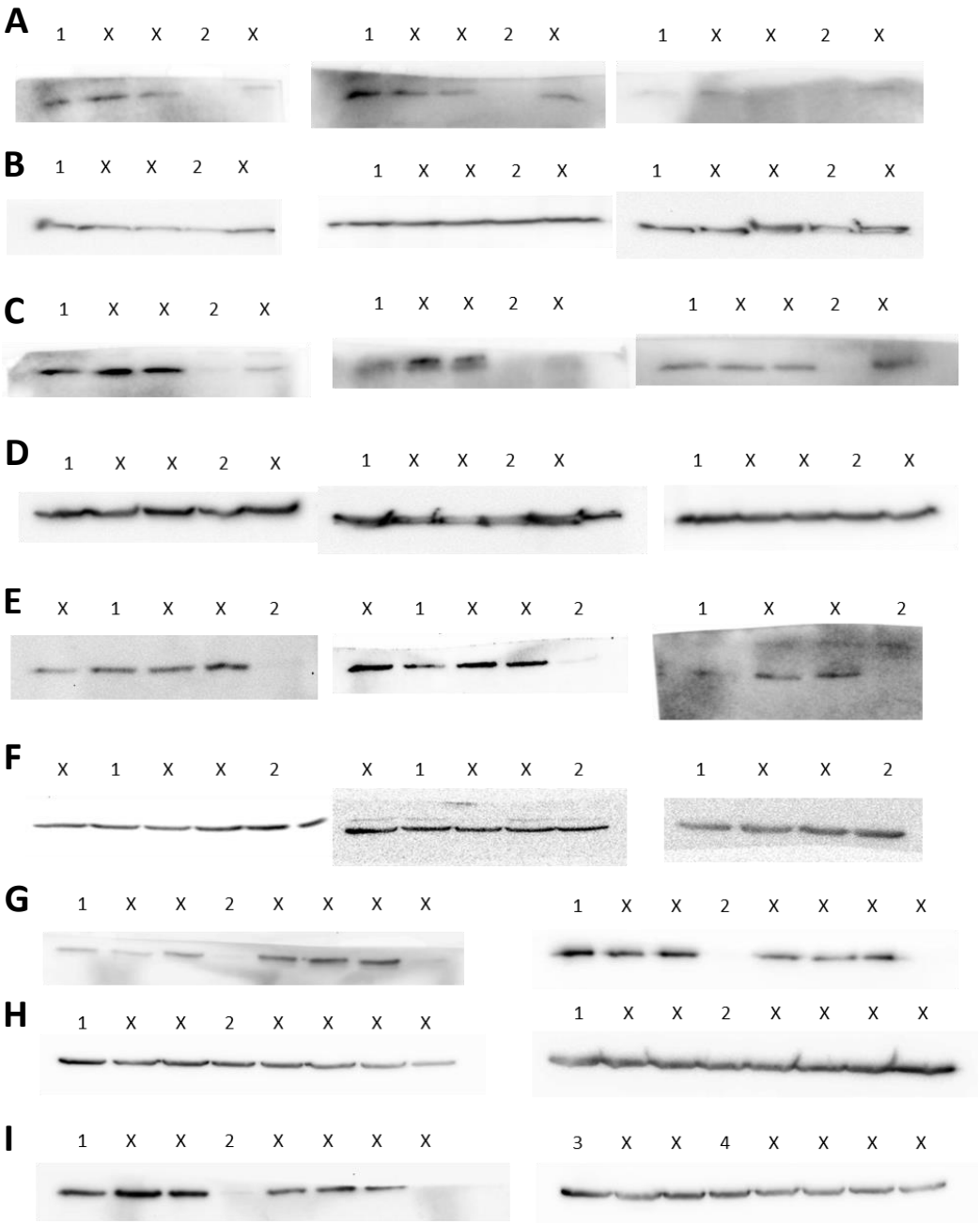

Figure S 15: Raw WB Images Related to Fig. 24 B

Expression of Gal-3 in BXPC-3, PA-TU-8988T, PANC-1 and MIA-PACA-2 cell lines. (A) Lanes 1-2: BXPC-3 cell protein extract incubated with the Gal-3 Antibody. (B) Lanes 1-2: BXPC-3 cell protein extract incubated with the βActin Antibody. (C) Lanes 1-2: PA-TU-8988T cell protein extract incubated with the Gal-3 Antibody. (D) Lanes 1-2: PA-TU-8988T cell protein extract incubated with the βActin Antibody. (E) Lanes 1-2: PANC-1 cell protein extract incubated with the Gal-3 Antibody. (F) Lanes 1-2: PANC-1 cell protein extract incubated with the βActin Antibody. (G) Lanes 1-2: MIA-PACA-2 cell protein extract incubated with the Gal-3 Antibody. (H) Lanes 1-2: MIA-PACA-2 cell protein extract incubated with the βActin Antibody. (I) Lanes 1-2: MIA-PACA-2 cell protein extract incubated with the Gal-3 Antibody and lanes 3-4 incubated with the βActin Antibody. Lanes X: Not included in figure.

Curriculum Vitae

Werdegang

01/2017 – 12/2023	*Martin-Luther-Universität Halle-Wittenberg* **Promotionsstudent (Dr. rer. nat.)** Titel der Dissertation: „Impact of Receptors for Advanced Glycation End Products in Development of Chronic Pancreatitis & Pancreatic Ductal Adenocarcinoma"
08/2016 – 08/2022	*Klinik für Innere Medizin I, MLU Halle-Wittenberg* **Wissenschaftlicher Mitarbeiter**
04/2020 – 04/2021	**Elternzeit**
04/2013 - 02/2016	*Julius-Maximilians-Universität Würzburg* **Masterstudium in Biologie** Titel der Masterthesis: „Strukturelle Studien zur Substratspezifität des mykobakteriellen Typ VII Sekretionssystems"
08/2014 – 12/2014	*Karolinska Institutet, Stockholm* **Erasmus-Internship** Forschungsarbeit zur Protein-Protein-Interaktion des Typ IV Sekretions-systems in *Streptococcus pneumoniae*
10/2009 – 03/2013	*Julius-Maximilians-Universität Würzburg* **Bachelorstudium in Biologie** Titel der Bachelorthesis: „Characterization of RNA binding proteins in *Campylobacter jejuni*"
10/2008 – 08/2009	**Wehrdienst (FWDL)**
08/2005 – 06/2008	*Staatliche Integrierte Gesamtschule, Erfurt* **Abitur**

Publikationsliste

Scientific Reports - submitted - November 2023

Induction of oxidative- and endoplasmic-reticulum-stress dependent apoptosis in pancreatic cancer cell lines by DDOST knockdown

Böhme R, Schmidt A, Hesselbarth N, Posern G, Sinz A, Ihling C, Michl P, Laumen H, Rosendahl J.

Pancreatology - 2020

Serum levels of advanced glycation end products and their receptors sRAGE and Galectin-3 in chronic pancreatitis

Böhme R, Becker C, Keil B, Damm M, Rasch S, Beer S, Schneider R, Kovacs P, Bugert P, Riedel J, Griesmann H, Ruffert C, Kaune T, Michl P, Hesselbarth N, Rosendahl J.

Pancreatology - 2018

Common variants in the CLDN2-MORC4 and PRSS1-PRSS2 loci confer susceptibility to acute pancreatitis

Weiss FU, Hesselbarth N, Párniczky A, Mosztbacher D, Lämmerhirt F, Ruffert C, Kovacs P, Beer S, Seltsam K, Griesmann H, Böhme R, Kaune T, Hollenbach M, Schulz HU, Simon P, Mayerle J, Lerch MM, Cavestro GM, Zuppardo RA, Di Leo M, Testoni PA, Malecka-Panas E, Gasirowska A, Głuszek S, Bugert P, Szentesi A, Mössner J, Witt H, Michl P, Hégyi P, Scholz M, Rosendahl J.

Microbiology - 2015

In vivo characterization of the scaffold activity of flotillin on the membrane kinase KinC of Bacillus subtilis

Schneider J, Mielich-Süss B, Böhme R, Lopez D.

Eidesstattliche Erklärung

Ich erkläre hiermit, dass ich diese Dissertation selbstständig, ohne Hilfe Dritter und ohne Benutzung anderer als der angegebenen Quellen und Hilfsmittel verfasst habe. Alle den benutzten Quellen wörtlich oder sinngemäß entnommenen Stellen sind als solche einzeln kenntlich gemacht.

Mit dieser Arbeit bewerbe ich mich erstmals um die Erlangung des Doktorgrades. Diese Arbeit ist bislang keiner anderen Prüfungsbehörde vorgelegt worden und auch nicht veröffentlicht worden.

Halle (Saale), den 06. Dezember 2023

Richard Böhme